Thesis for the Degree of Doctor of Philosophy

Constrained Blind Source Separation of Human Brain Signals

Tahir Rasheed

Department of Computer Engineering
Graduate School
Kyung Hee University
Seoul, Korea

February, 2010

Thesis for the Degree of Doctor of Philosophy

Constrained Blind Source Separation of Human Brain Signals

By

Tahir Rasheed

Supervised By

Prof. Young-Koo Lee

Department of Computer Engineering

Graduate School

Kyung Hee University

Seoul, Korea

February, 2010

Constrained Blind Source Separation of Human Brain Signals

by

Tahir Rasheed

Supervised by

Prof. Young-Koo Lee, Ph.D.

Submitted to the Department of Computer Engineering
and the Faculty of the Graduate School of
Kyung Hee University in partial fulfillment
of the requirements for the degree of
Doctor of Philosophy

Dissertation Committee:

Prof. Ok-Sam Chae, Ph.D. (chairman)

Prof. Sungyoung Lee, Ph.D.

Prof. Tae-Choong Chung, Ph.D.

Prof. Tae-Seong Kim, Ph.D.

Prof. Young-Koo Lee, Ph.D.

Abstract

Blind source separation (BSS) is a method of separating the underlying source signals from their mixtures, without or little information about the original sources or the mixing process. Blind signal separation relies on the independence criteria of original sources. There are different methods of blind source separation: Singular value decomposition, Principal components analysis, Independent component analysis etc. Recently, blind source separation by Independent Component Analysis (ICA) has gained considerable attention in the research areas such as pattern analysis, multimedia and medical signal processing. ICA has some inherent disadvantage which can be solved by incorporating more information about the desired source into the contrast function as is done in the case of constrained independent component analysis.

Related to every action, there is an electrical activity between the neurons of the brain. This activity can be monitored using invasive or non-invasive techniques. Electroencephalogram (EEG) and Magnetic resonance imaging (MRI) are the two common non-invasive techniques. EEG measures electrical activity of brain at the surface of head with millisecond temporal resolution. Whereas, MRI can measures magnetic activity at the surface of head with millimeter spatial resolution. The signals obtained with each of the two modalities, BSS methods can be applied to find the sources / signals of interest.

In neurophysiological signal analysis, artifact rejection in EEG signals is an important research area. Application of ICA for this purpose has some inherent disadvantages e.g., source ambiguity, un-ordered independent components and large number of independent components. Some time a priori information about the desired sources is available and can be utilized in the

extraction process. A complete artifact rejection system from EEG signals based on constrained independent component analysis is proposed. The proposed system can remove artifacts (e.g., BCG, EOG) from EEG signals measured inside MRI. The system has some peculiar advantages compared to the conventional system e.g. completely automatic artifact rejection system and any number of artifacts can be rejected at the same time.

Evoked potentials (EP) is the brain activity obtained by averaging the EEG activity time-locked to the presentation of some sort of stimulus like visual, somatosensory, or auditory. P300 is a positive evoked potential (EP), elicited approximately 300ms after an attended external stimulus. P300 can be used in brain control interface (BCI) applications. Until now, P300-based BCI has been slow, as it is difficult to detect a P300 response without averaging over a number of trials. An algorithm based on constrained independent component analysis for P300 extraction is proposed, which can extract only the relevant component by incorporating a priori information. The extracted P300 IC is segmented, averaged, and classified into target and non-target events by means of a linear classifier. The method is fast, reliable, computationally inexpensive as compared to conventional averaging and ICA based methods.

Some times the a priori information about the desired component / pattern is in frequency domain. Extracting an IC in specific frequency range has many applications like in medical diagnostic, brain computer interface (BCI) etc. The observations are in time domain and a priori information is in fourier domain. Combining the two is a difficult task, there is no algorithm in bio-signals analysis that can extract IC of specific frequency range. An algorithm is designed to accomplish this task. The performance of the proposed algorithm is presented by extracting the alpha signal from EEG data.

Spatiotemporal data; where sources are present in both space and time. Underlining independence criteria of ICA is difficult to met in both the domains. The conventional ICA algorithm extract sources of the one domain distorting the sources in the other domain. Few Spatiotemporal algorithms are available those have their own disadvantages e.g., source ambiguity, large number of independent and manual selection of independent components. I have proposed an

algorithm which tries to overcome the disadvantages of the conventional as well as the existing spatiotemporal algorithm.

In short, in this thesis new constrained blind source separation algorithm are presented along with their potential applications. Also, constrained BSS approach is used to solve the existing problems in non-invasive brain signal analysis.

Dedicated to my Family; I love you all

Acknowledgments

First and foremost, I render my humble and sincere thanks to the Almighty for showering His blessings in every possible form upon me. He gave me strength, courage, patience and introduced to me all those people who made my studies and stay in Korea a pleasant experience.

This dissertation represents a great deal of time and effort not only on my part, but also on part of my advisor, Prof. Young-Koo Lee and co-advisor Prof. Tae-Seong Kim. I am also obliged and thankful to Prof. Sungyoung Lee. They helped me to shape up my research from day one, pushed me to get through the inevitable research setbacks, and encouraged me to achieve the best of my abilities.

I am also thankful to my other thesis committee members Professors for providing insightful and constructive comments to improve the quality of this dissertation.

I am very much thankful to my friends Uzair Ahmad, Syed M. K. Raazi, Adil Mehmood Khan, Ozair Idrees Khan, Asad Masood Khattak, Zafar Khan and Zeeshan Pervez for making my time at Kyung Hee University as good as it was. I especially owe a lot to the support given by Bilal Ahmed, Syed Obaid Amin and Muhammad Shoaib Siddiqui; who are always there for providing every possible help during my studies.

I would also like to thank all the current and former members of my lab for their kind support and for providing a pleasant working environment. Every lab member is worthy to be praised and I appreciate them all.

I have no words to express my gratitude to my family for their endless support, love and prayers. I would like to acknowledge the sacrifices made by my parents for my better education

and upbringing. My loving thanks go to my wife, whose care and sacrifices have sustained me throughout this work. Lastly, once again I am thankful to the Almighty for gifting me with an adorable son and daughter; who are sources of constant joy and happiness in my life. They always takes away all of my worries and vexation by there sweet smile, hugs and kisses.

I love you and am thankful to you, my family.

Tahir Rasheed

February, 2010

Contents

List of Figures

List of Tables

Chapter 1

Introduction

1.1 Overview

Blind source separation (BSS), is a method of separating the under lying source signals from the observations, which are the mixtures of the original sources, without or little information about the original sources or the mixing process. Consider a scenario depicted in Fig. 1.1, there are some sources S_1, S_2, S_3, S_4, S_n producing the signals and some sensors at some distance (surface of head) from these sources measuring them. Depending on the distance from the sources each sensor will measure different mixture X_1, X_2, X_3, X_4, X_n of the sources. Assume that we have no idea of the nature of the sources and the mixing process and we are asked to estimate the original source signals from the mixtures only, then this is a blind source separation problem.

Blind signal separation relies on the assumption that the underlying sources are independent. The Central limit theorem (CLT) states that adding the sources makes the mixture gaussian. Blind source separation techniques transforms a set of data (mixture) into another set of data where the signals are independent of each other i.e., estimates of original signals. The transformation criteria is to increase the independence between the mixtures. There are different methods of blind source separation: Singular value decomposition, Principal components analysis,Independent component analysis etc.

Recently, blind source separation by Independent Component Analysis (ICA) has gained considerable attention in the research areas such as pattern analysis, multimedia, speech recognition systems, telecommunications and medical signal processing. By adding the whitening process

as a preprocessing stage, ICA not only de-correlates the signals but it also employs higher-order statistics to separate independent components. ICA find non-orthogonal components compared to principal component analysis (PCA), which is based on second order statistics, that can only find orthogonal components.

Various ICA algorithms has been developed which uses numerous contrast functions for optimization e.g., contrast function based on kurtosis, negentropy etc. ICA has some inherent disadvantage i). source ambiguity ii) undetermined variances of independent components etc. The problem mentioned above can be solved by incorporating more information about the desired source into the ICA contrast function. A procedure called constrained ICA uses Lagrange method to incorporate constrains.

There are numerous brain imaging technique e.g., electroencephalogram (EEG), magnetoencephalogram (MEG) and functional magnetic resonance imaging (fMRI). The data obtained from these techniques are multi-channel data, ICA or constrained ICA are ideally suited for their analysis. However, ICA analysis of the brain imaging data has limitations. The procedures and new algorithms based on constrained ICA has been presented in thesis for EEG and fMRI data analysis.

1.2 Problem Statement and Challenges

Highly complex and center of the human nervous system is the brain. It is made of a network of billions of neurons. There is an electrical communication between these neurons through synaptic connections for each and every activity of a human being. For functional understanding of the human brain, study of these communications is very important. The procedure to record these electrical activities can be grouped into two categories, Invasive techniques and non-invasive techniques. Electroencephalogram (EEG) and Magnetic resonance imaging (MRI) are two the non-invasive techniques used to study brain. EEG measures electrical activity at the surface of the head with millisecond temporal resolution and MRI measures magnetic activity at the

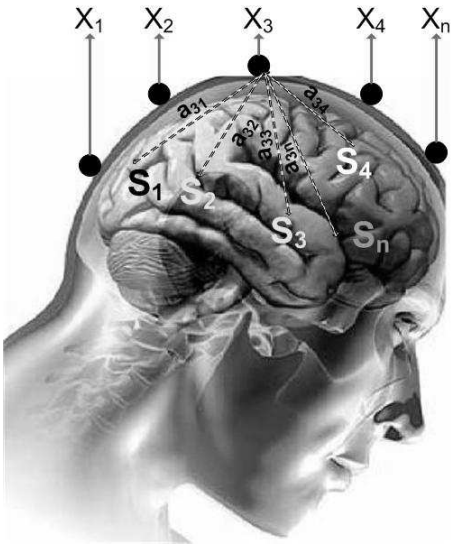

Figure 1.1: Brain signal analysis: Blind source separation problem

surface of head with millimeter spatial resolution. Even the two modalities can be combined for superior spatiotemporal resolution. In addition to functional understanding the EEG and fMRI signals can be employed for numerous applications like, medical diagnostics, brain computer interface applications, Telecare and U-health applications and brain games (games played simply by thinking).

In non-invasive techniques (EEG and fMRI), the sensors are placed at the surface or around the head at very close distance. For each activity of the human, large number of sources (neurons) are active. Each sensor is measuring a mixture of these activities from sources and each sensor measures a different mixture depending upon its distance from the sources. This scenario is depicted in Fig. 1.1. As these are non-invasive techniques, one has no idea about the sources and the mixing process that has taken place inside the head. Therefore, brain signal analysis can be treated as a blind source separation problem. The flow diagram of human brain signal analysis is given Fig.1.2. In the field of pattern analysis and bio-signal analysis ICA is very favorable choice and is extensively used. However, when applying ICA to artifact rejection in EEG signals

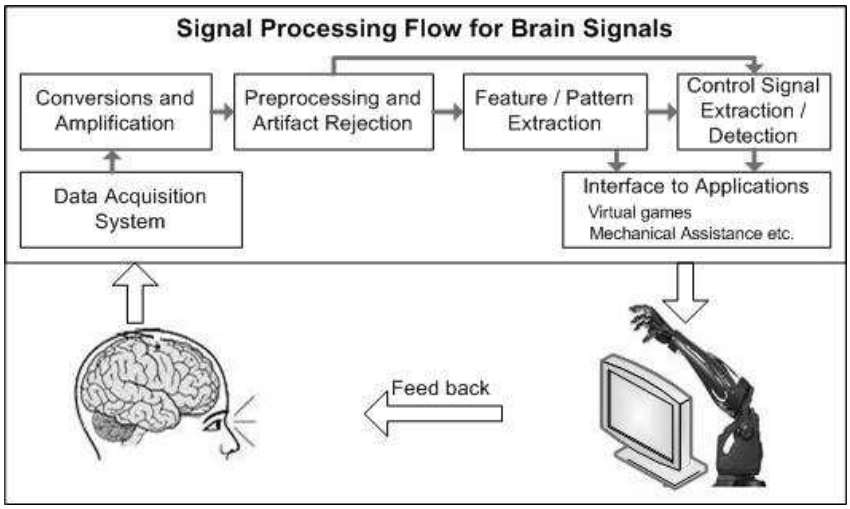

Figure 1.2: Flow diagram of brain signal analysis

it has some inherent disadvantages e.g., source ambiguity, un-ordered independent components and large number of independent components. With these problems, automated complete artifact rejection system from EEG signals based on ICA can not be devised. Event related potentials (ERP) is an EEG signal that is time locked averaged according to some external stimulus like auditory or visual stimulus. It is an important control signal in BCI applications. Conventional methods, large number of averaging and conventional ICA makes the whole process very slow and hard to be used in BCI applications. Similarly, There are cases where the requirement is to extract a component with known frequency range. Extracting an independent component in specific frequency range is important and has many applications like in brain computer interface (BCI) and multimedia applications. For today's BCI applications common control signals are alpha signal or mu signal, for these signals only known information is their frequency range. The signals are in time domain and a priori information is in Fourier domain. It is always challenging to fusion the information in two different domain, to our best knowledge there is no algorithm for bio-signals analysis that can extract independent component of specific frequency range. The other noninvasive technique (i.e., fMRI) produces sequence of images of brain. These sequence

of images (spatiotemporal data) has interesting sources in time as well as in spatial domain. Extracting the temporal as well spatial sources are crucial for fMRI analysis. However, there are cases, where underlining independence criteria of ICA is difficult to met. In such cases, the conventional ICA algorithm extract sources of the one domain distorting the sources in corresponding domain. Other available algorithm for spatiotemporal data has their own disadvantages e.g., source ambiguity, large number of independent and manual selection of independent components.

Briefly, the focus of this thesis is to present solutions to the problems of EEG and fMRI data analysis. Various, new approaches and new algorithm have been proposed based on constrained blind source separation to handle the difficulties of brain signal analysis.

1.3 Contributions

In bio-signal analysis some times a priori information is available about the desired sources. The a priori information is utilized in proposing a complete artifact rejection system from EEG signals [1],[2]. The proposed system is based on the constrained independent component analysis, it can remove artifacts (e.g., BCG, EOG) from EEG signals measured inside MRI. The proposed system has some peculiar advantages compared to the conventional system e.g. automatic complete artifact rejection system, any number of artifacts can be rejected at the same time. In an other application, a priori information about the desired event related potential (P300) has been utilized in constrained ICA to exact the P300 signal from EEG data. The proposed solution overcomes the problem associated with the conventional method with promising results.

An algorithm which take frequency information as constraint to extract the independent component in the desired frequency band is proposed. The performance of the proposed algorithm is presented by extracting the alpha signal from EEG data. The performance of the proposed algorithm is compared with the conventional methods. The results indicate better performance of the proposed algorithm. This algorithm is a valuable addition to the tools available for BSS

applications.

For spatiotemporal data analysis, an algorithm for spatiotemporal data which tries to overcome the disadvantages of the conventional as well as spatiotemporal algorithm is presented. With the proposed algorithm one or subset of independent components in both the domains can be extracted with out affecting the independent components in the corresponding domains. Better performance of the proposed algorithm is proved with application on simulated as well as real life applications.

In short we can summarize our contributions as follows

- Automated, complete artifact rejection system in electroencephalogram (EEG) signals.
- An algorithm for the analysis of spatiotemporal data, its application for real life data
- Algorithm to extract independent components in specific band, its application for real life data
- Constrained blind source separation based extraction of control signals like P300 for applications like Brain control interface (BCI) is also presented.

1.4 Structure of the Dissertation

- Chapter 2 provides the mathematical preliminaries required to understand this thesis.
- Chapter 3 provides basic information about the brain imaging techniques (i.e., EEG, MEG and fMRI.)
- Chapter 4 describes a complete solution for artifact rejection in electroencephalogram (EEG) signals.
- Chapter 5 describes the constrained spatiotemporal independent component analysis and its application for fMRI images.

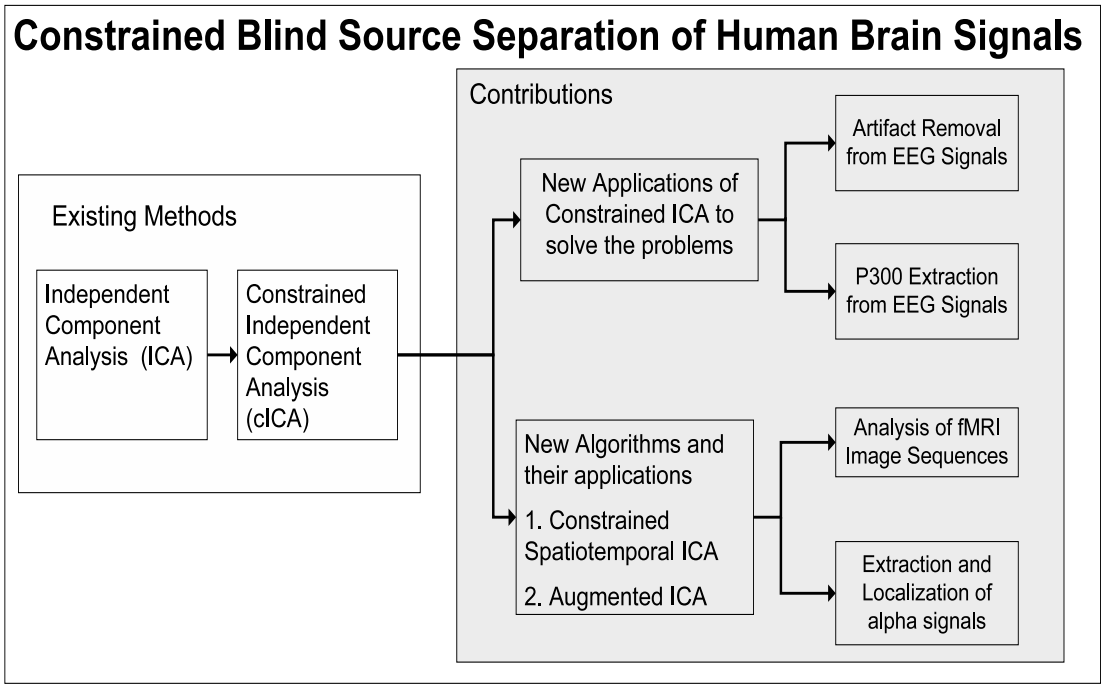

Figure 1.3: Contributions; block diagram

- Chapter 6 describes the extraction of a independent component of some particular frequency range using augmented independent component analysis.
- Chapter 7 constrained independent component analysis based extraction of P300,an ERP.
- Chapter 8 concludes this thesis and provides the possible future directions.

Chapter 2

Blind Source Separation

The mathematical preliminaries required to understand the basic concepts of independent component analysis (ICA) and constrained Independent component analysis (constrained ICA) is presented in this chapter. Knowledge of these concepts are important for understanding the concepts presented in this thesis.

2.1 Mathematical Preliminaries

2.1.1 Vector and Matrix Gradient

Consider a scalar valued function g of m variables $g = g(w_1, \ldots, w_m) = g(\mathbf{w})$. The $\mathbf{w} = (w_1, ..., w_m)^t$ is a column vector. The vector gradient of function g can be written as.

$$\frac{\partial g}{\partial \mathbf{w}} = \begin{pmatrix} \frac{\partial g}{\partial w_1} \\ \cdot \\ \\ \cdot \\ \frac{\partial g}{\partial w_n} \end{pmatrix} \tag{2.1}$$

The notation $\frac{\partial g}{\partial \mathbf{w}}$ is the shorthand for the gradient, other commonly used notations would be ∇_g or $\nabla_{\mathbf{w}} g$. The second order gradients of a function g with respect to **w** can be written as

$$\frac{\partial^2 g}{\partial \mathbf{w}^2} = \begin{pmatrix} \frac{\partial^2 g}{\partial w_1^2} & \cdots & \frac{\partial^2 g}{\partial w_1 w_m} \\ \vdots & \ddots & \vdots \\ \frac{\partial^2 g}{\partial w_m w_1} & \cdots & \frac{\partial^2 g}{\partial w_m^2} \end{pmatrix} \tag{2.2}$$

The above matrix is called the Hessian matrix of the function $g(\mathbf{w})$. This matrix is always symmetric. These concepts can be generalized to the vector-valued functions.

$$\mathbf{g}(\mathbf{w}) = \begin{pmatrix} g_1(\mathbf{w}) \\ . \\ . \\ g_n(\mathbf{w}) \end{pmatrix} \tag{2.3}$$

The first order derivative of g with respect to $\mathbf{w}$ known as *jacobian matrix* of $\mathbf{g}$ can be written as

$$\frac{\partial \mathbf{g}}{\partial \mathbf{w}} = \begin{pmatrix} \frac{\partial g_1}{\partial w_1} & \cdots & \frac{\partial g_n}{\partial w_1} \\ \vdots & \ddots & \vdots \\ \frac{\partial g_1}{\partial w_m} & \cdots & \frac{\partial g_n}{\partial w_m} \end{pmatrix} \tag{2.4}$$

The Jacobian matrix is sometimes denoted by $J_{\mathbf{g}}$.

Now, consider a scalar-valued function g of the elements of mxn matrix $\mathbf{W} = (w_{ij})$. Similar to the vector gradient, the matrix gradient can be written as:

$$\frac{\partial g}{\partial \mathbf{W}} = \begin{pmatrix} \frac{\partial g}{\partial w_{11}} & \cdots & \frac{\partial g}{\partial w_{1n}} \\ \vdots & \ddots & \vdots \\ \frac{\partial g}{\partial w_{m1}} & \cdots & \frac{\partial g}{\partial w_{mn}} \end{pmatrix} \tag{2.5}$$

2.1.2 The Lagrange Method

The most common and prominent method to take the constraints into account is the Lagrange multipliers method. The lagrange method can handle problems with both equality and inequality constraints. The general form with which the lagrange method deals is given as follows:

$$minimize \ f(\mathbf{X}), \quad subject \ to \ \mathbf{g}(\mathbf{X}) \leq 0, \quad \mathbf{h}(\mathbf{X}) = 0 \tag{2.6}$$

where $f(\mathbf{X})$ is an objective function, $\mathbf{X}$ is a matrix or a vector of the problem arguments, $\mathbf{g}(\mathbf{X})$ are the inequality constraints and $\mathbf{h}(\mathbf{X})$ defines the equality constraints. Lagrange method does

not directly deals with the inequality constraints therefore they are converted onto equality constraints by introducing the the slack variables $\mathbf{z}$ i.e., $\hat{\mathbf{g}}(\mathbf{X}) = \mathbf{g}(\mathbf{X}) + \mathbf{z}$. Based on this transformation equation 2.6 can be written as:

$$\Gamma(\mathbf{X}, \boldsymbol{\mu}, \boldsymbol{\lambda}, \boldsymbol{z}) = f(\mathbf{X}) + \boldsymbol{\mu}^t \hat{\mathbf{g}}(\mathbf{X}) + \tfrac{1}{2}\gamma||\hat{\mathbf{g}}(\mathbf{X})||^2 + \boldsymbol{\lambda}^t \mathbf{h}(\mathbf{X}) + \tfrac{1}{2}\gamma||\mathbf{h}(\mathbf{X})||^2 \tag{2.7}$$

where $\boldsymbol{\mu} = [\mu_1, \ldots, \mu_m]^t$ and $\boldsymbol{\lambda} = [\lambda_1, \ldots, \lambda_n]^t$ are two sets of lagrange multipliers, γ is the scalar penalty parameter, $||.||$ denotes Euclidean norm and $\frac{1}{2}\gamma||.||$ is the penalty term that ensures that the optimization problem remains in the condition of local convexity assumption ($\nabla^2_{\mathbf{XX}}\Gamma > 0$).

2.1.3 Independent and Uncorrelated Variables

Independence can be defined as: consider two scalar random variables v_1 and v_2, knowing some thing about one variable does not give any sort of information about other variables then the two variables are said to independent. Mathematically we can write as:

$$p(v_1, v_2) = p(v_1)p(v_2) \tag{2.8}$$

where $p(v_1, v_2)$ is the joint pdf of the two variables and $p(v_1), p(v_2)$ are the marginal pdf of the two scalar variables. In words the equation 2.8 stats that: if the joint pdf of variables is equal to the product of the their marginal pdf then the variables are independent.

On the other side, if the covariance between two random variables is zero they are said to be uncorrelated. The uncorrelatedness is a weaker concept than the independence. Mathematically uncorrelatedness can be written as:

$$cov(v_1, v_2) = E\{(v_1 - \bar{v_1})(v_2 - \bar{v_2})^t\} = 0 \tag{2.9}$$

where $\bar{v_1}, \bar{v_2}$ are the mean values of the random variables.

2.1.4 Nongaussian is Independent

The Central Limit Theorem, a classical result in probability theory, tells that the distribution of a sum of independent random variables tends toward a gaussian distribution, under certain conditions. Thus, a sum of two independent random variables usually has a distribution that is closer to gaussian than any of the two original random variables. Based on this theorem on can say that nongaussian is independent.

2.1.5 Measures of Nongaussianity

A quantitative measure of nongaussianity of a random variable can be kurtosis or negentropy. Assume the random variable under consideration is centered (zero-mean) and has variance equal to one.

2.1.5.1 Kurtosis

Kurtosis, the fourth order cumulant can be a measure of nongaussianity. The kurtosis of a random variable y can be defined as:

$$\mathrm{kurt(y)} = \mathrm{E\{y^4\}} - 3(\mathrm{E\{y^2\}})^2 \tag{2.10}$$

As we have assumed that y is of unit variance, the right-hand side of above equation can be written as $Ey^4 - 3$, indicating that kurtosis is a normalized version of the fourth moment Ey^4. kurtosis is zero for a gaussian random variable because the fourth moment for them equals to $3(Ey^2)^2$. Therefore, for most (but not quite all) of nongaussian random variables the kurtosis is nonzero. Kurtosis can be both positive or negative. Random variables that have a negative kurtosis are called subgaussian, and those with positive kurtosis are called supergaussian.

In practice, using Kurtosis as a measure of nongaussianity has some drawbacks. The main problem is that kurtosis can be very sensitive to outliers [3]. Its value may depend on only a few erroneous or irrelevant observations in the tails of the distribution. In other words, kurtosis is not a robust measure of nongaussianity.

2.1.5.2 Negentropy

The other very important and mostly used measure of nongaussianity is given by negentropy. Negentropy is based on differential entropy. A slightly modified version of differential entropy is used to obtain a measure of nongaussianity that is always nonnegative and zero for a gaussian variable. This measure is called negentropy. Negentropy J is defined as follows:

$$J(y) = H(ygauss) - H(y) \tag{2.11}$$

where $ygauss$ is a Gaussian random variable of the same covariance matrix as the random variable y. In addition to have nonnegative valuse and zero for Gaussian variable, Negentropy has the additional interesting property that it is invariant for invertible linear transformations [4] [5]. A very useful approximation of negentropy were developed by Hyvarinen. These approximation were based on the maximum-entropy principle:

$$J(y) \approx \sum_{i=1}^{p} k_i[E\{G_i(y)\} - E\{G_i(v)\}]^2 \tag{2.12}$$

where k_i are some positive constants, and v is a Gaussian variable of . y is zero mean and unit variance random variable. G_i are nonquadratic functions [5].

2.2 Independent Component Analysis

Consider a situation where there are number of signals emitted by some physical sources (for simplicity consider four sources), for example, people speaking in the same room, thus emitting speech signals; different brain areas emitting electric signals; or mobile phones emitting their radio waves. Assume that there are four sensors at different positions, so that each records a mixture of the original source signals with slightly different weights. Denote the observed signals by $x_1(t), x_2(t)$, $x_3(t)$ and $x_4(t)$ and $s_1(t), s_2(t)$, $s_3(t)$ and $s_4(t)$ the original signals. The $x_i(t)$ are the weighted sums of the $s_i(t)$, where the coefficients depend on the distances between the

sources and the sensors:

$$\begin{aligned} x_1(t) &= a_{11}s_1(t) + a_{12}s_2(t) + a_{13}s_3(t) + a_{14}s_4(t) \\ x_2(t) &= a_{21}s_1(t) + a_{22}s_2(t) + a_{23}s_3(t) + a_{24}s_4(t) \\ x_3(t) &= a_{31}s_1(t) + a_{32}s_2(t) + a_{33}s_3(t) + a_{34}s_4(t) \\ x_4(t) &= a_{41}s_1(t) + a_{42}s_2(t) + a_{43}s_3(t) + a_{44}s_4(t) \end{aligned} \tag{2.13}$$

where a_{ij} are the unknown mixing weights. The weights are unknown; the original sources are unknown as well as those cannot be recorded directly. As an illustration, consider the waveforms in Fig. 2.2. These are linear mixtures of source signals shown in Fig. 2.2(a). Our task is to find the original signals from these mixtures. This is the blind source separation (BSS) problem. We can safely assume that the matrix made by mixing coefficients a_{ij} is invertible (i.e., full rank matrix). Thus there exists a matrix $\mathbf{W}$ with coefficients w_{ij}, such that we can separate them as:

$$\begin{aligned} s_1(t) &= w_{11}x_1(t) + w_{12}x_2(t) + w_{13}x_3(t) + w_{14}x_4(t) \\ s_2(t) &= w_{21}x_1(t) + w_{22}x_2(t) + w_{23}x_3(t) + w_{24}x_4(t) \\ s_3(t) &= w_{31}x_1(t) + w_{32}x_2(t) + w_{33}x_3(t) + w_{34}x_4(t) \\ s_4(t) &= w_{41}x_1(t) + w_{42}x_2(t) + w_{43}x_3(t) + w_{44}x_4(t) \end{aligned} \tag{2.14}$$

One approach to solving this problem is to assume that $s_i(t)$ are statistically independent at each time instant t. Independent component analysis (ICA), a method for finding underlying factors or components from multivariate (multidimensional) statistical data, based on the information of independence and nongaussianity can estimate w_{ij}, which allows us to separate the original source signals $s_i(t)$ from their mixtures $x_i(t)$. Fig. 2.2(b) gives the signals estimated by the ICA method. As can be seen, these are very close to the original source signals.

The above example can be extended to m number of sources ($\mathbf{s}(t) = (s_1(t), s_2(t)) \ldots, s_m(t))^T$ and n number of multi-channel observations ($\mathbf{x}(t) = (x_1(t), x_2(t), \ldots, x_n(t))^T$). The Linear ICA equations for these sources and mixtures can be written in vector form as:

$$\mathbf{x}(t) = \mathbf{A}\mathbf{s}(t) \tag{2.15}$$

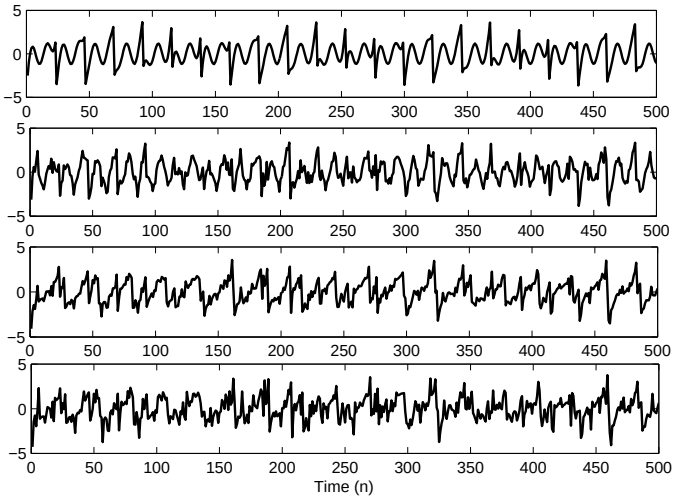

Figure 2.1: The observed signals that are assumed to be mixtures of some underlying source signals.

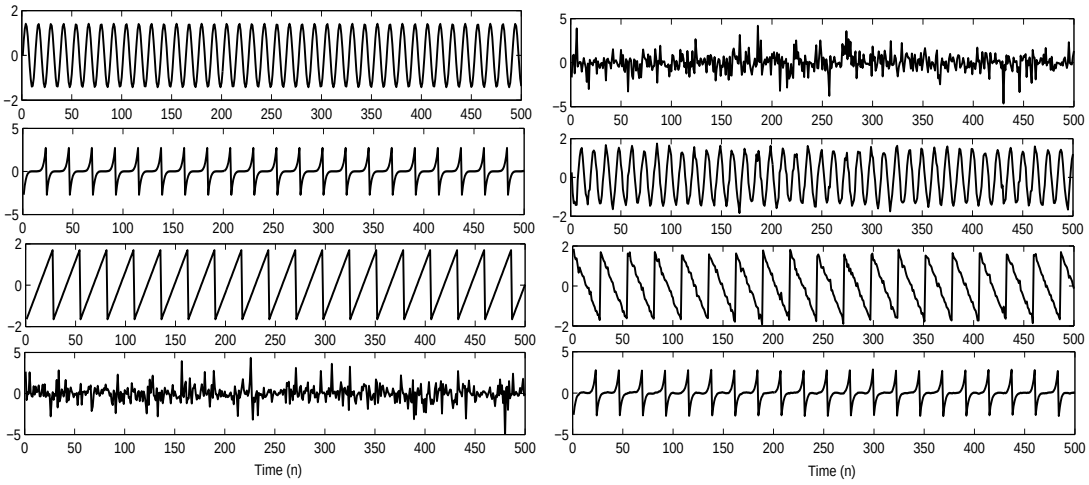

(a) Original source signals (b) The estimates of the original source signals

Figure 2.2: The original source signals and the recovered signals using ICA.

where the matrix A of size *n* × *m* represents linear memory-less mixing channels. The ICA algorithm, based on the independence criterion and non-gaussian distribution of under lying sources, must find a separating or de-mixing matrix such that

$$\mathbf{s}(t) = \mathbf{W}\mathbf{x}(t) \tag{2.16}$$

where $\mathbf{W} = [\mathbf{w}_1, \mathbf{w}_2, \ldots, \mathbf{w}_n]$ is the un-mixing matrix of size *m* × *n*. For the complete ICA, the number of channels are assumed to be equal to the number of underlying independent sources i.e., n=m. General implementations of ICA can be found in the literature [6, 7, 8].

2.3 Ambiguities of ICA

In ICA model (**x=As**) presented above has following ambiguities: *1. The variances (energies) of the independent components can not be determined., 2. The order of the output independent components can not be determined.* The details about these ambiguities can be found in [8].

2.4 Constrained Independent Component Analysis

The conventional ICA algorithms have some limitations like, the output number of components are equal to observations. This is big drawback in case of large number of observation channels. The conventional ICA got extended by Lu and Rajapakse such that only a desired source or a subset of sources can be found. They named it as a constrained ICA. With the constraints in place, the constrained ICA deals with the following minimization problem:

$$\begin{aligned} &maximize: && \mathcal{C}(\mathbf{y}) \\ &subject\ to: && g(\mathbf{y}:\mathbf{W}) \leq \mathbf{0}, \quad \mathbf{h}(\mathbf{y}:\mathbf{W}) = \mathbf{0} \end{aligned} \tag{2.17}$$

where $\mathcal{C}(\mathbf{y})$ is the ICA contrast function, $y_i = \mathbf{w}_i^T\mathbf{x}$ is the estimated output, ρ is a positive constant, v is a zero mean and unit variance Gaussian variable, $G(.)(= logcosh(.))$ is a non-quadratic function as defined in [8],

$\mathbf{g}(\mathbf{y}:\mathbf{W}) = (g_1(\mathbf{y}:\mathbf{W}), g_2(\mathbf{y}:\mathbf{W}), \ldots, g_u(\mathbf{y}:\mathbf{W}))$ is the inequality closeness constraint and $\mathbf{h}(\mathbf{y}:\mathbf{W}) = (h_1(\mathbf{y}:\mathbf{W}), h_2(\mathbf{y}:\mathbf{W}), \ldots, h_v(\mathbf{y}:\mathbf{W})$ constrains the outputs to have a unit variance (equality constraints). Transform the original inequality constraints $\mathbf{g}(\mathbf{y}:\mathbf{W}) \leq \mathbf{0}$ into equality constraints with a vector of slack variables $\mathbf{z} = (z_1, z_2, \ldots, z_u)^t$, we have

$$g_i(\mathbf{y}:\mathbf{W}) \leq \mathbf{0} \quad \Leftrightarrow \quad g_i(\mathbf{y}:\mathbf{W}) + \mathbf{z}_i^2 = 0 \tag{2.18}$$

let

$$\begin{aligned} &g_i(\mathbf{y}:\mathbf{W}) + \mathbf{z}_i^2 = \hat{g}_i(\mathbf{y}:\mathbf{W}) \\ &\hat{\mathbf{g}}(\mathbf{y}:\mathbf{W}) = (\hat{g_1}(\mathbf{y}:\mathbf{W}), \hat{g_2}(\mathbf{y}:\mathbf{W}), \ldots, \hat{g_u}(\mathbf{y}:\mathbf{W}))^t \end{aligned} \tag{2.19}$$

Using the augmented Lagrangian function as described by [9], equation 2.17 can be written as follows:

$$\begin{aligned} \Gamma(\mathbf{W}, \boldsymbol{\mu}, \boldsymbol{\lambda}, \mathbf{z}) = \mathcal{C}(\mathbf{y}) + \boldsymbol{\mu}^{\mathbf{t}}\hat{\mathbf{g}}(\mathbf{y}:\mathbf{W}) + \tfrac{\mathbf{1}}{\mathbf{2}}\gamma||\hat{\mathbf{g}}(\mathbf{y}:\mathbf{W})||^{\mathbf{2}} \\ +\boldsymbol{\lambda}^T\mathbf{h}(\mathbf{y}:\mathbf{W}) + \tfrac{\mathbf{1}}{\mathbf{2}}\gamma||\mathbf{h}(\mathbf{y}:\mathbf{W})||^{\mathbf{2}} \end{aligned} \tag{2.20}$$

where $\mu = (\mu_1, \mu_2, \ldots, \mu_u)^t$ and $\lambda = (\lambda_1, \lambda_2, \ldots, \lambda_v)^t$ are the vectors of Lagrange parameters, $\gamma(> 0)$ is the penalty parameter and $||.||$ denotes the Euclidean norm (dot product). let

$$\begin{aligned} &G(\mathbf{y}:\mathbf{W}, \boldsymbol{\mu}, \mathbf{z}) = \boldsymbol{\mu}^t\hat{\mathbf{g}}(\mathbf{y}:\mathbf{W}) + \tfrac{\mathbf{1}}{\mathbf{2}}\gamma||\hat{\mathbf{g}}(\mathbf{y}:\mathbf{W})||^{\mathbf{2}} \\ &H(\mathbf{y}:\mathbf{W}, \boldsymbol{\lambda}) = \boldsymbol{\lambda}^T\mathbf{h}(\mathbf{y}:\mathbf{W}) + \tfrac{\mathbf{1}}{\mathbf{2}}\gamma||\mathbf{h}(\mathbf{y}:\mathbf{W})||^{\mathbf{2}} \end{aligned}$$

Therefore equation 2.20 can be written as:

$$\Gamma(\mathbf{W}, \boldsymbol{\mu}, \boldsymbol{\lambda}, \mathbf{z}) = \mathcal{C}(\mathbf{y}) + \mathbf{G}(\mathbf{y}:\mathbf{W}, \boldsymbol{\mu}, \mathbf{z}) + \mathbf{H}(\mathbf{y}:\mathbf{W}, \boldsymbol{\lambda}) \tag{2.21}$$

Our goal is to find $min\{\Gamma(\mathbf{W}, \boldsymbol{\mu}, \boldsymbol{\lambda}, \mathbf{z}) : \mathbf{W}, \mathbf{z}\}$ i.e., minimize the final cost function w.r.t $\mathbf{W}$ and $\mathbf{z}$. We can rewrite our goal as follow:

$$min\{\Gamma(\mathbf{W}, \boldsymbol{\mu}, \boldsymbol{\lambda}, \mathbf{z}) : \mathbf{W}, \mathbf{z}\} = \mathbf{min}\{\mathbf{min}\{\boldsymbol{\Gamma}(\mathbf{W}, \boldsymbol{\mu}, \boldsymbol{\lambda}, \mathbf{z}) : \mathbf{z}\} : \mathbf{W}\} \tag{2.22}$$

First, lets analyze $min\{\Gamma(\mathbf{W}, \boldsymbol{\mu}, \boldsymbol{\lambda}, \mathbf{z}) : \mathbf{z}$ to eliminate $\mathbf{z}$ from the problem. From equation 2.21 we have;

$$min\{\Gamma(\mathbf{W}, \boldsymbol{\mu}, \boldsymbol{\lambda}, \mathbf{z}) : \mathbf{z} = \mathbf{C} + \mathbf{min}\{\mathbf{G}(\mathbf{y}:\mathbf{W}, \boldsymbol{\mu}, \mathbf{z}) : \mathbf{z}\} + \mathbf{H} \tag{2.23}$$

For simplicity remove index inside the function, rewrite $G(\mathbf{y} : \mathbf{W}, \boldsymbol{\mu}, \mathbf{z})$ as follow:

$$\begin{aligned} G(\mathbf{y} : \mathbf{W}, \mu, \mathbf{z}) &= \sum_{i=1}^{u} \{u_i[g_i + z_i^2] + \tfrac{1}{2}\gamma[g_i + z_i^2]^2\} \\ &= \sum_{i=1}^{u} G_i(\mathbf{W}, \mu_i, z_i) \quad or \quad \sum_{i=1}^{u} G_i(z_i) \end{aligned} \tag{2.24}$$

The function $G_i(z_i)$ is a quadratic function of variable z_i^2, differentiating w.r.t. to z_i^2 the minimizer comes to be $\mu_i + \gamma g_i + \gamma z_i = 0 \;\; i.e., \;\; z_i^2 = -\frac{\mu_i}{\gamma} - g_i$. If $(-\frac{\mu_i}{\gamma} - g_i) < 0$ then clearly $z_i = 0$ minimizes G_i. So the optimal value of z_i^2 is given by

$$z_i^{*2} = \begin{cases} -\frac{\mu_i}{\gamma} - g_i & g_i \leq -\frac{\mu_i}{\gamma} \\ 0 & g_i \geq -\frac{\mu_i}{\gamma} \end{cases} \tag{2.25}$$

placing this optimal value into the equation 2.24 and after a little calculation the optimal value of $G_i(z_i^*)$ comes out to be:

$$G_i(z_i^*) = \begin{cases} -\frac{\mu_i^2}{2\gamma} & g_i \leq -\frac{\mu_i}{\gamma} \\ \frac{1}{2}\gamma g_i^2 + \mu_i g_i & g_i \geq -\frac{\mu_i}{\gamma} \end{cases} \tag{2.26}$$

$\frac{1}{2}\gamma g_i^2 + \mu_i g_i$ can be written like $\frac{1}{2\gamma}(\mu_i + \gamma g_i)^2 - \frac{\mu_i^2}{2\gamma}$, therefore the above equation can be written as

$$G_i(z_i^*) = \frac{1}{2\gamma}\{(max\{0, \mu_i + \gamma g_i\})^2 - \mu_i^2\} \tag{2.27}$$

Therefore

$$min\{G(\mathbf{y} : \mathbf{W}, \boldsymbol{\mu})\} = \frac{1}{2\gamma}\sum_{i=1}^{u}\{(max\{0, \mu_i + \gamma g_i(\mathbf{y} : \mathbf{W}\})^2 - \mu_i^2\} \tag{2.28}$$

Lets denote $min\{G(\mathbf{y} : \mathbf{W}, \mu)\} = \mathbf{K}(\mathbf{W}, \mu)$. After eliminating the slack vectors $\mathbf{z}$, equation 2.21can be written as:

$$\Gamma(\mathbf{W}, \boldsymbol{\mu}, \boldsymbol{\lambda}) = \mathcal{C}(\mathbf{W}) + \mathbf{K}(\mathbf{W}, \mu) + \mathbf{H}(\mathbf{y} : \mathbf{W}, \boldsymbol{\lambda}) \tag{2.29}$$

By partially differentiating the objective function Γ w.r.t.$\mathbf{w}$ i.e. $\nabla_W \Gamma = \nabla_W \mathcal{C} + \nabla_W K + \nabla_W H$

$$\begin{aligned} \nabla_W H &= \boldsymbol{\lambda}^t . \nabla_W h(\mathbf{y} : \mathbf{W}) + \gamma \mathbf{h}(\mathbf{y} : \mathbf{W}) . \nabla_{\mathbf{W}} \mathbf{h}(\mathbf{y} : \mathbf{W}) \\ &= (\boldsymbol{\lambda}^t + \gamma h(\mathbf{y} : \mathbf{W})) . \nabla_{\mathbf{W}} \mathbf{h}(\mathbf{y} : \mathbf{W}) \end{aligned}$$

$$\nabla_W K = \sum_{i=1}^{u} \{\nabla_{g_i} G_i(z_i^*).\nabla_W g_i\} \quad where \qquad \nabla_{g_i} G_i = \begin{cases} 0 & g_i \leq -\frac{\mu_i}{\gamma} \\ \gamma_{g_i} + \mu_i & g_i > -\frac{\mu_i}{\gamma} \end{cases}$$

$$\nabla_{g_i} G_i = max(0, \lambda_{g_i} + \mu_i)$$

$$= max\{\mathbf{0}, \gamma_{\mathbf{g}} + \boldsymbol{\mu}^{\mathbf{t}}\}.\nabla_{\mathbf{W}}\mathbf{g}$$

$$= (\boldsymbol{\mu}^t + max\{-\boldsymbol{\mu}^t, \gamma_g\}).\nabla_W g$$

Learning of the weights is achieved through a Newton-like learning process and Lagrange parameters through the gradient-ascent method.

$$\begin{aligned} \mathbf{W_{k+1}} &= \mathbf{W_k} - \eta(\mathbf{\Gamma}'')^{-\mathbf{1}}\mathbf{\Gamma}' \\ \mu_{\mathbf{k+1}} &= \mathbf{max}\{-\boldsymbol{\mu}_{\mathbf{k}}, \gamma\mathbf{g}(\mathbf{y} : \mathbf{W})\} \\ \boldsymbol{\lambda}_{k+1} &= \boldsymbol{\lambda}_k + \gamma\mathbf{h}(\mathbf{y} : \mathbf{W}) \end{aligned} \tag{2.30}$$

where η is the learning weight. More details of the optimization procedure can be found in [10],[11][9].

2.4.1 Less Complete ICA

The problem of finding the less number of components, which is a subspace of the original ICs, than those originally mixed in the signal is addressed by less-complete ICA. In 1996, Cao and Liu proved [12] that the criterion of statistical independence is insufficient for extracting a subset of original sources. One-unit ICA algorithms based on deflation process can extract ICs one by one [13][14], the process can be treated as a sequential solution to extract a subspace of ICs. Cichocki et al. claimed that the enhanced nonlinear PCA with a whitening process was able to extract less number of ICs than the sources [15]. However, the necessary preprocessing (whitening) stage results in failure of separation due to data distortion when ill-conditioned mixing matrices or weak sources are involved.

Neqentropy has been used as a measure to separate ICs from their mextures [6][14] because underlying sources are normally considered non-Gaussian. For the Gaussian signals the value of negentropy is zero, negentropy is always nonnegative for non guassian signals [16]. One can

project the data onto a low dimensional space by maximizing the marginal negentropies and thus can finds the structure of non-Gaussianity in the projection [17]. The fastICA algorithm based on negentropy, proposed by Hyvrinen [6], can separate a subset of ICs in parallel manner, but the interference caused by an explicit de-correlation process after each iteration is too rigid to orient the learning process toward the correct convergence trend. Therefore, the uncorrelation among estimated ICs is introduced as constraints to prevent same IC being converged at all the outputs [6]. The contrast function for the less-complete ICA with constraints can be defined as:

$$\begin{aligned} &maximize \;\; \mathcal{J}(y) = -\sum_{i=1}^{l} J(y_i) \\ &subject \;\; to \;\; h_{ij}(y_i, y_j) = (E\{y_i y_j\})^2 = 0 \quad \forall i, j = 1, 2, \ldots, l; i \neq j \end{aligned} \tag{2.31}$$

where $J(y_i) \approx \rho[E\{G(y_i)\} - E\{G(v)\}]^2$ is the contrast function [8][18], ρ is a positive constant, $G(.)$ is a nonquadratic function and v is a Gaussian variable having zero mean and unit variance. The constraints in Equation 2.31 can be included into the contrast function using lagrange methods and it can be optimized according to procedure mentioned in section 2.4.

2.4.2 ICA with Reference

The one-unit ICA algorithms extracts one source at a time, the extraction of the sources depends on the contrast function used. If negentropy is used as a contrast function, the one unit algorithm will extract a source with maximum entropy. When one desires a source other than the maximum entropy then one unit ICA (section 2.2) is of little use.

In blind source extraction applications, most of the time only one particular component or a set of components are desired. Previously, additional conditions, sparse decomposition of signals [19] and fourth order cumulants [20], have been incorporated into the contrast function by using to find the desired components. However, if the desired number of sources or their density types are unknown then the components obtained is not useful. If some information about the desired sources is available then that it can be incorporated into the ICA contrast function [9] as *a priori* information. *a priori* information referred to as reference signal carries some

information about the desired source. It does not need to be a prefect match, but it should be close enough to point the algorithm into the direction of a particular IC. Let the reference be $\mathbf{r}(t) = (r_1(t), r_2(t), ..., r_k(t))^T$. The closeness constraint for single IC can be written as

$$g_i(\mathbf{w}_i) = \varepsilon(\mathbf{w}_i^T\mathbf{x},\ r_i) - \xi \leq 0 \tag{2.32}$$

where ε is some closeness measure between the estimated output $\mathbf{w}_i^T\mathbf{x}$ and the reference signal r_i. The number of column of $\mathbf{W} = [\mathbf{w}_1, \mathbf{w}_2, \ldots, \mathbf{w}_n]$ in the case of ICA-R will be equal to the number of reference signals i.e., *n=k*. Both the output and reference signal must have zero-mean and unit variance. The closeness threshold parameter is denoted by ξ. The optimization equations will become:

$$\begin{aligned} &maximize && \mathcal{J}(y) = -\sum_{i=1}^{l} J(y_i) \\ &subject\ to: && g(\mathbf{y} : \mathbf{W}) \leq \mathbf{0}, \quad \mathbf{h}(\mathbf{y} : \mathbf{W}) = \mathbf{0} \end{aligned} \tag{2.33}$$

where l is the number of sources to be extracted. $\mathbf{g}(\mathbf{W})$ are the inequality constraints and $\mathbf{h}(\mathbf{W})$ are the equality constraints. The constrains are included into the contrast function according to the procedure mentioned in section 2.4 by using the augmented lagrange method. The equation 2.33 will become:

$$\Gamma = \sum_{i=1}^{l}(j(y_i) - \frac{max^2\{\mu_i + \gamma_i g_i(w_i), 0\} - \mu_i^2}{2\gamma_i}) - \boldsymbol{\lambda}^{\boldsymbol{t}}\mathbf{h}(\mathbf{W}) - \frac{1}{2}\gamma^t||\mathbf{h}(\mathbf{W})||^2 \tag{2.34}$$

Equation 2.34 is the final contrast function that needs to optimized. Newton-like learning process can be used to learn the weights and Lagrange parameters through the gradient-ascent method.

$$\mathbf{W_{k+1}} = \mathbf{W_k} - \eta < \bar{\mathbf{s}}(\mathbf{W}) > \mathbf{\Gamma}'_{\mathbf{W}}\mathbf{R_{XX}}^{-\mathbf{1}} \tag{2.35}$$

where η is the learning weight, $\bar{\mathbf{s}}(\mathbf{W})$ is a vector equals to $(\frac{1}{s_1(\mathbf{w}_1),\ldots,s_l(\mathbf{w}_l)})^t$ in which $s_i(\mathbf{w}_i) = \bar{\rho}_i E\{G''_{y_i^2}(y_i)\} - \frac{1}{2}\mu_i E\{g''_{y_i^2}(\mathbf{w}_i)\} - \lambda_i$ for $\forall i = 1, \ldots, l$ obtained from the Hessian matrix $\Gamma''_{\mathbf{W^2}}$, $< . >$ represents a diagonal matrix whose off-diagonal elements are all zeros and the diagonal is given by the vector inside and the gradient $\Gamma''_{\mathbf{W^2}}$ is given as:

$$\Gamma'_{\mathbf{W}} = < \bar{\boldsymbol{\rho}} > E\{G'_{\mathbf{y}}(\mathbf{y})\mathbf{x}^{\mathbf{t}}\} - \frac{1}{2} < \boldsymbol{\mu} > E\{g'_{\mathbf{y}}(\mathbf{W})\mathbf{x}^t\} - < \boldsymbol{\lambda} > E\{\mathbf{y}\mathbf{x}^t\} \tag{2.36}$$

where $G'_{\mathbf{y}}$ and $g'_{\mathbf{y}}$ are the first derivatives of $G(\mathbf{y})$ and $(\mathbf{g}(\mathbf{W})$ with respect to the corresponding y_i in $\mathbf{y}$.The learning of Lagrange multipliers μ and λ can be found using gradient ascent method

$$\begin{aligned} \boldsymbol{\mu}_{k+1} &= max\{\mathbf{0}, -\boldsymbol{\mu}_k + < \gamma > \mathbf{g}(\mathbf{y} : \mathbf{W})\} \\ \boldsymbol{\lambda}_{k+1} &= \boldsymbol{\lambda}_k + < \gamma > \mathbf{h}(\mathbf{y} : \mathbf{W}) \end{aligned} \tag{2.37}$$

More details of the optimization procedure can be found in [10],[11][9].

The measure of closeness can take any form, such as mean squared-error (MSE), correlation or any other suitable closeness (or similarity) measures. In our implementation of the algorithm, we have used MSE as a measure of closeness and to adjust the value of the thresholding parameter we used the same procedure mentioned in [9].

Chapter 3

BSS for Brain Imaging Applications

Related to every action there is an electrical activity between the neurons of the brain. With the advancement of science it is now possible to measure these neuron signals. The techniques used to measure these activities can be invasive or non-invasive. Non-invasive brain imaging techniques are well suited for human brain recordings. The non-invasive brain imaging techniques could be electroencephalogram (EEG), magnetoencephalogram (MEG) and magnetic resonance imaging (MRI). The EEG, MEG or MRI data is multichannel data and can be quite well described by ICA model. ICA and constrained ICA has proved to be very effective tools to extract the essential features from the data to allow an easier representation or interpretation of their properties.

3.1 Electroencephalogram, Magnetoencephalogram and Functional Magnetic Resonance Imaging

The human brain is very complex and is the center of the nervous systems. All human activities are controlled by the brain. From structural point of view, it has white matter which is covered by the gray matter, then comes the skull and skin. Approximately 10^{10} to 10^{11} neurons are there in the white matter; which is the basic information-processing units. There is communication between the neurons for every activity. The communication is done by transmitting very short bursts of electrical signals generated by action potentials. The receiving neurons transform these potentials to postsynaptic potential that are longer in duration. Single action potentials

and postsynaptic potentials are very weak and cannot be detected as such by present noninvasive measurement devices. Fortunately at any given time, the relatively longer and strong postsynaptic potentials tend to be clustered in the brain. Such a cluster produce enough total electric current that it can be detected by noninvasive methods. The potential distribution on the scalp can be measured by placing electrodes on it, which is the method used in EEG. On the other hand, MEG measure the magnetic fields associated with the current.

The electric current of the brain can be modeled in different ways however the current dipole model is the most often used. It assumed that at any given point of time the electric activity of the brain can be modeled by small number of dipoles. The electric and magnetic potentials produced by these dipoles is strong enough that it can be measured on the surface of head. EEG is used extensively for monitoring the electrical activity within the human brain. It is the most widespread technique used to study the brain functions. EEG can be used for the measurement of continuous activity as well as for evoked potentials. Brain's spontaneous electrical activity over a short period of time, recorded with multiple electrodes placed on the scalp, is termed as continuous EEG. Evoked potentials involves averaging the EEG activity time-locked to the presentation of a stimulus of some sort like visual, somatosensory, or auditory. Typical temporal resolution of EEG is in the range of millisecond. Normally the number of electrodes used for EEG recording are in range of 20 to couple of hundred. The continuous EEG signals have very low signal to noise ratio. Evoked potentials are even many fold smaller than continuous EEG.

Different brain areas between the measuring devise and the assumed dipole have different conductivities. These different conductivities cause seaming effect in EEG. However, this effect is not present in the case of magnetic field resulting in much higher spatial resolution of MEG compared to EEG. The information content of MEG is essentially the same as that of EEG but with higher spatial resolution. MEG is mainly used for basic cognitive brain research. To measure the weak magnetic fields of the brain, superconducting quantum interference devices (SQUIDs) are needed. The measurements are carried out inside a magnetically shielded room. The superconducting characteristics of the device are guaranteed through its immersion in liquid

helium, at a temperature of -269^oC [8].

Functional magnetic resonance imaging (fMRI) is an MRI scan that measures the change in blood flow and blood oxygenation (collectively known as hemodynamic response) related to neural activity in the brain. The firing of the neurons requires energy, blood releases oxygen (energy) to them at a greater rate than to inactive neurons through hemodynamic response. Hemoglobin is diamagnetic when oxygenated but paramagnetic when deoxygenated [21]. The magnetic resonance (MR) signal of blood, BOLD (Blood oxygen level dependent) signal, is therefore slightly different depending on the level of oxygenation. Inside the MRI: with magnetic susceptibility sensitive parameters, changes in the BOLD contrast can be measured. The changes are very small however based on statistical techniques active brain areas for a particular task can be distinguished. Almost all current fMRI research uses BOLD as a method of determining the active brain regions for a particular task.

EEG has temporal resolution in the range of milliseconds and fMRI has spatial resolution in the range of millimeters. By combining these two brain imaging modalities the functionality of the brain can be studied as higher spatiotemporal resolution. However, simultaneous recording is hindered by the fact that the EEG artifacts like imaging artifacts, ballistocardiogram and electro-occulogram get amplified inside MRI scanner. For EEG studies inside MRI scanner careful consideration of these artifacts is very important.

3.2 Basic ICA Model Validity

ICA or constrained ICA statistically extract independent sources from EEG or MEG without regard to physical location or configuration of the source generators. EEG or MEG is assumed to be the output of a number of statistically independent but spatially fixed potential generating dipoles, these dipoles can either by spatially restricted or widely distributed [22].

The ICA or constrained ICA techniques appear ideally suited for performing source separation in domains where, i) statistically independent source signals are present, ii) linear mixing at

the sensors is instantaneous, iii) mixing and the independent components (ICs) are stationarity, iv) number of independent sources signal is the same as the number of sensors. The independence criterion is a statistical relation between the amplitude of the recorded signals. It mainly depends on the experimental conditions and not on the morphology or physiology of neurons. One can safely assume that EEG or MEG recordings is a linear mixture of statistically independent brain processes. The time instance of EEG and MEG signals can be considered separately [23]; the quasi static approximation of Maxwell equations holds as their energy lies below 1 kHz. The propagation of the EEG and MEG signals is immediate (without any time-delays) and the instantaneous mixing is valid. In 1995, Blanco [24] discussed the nonstationarity of EEG and MEG signals. The data are considered as random variables in batch ICA algorithms, and their distributions are estimated from the whole data set. Therefore, the nonstationarity of the signals is not really a violation of the assumptions of the model. However, The assumption of stationarity of the mixing matrix A agrees with widely accepted neuronal source models [25][26]. Details about the validity of ICA model for EEG and MEG signals can be found in [8]

It is believed that for every task only certain areas of brain are active and there is a connection / communication between them to achieve the task i.e. functional principal of brain is localization and connectionism. Consistent with this principles, [27] for the first time for fMRI data suggested that the multifocal brain areas activated by performance of a psychomotor task should be unrelated from the brain areas whose signals are affected by artifacts. Mackeown and his colleagues made the following assumptions for fMRI data analysis by ICA, i) Each separate processes may be represented by one or more spatially-independent components, each associated with a single time course of enhancement and/or suppression and a component map, ii) the component maps is assumed to be a fixed spatial distribution of possibly overlapping, multifocal brain areas of statistically dependent fMRI signal influence, iii) the component map distributions are spatially independent and hence uniquely specified, iv) The maps will be independent if active voxels in the maps are sparse and mostly non-overlapping, v) the observed fMRI signals are the linear sum of the contributions of the individual component processes at each voxel. Based on these assump-

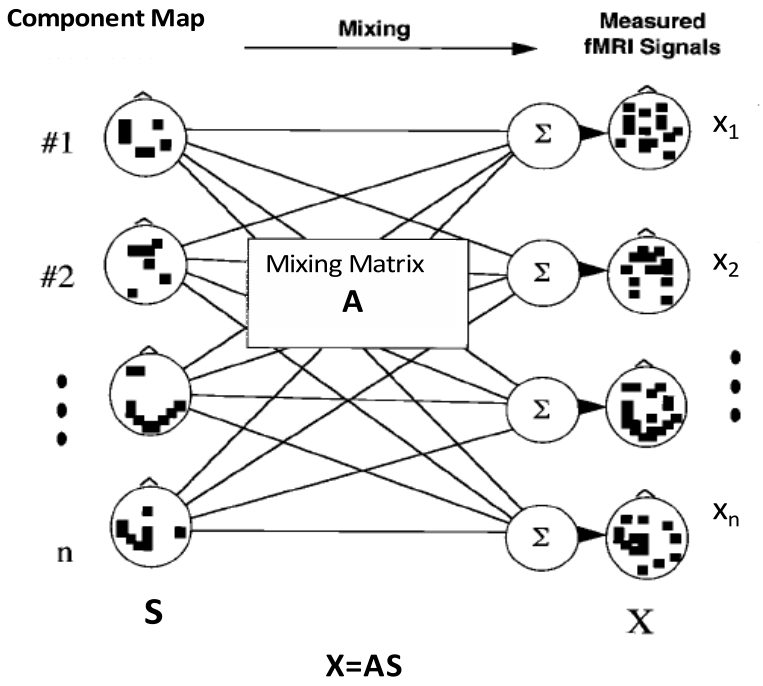

Figure 3.1: ICA can separate the fMRI into independent component maps and activation waveforms

tions, An ICA algorithm can decompose the fMRI signals, recorded during the performance of tasks, into a number of independent component maps and their associated component activations [28]. The process is illustrated in the Fig. 3.1.

3.3 Summary

In this chapter basic knowledge about brain imaging techniques has been presented. This chapter also provides information on how the the EEG and MEG data fulfils the requirement of basic ICA model. Finally, some examples of ICA and constrained ICA application of EEG and MEG and their reference are provided for further insight.

Chapter 4

Artifact Rejection in EEG signals

Integration of electroencephalography (EEG) and functional magnetic imaging (fMRI) resonance will allow analysis of the brain activities at superior temporal and spatial resolution. However simultaneous acquisition of EEG and fMRI are hindered by the enhancement of artifacts in EEG. The most prominent of which are Ballistocardiogram (BCG) and Electro-oculogram (EOG) artifacts. The situation even gets worse if evoked potentials are measured inside MRI for their minute responses in comparison to the spontaneous brain responses. In this chapter, a new method of attenuating these artifacts from the spontaneous and evoked EEG data acquired inside a MRI scanner using constrained independent component analysis with *a priori* information about the artifacts as constraints will be discussed. With the proposed techniques of reference function generation for the BCG and EOG artifacts as constraints, the new approach presented in this chapter performs significantly better than the averaged artifact subtraction (AAS) method. The proposed method could be an alternative to the conventional ICA method for artifact attenuation with some advantages. As a performance measure we have achieved much improved normalized power spectrum ratios (INPS) for continuous EEG and correlation coefficient (cc) values with outside MRI visual evoked potentials for visual evoked EEG as compared to those obtained with the AAS method. The results show that the new approach is more effective than the conventional methods, almost fully automatic, and no extra ECG signal measurements are involved.

4.1 Introduction

Simultaneous acquisition of electroencephalography (EEG) and functional magnetic resonance imaging (fMRI) holds promise toward mapping brain activities at superior spatiotemporal resolution. EEG provides temporal resolution in the order of mili-second and fMRI provides spatial resolution in mili-meter scale: researchers believe that combining these two imaging modalities is a critical requirement to decipher the functions of the brain [29, 30, 31, 32, 33].

However, one of the limitations in the simultaneous acquisition of EEG and fMRI is that EEG signals measured inside the MR scanner get significantly corrupted by artifacts: most significant of which are gradient, ballistocardiogram (BCG) and electro-oculogram (EOG) artifacts. It is known that the gradient artifact is due to changing fMRI magnetic fields, BCG artifact due to the tiny movement of EEG electrodes inside the MRI scanner because of the pulsatile changes in blood flow tied to cardiac cycle and EOG artifact by the movement of eyes of the subject. It has been reported that the magnitude of these artifacts is much higher compared with the alpha rhythm of EEG [34, 35, 36, 37].

Most approaches used to date for the BCG and EOG artifacts rejection can be grouped into three main classes: (i) averaged artifact subtraction (AAS) methods, (ii) adaptive filtering techniques (AFT) and (iii) independent component analysis based procedures (ICAP). The AAS method was first proposed in [34] and lately the concept of adaptive weighting to the original procedure to reduce the time variability in the BCG templates was introduced by [31]. In this method, an artifact template for each channel was obtained by averaging the artifacts per each heart beat and then was subtracted from the corresponding EEG signals. The standard AAS method is the most common technique used in available commercial softwares for artifact attenuation. Attempts have been made using this procedure not only for spontaneous EEG but also to recover the visual evoked potentials measured during fMRI [38, 39]. One critical requirement for AAS is the simultaneous acquisition of ECG to identify each heart beat. However, as the ECG is a non-stationary signal and gets affected by the magnetic field as well, this method is associated with less representative templates. The AAS method is also a popular method for attenuating the

gradient artifact [35] in addition to the above mentioned BCG artifact.

A concept of adaptive (median) filtering was proposed by [36] to generate more accurate templates for the artifacts. Attempts for real time artifact attenuation have also been made. In one such attempt, motion sensors were used to measure the head movements and the adaptive filters were utilized to remove the artifacts [37]. Improved BCG artifact attenuation technique using an efficient heart beat detector was proposed by [40]. Later Kalman filtering of EEG signals for the BCG artifact attenuation has been done by our group [41]. Usually these adaptive filtering techniques assume known variances and therefore require reference channels for generating the artifacts.

An interesting alternative to the above mentioned techniques for neurophysiological signal analysis applications are procedures based on ICA [42, 43, 44, 45]. ICA is a well established technique for blind source separation. It extracts statistically independent components when linear memory-less mixing is the fundamental assumption [4, 7, 6, 46, 18, 8]. In the field of biomedical signal analysis, researchers have used ICA for different artifact attenuation from spontaneous EEG data such as line artifact, EOG artifact and BCG artifact [47, 43, 44]. Some researchers have used ICA for artifact attenuation from evoked potentials measured inside MRI [48, 45]. In 2006, a comprehensive study [49] has been conducted on different conventional ICA algorithms to evaluate their performance for the BCG artifact attenuation from EEG signals measured inside MRI. However standard implementations of ICA have some disadvantages associated with them: (i) the number of ICs are equal to the number of observations, making the subsequent manual IC selection very cumbersome and subjective, (ii) neither the energies nor the signs of ICs can be predefined, (iii) ordering of ICs is random and (iv) possibility of breaking up of the artifacts into multiple ICs, making the selection task even difficult. However, in comparison to the AAS methods, ICAPs has shown to produce improved results and also do not require separate ECG measurement.

In general, for neurophysiological signal analysis we are not interested in the complete set of ICs but only few ICs are of interest: artifact ICs. We can extract these ICs by incorporating some

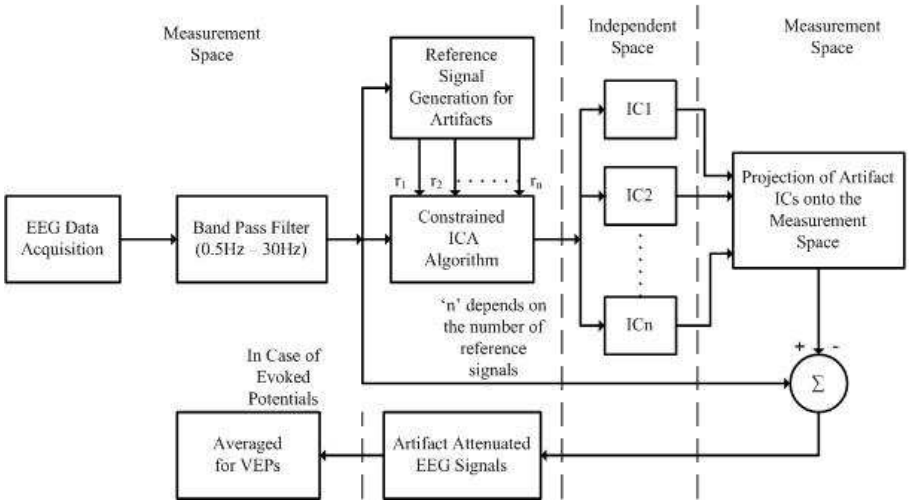

Figure 4.1: Schematic diagram of our proposed artifact attenuation procedure using constrained ICA

a priori information about the artifacts into the ICA algorithm. Constrained ICA [9] uses the augumented Lagrangian method to incorporate *a priori* information about the signal to be sought as constrains in the ICA contrast function. With constrained ICA one can extract only a subset of ICs thus overcoming the disadvantages of the conventional ICA. Application of temporally constrained ICA to attenuate the EOG and line artifacts from EEG (not measured inside MRI) and BCG artifact from MEG data respectively have been explored by [50]. The non-stationary effect of BCG artifact in EEG measured inside MRI is not present in the case of MEG recordings. To the best of our knowledge, attenuation of the BCG and EOG artifacts from EEG (spontaneous as well as evoked) measured inside MRI with constrained ICA has not been attempted before. In the frame work of blind un-mixing, if the BCG and EOG artifacts are assumed to be linearly mixed into the EEG measurements and some *a priori* knowledge is available or can be extracted form EEG data then *constrained ICA with reference* should extract them as ICs. In the work presented in this chapter, we present an artifact attenuation method based on constrained ICA for spontaneous as well as visual evoked potential EEG signals measured inside MRI. The advantages of

this method are: (i) single artifact template is not required thus overcoming some requirements associated with the AAS methods, (ii) it does not require any ECG measurements or any extra information, (iii) we can overcome the problems of the conventional ICA as mentioned above), (iv) with our proposed methods, various references for the constrained ICA can be generated from the EEG data, (v) several artifacts can be attenuated at the same time and (vi) with this method not only artifacts but also any desired information can be extracted from the data if *a priori* information is available or if some traces of desired information, which can be used as *a priori* information, can possibly be extracted from the data. With the procedure presented in this chapter, BCG and EOG artifacts are successfully attenuated, simultaneously and automatically, from the EEG signals measured inside MRI. In this chapter, we illustrate the effectiveness of our technique for artifact attenuation with comparative results. For spontaneous EEG signals, we evaluated our technique by examining the EEG signals and power spectrums before and after artifact attenuation. We have compared the performance against the standard AAS method. The higher normalized power spectrum ratios (INPS) for the constrained ICA method indicate better performance compared to the standard AAS method. Similarly, the higher correlation coefficient values (cc) calculated between the VEPs obtained from the outside EEG signals and to those obtained with the constrained ICA and the standard AAS method indicates better performance of the constrained ICA method. The significance of our approach is that we have proposed the use of constrained ICA for the first time for BCG and EOG artifacts attenuation from EEG (spontaneous as well as evoked) measured inside MRI. We have also proposed three techniques for the reference function generation from the EEG data. Our results clearly demonstrate that the proposed approach is more effective, convenient, fully automatic (except for careful generation of reference functions in the first two proposed techniques) and outperforms the conventional techniques. Some partial results have been reported in the conference proceedings [1, 51].

4.2 Methodology

Details about the independent component analysis (ICA) and constrained ICA (cICA) can be found in sections 2.2 and 2.4 respectively. We need to attenuate multiple artifacts so constrained ICA with multi-reference is used.

4.2.1 Design of Reference Functions for Artifacts

The BCG artifact is known to be non-stationary and vary channel-to-channel in its timing and waveforms, making difficult to generate a single reference template. The reference signal generation depends on the application area and the type of the signal one wants to extract. In the field of electromagnetic brain signal analysis, a trace of desired signal (i.e., artifact) is available at some instance. For example, in the case of artifact rejection, the morphologies and relative timings of contaminating eye blinks or movements can easily be derived in an automated fashion from the observed EEG data. Here we propose three different techniques to generate the reference signals as described below. While designing a reference signal for the EOG artifact from EOG channel, note the fact that this channel is also affected by BCG.

1. CH-Reference (CH-R)

   A filtered EEG channel that is most representing the BCG artifact is taken as the reference for BCG and the EOG channel is taken as the second reference. The BCG artifact is prominent in all electrodes and there shape is better represented in the EEG channels compared to the ECG channel. Therefore, the channel that is most representing the BCG artifact can be used directly as a reference for the BCG artifact under the assumption that the variation of the BCG artifact in the rest of channels is small or insignificant.

   $$r_i(t) = f(q_j(t)) \qquad i = 1, 2, \ldots, k \quad j = 1, 2, \ldots, l \tag{4.1}$$

   where i is the number of reference signals used, (two in our implementation i.e., k=2), q the recorded signal, j the channel number, l the total number of channels recorded and f

denotes a transformation such as filtering. Each reference function $r_i(t)$ depends on the selected channel.

2. Template Train-Reference (TT-R)

   As mentioned above it is difficult to make a single template for the BCG artifact. However, if a train of templates at approximate timings is taken as a reference then the variation in the shape of the template with respect to time can approximately be accommodated. *In this technique a filtered EEG channel that is most representing the BCG artifact is converted into a train of templates and used as a reference for BCG.* Reference signal only needs to have some traces of the desired signal, in this case the approximate timing and the representative shape information is retained (as shown in Fig. 4.3).

$$\left.\begin{array}{l} r_i(t+v) = f(q_j(t+v)) \\ v = [-a, -a+1, ..., b] \\ \quad t \leftarrow t+b \end{array}\right\} if \;\; f(q_j(t)) \geq \pm\Upsilon \tag{4.2}$$

$$\begin{array}{ll} r_i(t) = 0 & Otherwise \\ i = 1, 2, \ldots, k & j = 1, 2, \ldots, l \end{array}$$

   where Υ is the selected threshold value, a and b are the number of samples selected before and after the time t at which the threshold is crossed. The variable v is a set that indicates the total number of samples assigned at each threshold crossing. After the assigning the samples to the reference signal time t is updated to $t + b$. The typical values of a and b in our implementation are in the range of 10 to 15 and 350 to 360 respectively.

3. PC-Reference (PC-R)

   PCA which is based on second order statistics finds orthogonal components. It is believed that EEG and artifacts are not orthogonal [42]. The use of PCA cannot completely separate eye-movement artifacts from the EEG signals, especially when they have comparable amplitudes and even it can distort the signal if the artifacts overlap with the signal [52].

The BCG artifact, which vary in amplitude and form with the heart rate and blood pressure [29] and also overlap with the true EEG signals, are very difficult to remove with PCA. In [53], the performance of PCA and ICA for the BCG artifact removal in EEG spike data measured inside MRI is presented and it is suggested that ICA performs significantly better than PCA. The general observation about the artifacts is that they have much higher amplitude as compared to the EEG signals, although the amplitude of the signals in different channels vary significantly i.e., ranging between 600μV to 15μV. The energy spectrum of the BCG artifact is localized in time because it reflects cardiac activity and cycle. Inside the MRI, average energy of the artifacts is greater than that of true EEG signals. With PCA (which decomposes the signals on the basis of variance) for this highly amplitude varying data, we cannot collect all the artifacts variance in the first two components. However if we project the EEG data onto the two major principal components (those corresponding to the highest eigenvalues) the projected data should represent the general features of the BCG and EOG artifacts. Therefore in this technique *data projected on the two major PC's are used as reference signals for the BCG and EOG artifacts.*

$$\begin{aligned} \mathbf{pc}(t) = \mathbf{E}^T\mathbf{x}(t) \quad with \quad \mathbf{pc}(t) &= [pc_1(t), pc_2(t), \ldots, pc_n(t)]^T \\ r_i(t) = pc_i(t) \qquad\qquad & i = 1, 2, \ldots, k \end{aligned} \tag{4.3}$$

where **E** is a matrix of eigenvectors of the covariance matrix of $\mathbf{X}^T$, with one signal per row. **pc** is a vector of projections on the eigenvectors and i is the number of principal components selected.

The reference signals from any one of the above techniques and mean square error (MSE) as a closeness measure, the inequality constraints **g(W)** in equation (4) become:

$$\begin{aligned} g_1(\mathbf{w}) &= E\{(\mathbf{w}^T\mathbf{x} - r_1)^2\} - \xi \leq 0 \\ g_2(\mathbf{w}) &= E\{(\mathbf{w}^T\mathbf{x} - r_2)^2\} - \xi \leq 0 \\ \mathbf{g}(\mathbf{W}) &= (g_1(\mathbf{w}), g_2(\mathbf{w}))^T \leq \mathbf{0} \end{aligned} \tag{4.4}$$

where ξ is a threshold parameter. The first two techniques of reference generation require some user intervention in terms of selecting and designing the reference signals, making the proposed techniques semi-automatic. However, with PC-R the reference is generated automatically with no arbitrariness.

4.2.2 Artifact Attenuation with the Proposed Method

The total number of channels used for data recording were 32, out of which the 29 channels were used for EEG, one channel was allocated for EOG and two for ECG signals. We recorded the ECG channels but those were not used at any stage of artifact attenuation. The focus of this chapter was the attenuation of BCG and EOG artifacts therefore the recorded EEG data was free of gradient artifact. The EEG data recorded was filtered (0.5Hz - 30Hz) with the Butterworth filter of order 4 and zero phase distortion to remove the noise such as line artifacts. The 29 channel filtered EEG data denoted by $\mathbf{x}(t)$ was centered and whitened. The reference signals for the artifacts were generated using one of the techniques presented in section 4.2.1. The reference signals were also centered and whitened. The data along with the reference signals were then given to the constrained ICA algorithm. The ICs (i.e., $\boldsymbol{S}$) recovered by the constrained ICA correspond to the artifacts. The ICs were projected back in to the measurement space to determine the mixing matrix, $\boldsymbol{A} = \boldsymbol{X}\boldsymbol{S}^{\dagger}$. Where $\dagger$ represents the pseudoinverse. The artifacts attenuated EEG signals $\mathbf{X_c}$ were obtained by

$$\mathbf{X_c} = \mathbf{X} - \mathbf{AS}. \tag{4.5}$$

In the case of evoked potentials averaging according to event timings was done to recover VEPs. The schematic diagram that depicts the whole process is shown in Fig. 4.1.

4.2.3 Performance Criteria

In order to assess the performance of artifact attenuation of our proposed techniques, we have used the following performance criteria for the continuous and evoked EEG.

1. Spontaneous EEG signals

   The performance of the proposed constrained ICA method for BCG artifact attenuation is evaluated by comparing the normalized power spectrum ratios (INPS) with those obtained from the standard AAS procedure (i.e., the Allen's method). INPS is a commonly used measure for evaluating the performance of BCG artifact attenuation in EEG data [54]. The higher values of INPS indicate better performance. The INPS is expressed as

   $$INPS = \frac{\sum_{l=1}^{N} P_l^{before-cICA}}{\sum_{l=1}^{N} P_l^{after-cICA}} \tag{4.6}$$

   where N is the number of harmonics of the artifact and P_i is the spectral power at the l^{th} BCG component. In our calculations we have used N = 10, that is the fundamental ECG frequency (approximately 1.1 Hz) and four harmonics are included. The 2048 point FFT at the sampling frequency of 1KHz is performed for spectral calculations. Furthermore, the performance is evaluated visually by inspecting the reduction in power at the artifact related frequencies after artifacts attenuation.

2. Evoked potentials

   In the case of visual evoked potentials, VEPs are recovered using the standard AAS procedure and our proposed constrained ICA method. For visual inspection both are plotted against the VEPs from the outside MRI EEG data, which is considered as a gold standard. For analytical comparison the Pearson correlation coefficients (cc) are calculated between the VEPs obtained from outside MRI EEG data and VEPs obtained with the standard AAS method and those obtained by the constrained ICA method.

4.2.4 Experimental Setup

Spontaneous EEG data and visual evoked potentials upon checker board reversals (1 or 2Hz) were acquired from six volunteers (mean age of 26.6) with no history of neurological and psychiatric disorders, recruited from an academic environment. We used a MRI-compatible 32-channel EEG recording system (Brain Amp MR, Brain products GmbH, Germany) for EEG data acquisition

inside a 3.0 T magnet of the whole body MRI scanner (Magnum 3.0, Medinus, Korea), thus from the MRI related artifacts only the BCG artifact is induced in the EEG signals. The EEG electrodes (Ag-AgC1) and lead wires were made of non-magnetic material to reduce the magnetic field effect on the electrodes. The distance between the EEG cap and the EEG amplifier was approximately 1m, and the EEG amplifier was placed at the rear end-side of the magnet. The EEG signals were amplified and then transformed into optical signals in the EEG amplifier, to be transmitted to the EEG data acquisition system placed outside the MRI shield room. The EEG data acquisition system has 16 bit depth with the voltage resolution of 100nV and the dynamic range of 3.2mV. The typical sampling rate used in this chapter was 1 KHz and the bandwidth of the band pass filter was 1-60Hz. All the EEG recordings were performed with the standard 10-20 uni-polar system referenced to the FCz electrode. Electrode skin impedance was kept below 1K Ohm. To minimize motion artifact in EEG on the scalp electrode of the subject, we tightly fixed the EEG cap on the scalp using adhesive tapes. Furthermore, to minimize the motion artifacts of the EEG lead wires between the EEG cap and the EEG amplifier, we fixed the lead wires to a supportive structure using plastic ties. The study presented in chapter was approved by the institutional ethics review committee of Kyung Hee University, Korea, and written informed consent was obtained from each subject.

4.3 Results

4.3.1 Spontaneous EEG

An example of a 5-s epoch of the multi-channel scalp EEG recorded inside MRI is shown in Fig. 4.2(a). The BCG and EOG artifacts shown by a rectangular box can be seen throughout the normal EEG. The reference signals for constrained ICA is generated using one of the techniques mentioned in the section 4.2.1. For the CH-R, one of the EEG channel is used as reference signal for BCG artifact and EOG channel is used as reference for BCG and EOG artifacts. Although the plot is not given in Fig. 4.2 due the space constraints, the results are given in table 4.1. For

the TT-R technique, a reference for BCG is obtained from the channel O1 and for both the BCG and EOG artifacts it is derived from the EOG channel according to the equation 4.2. Illustration of the method is shown in Fig. 4.3. The two recovered ICs overlayed with the corresponding reference signals are shown in Fig. 4.4. In the PC-R technique, the two principal components with the highest eigenvalues are selected and the data projected on these components are used as two references. The two recovered ICs, in our case, are then projected back into the measurement space and subtracted from the original EEG signals according to equation 4.5 to get artifact attenuated signals. Comparative results of artifact attenuation in one representative channel, when the reference functions are generated from different channels using the TT-R technique, are shown in Fig. 4.5. All the channels after artifact attenuation, reference function generated using TT-R and PC-R, are shown in Figs'. 4.2(b) and 4.2(c) respectively. Upon comparing Fig. 4.2(a) with Figs 4.2(b) and 4.2(c), it is clear that the artifacts related to BCG and EOG are attenuated. The artifacts are assumed to be linearly mixed with normal brain activities and have high amplitudes therefore the energy associated with frequencies (1-6Hz) related to the artifacts is much higher compared with those of normal brain activities. The power spectrum plots of channel O2, before and after artifact attenuation, is shown in Fig. 4.6. This figure clearly demonstrates that the power at frequencies related to the artifacts is significantly reduced after artifact attenuation. For comparison, we have implemented the standard AAS method and attenuated the artifacts. The quantitative and comparative results of the proposed procedure are summarized in table 4.1. The gain in the INPS values for the constrained ICA method clearly illustrate the effectiveness of our proposed method compared to the AAS method. A performance comparison in terms of INPS values between the constrained ICA method with the PC-R technique for reference generation and the PCA attenuation method (where only the first two PCs are subtracted from the data) is presented in table 4.2. The INPS values for the constrained ICA method lies in the range of 8.2 to 12.8. However, for the PCA method it lies in the range of 3.4 to 10.7. We observed that the INPS values with the PCA method for some channels are even less than that of the AAS method. We also observed distortion in the EEG signals if the artifacts are attenuated with the PCA method,

as observed by other researchers [52].

4.3.2 Visual Evoked EEG

In the case of evoked potentials, the VEPs were obtained from the artifact attenuated EEG signals averaged according to the event timings. For comparison, the VEPs from the EEG signals acquired outside MRI under the identical experimental settings are taken as the gold standard. The VEPs from some representative channels, before and after artifact attenuation against the outside VEPs are shown in Fig. 4.7. Results clearly depict that the VEPs obtained after artifact attenuation are much similar to those of outside MRI VEPs. The cc values are computed to measure the similarity of the VEPs after correcting a few msec time delay of the VEPs inside MRI, as performed by other groups [38, 39]. The cc values for the VEPs after artifact attenuation using constrained ICA lies in the range of 0.5 to 0.9. It is clear that the recovered VEPs is much similar to the outside VEPs. The occipital P1 and N1 peaks can be identified at similar latencies in both recording conditions. The P1-N1 complex was detected in all cases. To test our technique against the standard AAS method, we have implemented the AAS method and obtained the VEPs. The VEPs acquired with both the techniques are compared with the outside MRI VEPs and the plots with corresponding cc values are shown in Fig. 4.8. Visual inspection of the VEPs as well as the cc values indicate that the constrained ICA method performs better than the AAS method. The cc values for the constrained ICA and AAS method against the outside VEPs for six subjects are given in table 4.3. The values are higher for the constrained ICA, illustrating the effectiveness of the constrained ICA method for artifact attenuation for the evoked potentials compared to the standard AAS method.

4.4 Summary

The use of ICA for artifact rejection in an effective technique in the field of bio-medical signal analysis. However, because of the disadvantages mentioned in the introduction section there are

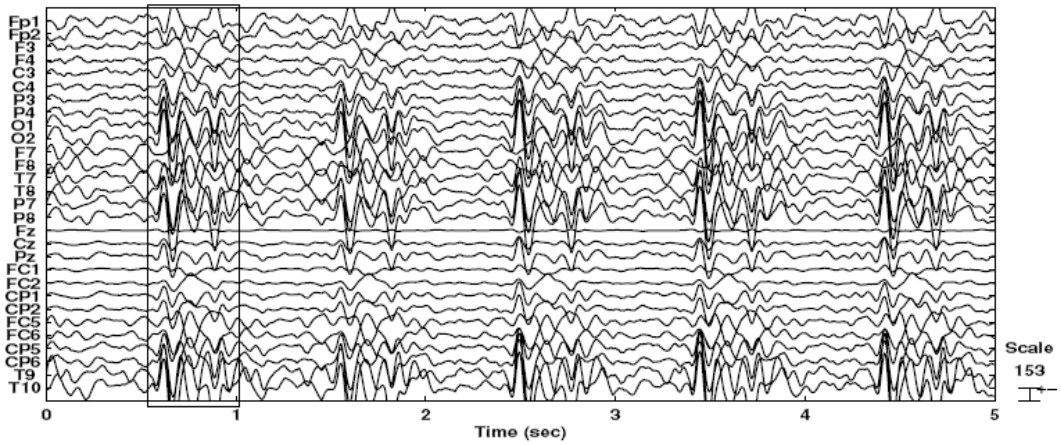

(a) EEG inside MRI

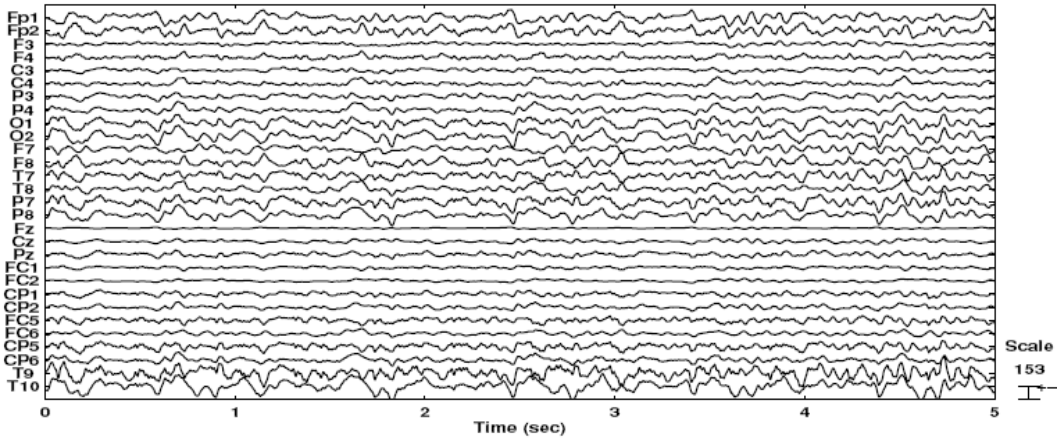

(b) EEG inside MRI - artifacts attenuated using TT-R

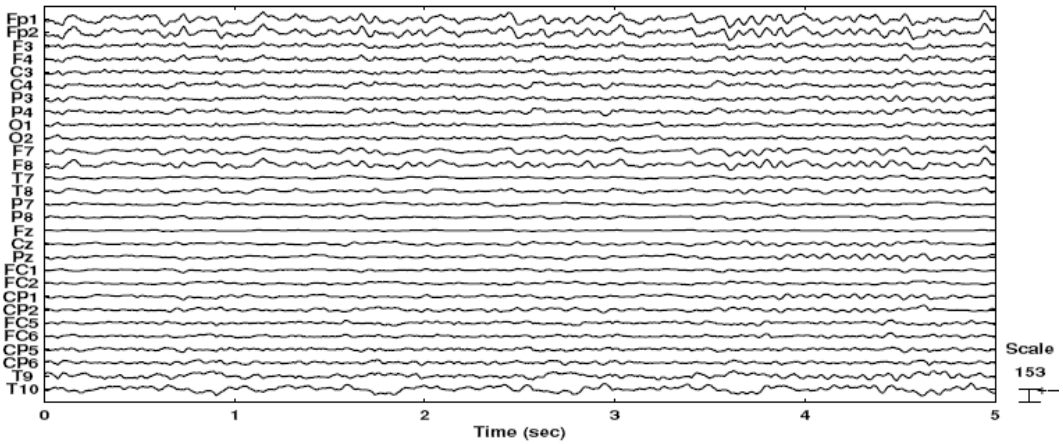

(c) EEG inside MRI - artifacts attenuated using PC-R

Figure 4.2: Attenuation of artifacts from spontaneous EEG recordings. (a) EEG recordings inside MRI: 29 channels, contaminated with the BCG and EOG artifacts as indicated by a rectangular box, (b) EEG recordings after artifact attenuation using the TT-R technique and (c) EEG recordings after artifact attenuation using the PC-R technique.

Table 4.1: INPS(dB) values for the constrained ICA with different ref. function generation techniques and the AAS method.

	Constrained ICA method												AAS method			
	CH-R				TT-R				PC-R							
Sub.	O1	O2	P8	FC6	O1	O2	P8	FC6	O1	O2	P8	FC6	O1	O2	P8	FC6
S1	5.9	5.8	5.9	7.2	9.6	10.1	8.7	10.1	11.2	12.3	11.2	12.1	2.1	3.2	3.5	4.9
S2	7.0	6.3	6.3	7.4	8.9	6.8	8.7	9.4	11.8	12.0	12.6	11.8	3.1	4.5	5.1	6.7
S3	7.1	6.2	5.8	8.0	8.6	11.1	11.8	9.2	15.4	12.8	12.7	10.9	3.9	4.8	5.2	6.9
S4	5.6	6.1	6.9	10.1	9.8	10.1	9.6	10.4	11.4	13.7	14.8	12.4	3.1	4.4	5.1	6.8
S5	5.7	5.8	5.3	7.8	8.6	10.8	9.1	8.8	10.3	13.7	11.2	11.4	6.7	6.2	5.9	7.1
S6	6.4	5.7	6.6	7.3	9.7	11.3	10.1	10.3	15.6	11.6	14.2	10.8	4.6	3.5	4.6	6.1
Mean	6.3	6.0	6.1	8.0	9.2	10.0	9.7	9.7	12.6	12.7	12.9	11.6	3.9	4.4	4.9	6.40
SD	±0.66	±0.25	±0.58	±1.10	±0.56	±1.66	±1.18	±0.66	±2.3	±0.9	±1.4	±0.65	±1.6	±1.1	±0.8	±0.8

Table 4.2: INPS(dB) values for constrained ICA with the PC-R ref. function generation technique and the PCA method.

	Constrained ICA method							PCA method						
Sub.	F3	P4	O1	O2	P8	CP2	CP6	F3	P4	O1	O2	P8	CP2	CP6
S1	9.3	7.9	11.2	12.3	11.2	8.6	12.4	1.3	7.2	8.0	9.2	11.0	5.3	9.1
S2	7.1	7.2	11.8	12.0	12.6	7.9	11.1	4.3	6.9	8.3	8.4	10.7	4.9	7.9
S3	8.9	7.1	15.4	12.8	12.7	8.1	11.8	4.7	7.2	8.7	8.9	10.3	5.1	8.8
Mean	8.4	8.4	12.8	12.4	12.2	8.2	11.8	3.4	7.1	8.3	8.8	10.7	5.1	8.6
SD	±1.2	±0.4	±2.3	±0.4	±0.8	±0.4	±0.65	±0.85	±0.2	±0.4	±0.4	±0.4	±0.2	±0.6

Table 4.3: Correlation coefficients between the outside VEPs and the VEPs after artifact attenuation with the constrained ICA and the AAS method.

	Constrained ICA Method						AAS Method					
Sub.	C3	P3	O1	O2	P8	CP6	C3	P3	O1	O2	P8	CP6
S1	0.90	0.93	0.88	0.64	0.89	0.83	0.70	0.83	0.73	0.72	0.80	0.81
S2	0.83	0.80	0.77	0.79	0.87	0.53	0.44	0.61	0.82	0.71	0.86	0.53
S3	0.65	0.73	0.70	0.77	0.64	0.69	0.57	0.78	0.67	0.62	0.77	0.69
S4	0.66	0.32	0.81	0.88	0.75	0.82	0.46	0.63	0.81	0.86	0.65	0.67
S5	0.56	0.75	0.87	0.76	0.89	0.85	0.63	0.71	0.85	0.60	0.80	0.84
S6	0.69	0.54	0.82	0.85	0.84	0.50	0.59	0.13	0.44	0.43	0.55	0.59
Mean	0.72	0.68	0.81	0.78	0.81	0.70	0.57	0.70	0.72	0.66	0.74	0.69
SD	$\pm$0.13	$\pm$0.22	$\pm$0.06	$\pm$0.08	$\pm$0.1	$\pm$0.16	$\pm$0.10	$\pm$0.10	$\pm$0.15	$\pm$0.14	$\pm$0.12	$\pm$0.12

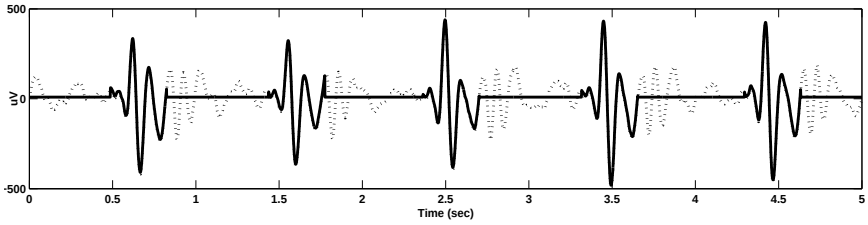

(a) EEG channel O1

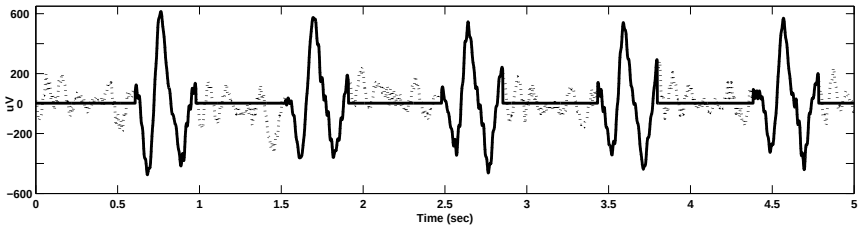

(b) EOG Channel

Figure 4.3: EEG signals inside MRI (dotted) and the derived reference functions (solid) using the TT-R technique.

difficulties to neither standardize nor automate the ICA-based artifact attenuation procedures. In the study presented in this chapter, we have introduced a simple, standardized and almost automatic way of attenuating the BCG and EOG artifacts simultaneously from the EEG signals measured inside MRI. The technique uses constrained ICA with *a priori* information about the artifacts as references or constraints. Since constrained ICA shares the same measure as that of fastICA [6] i.e., negentropy, it enjoys all the benefits of ICAP in addition to its own unique advantages as discussed in the introduction section. Detailed comparisons and analysis indicate that our proposed technique significantly reduce the artifacts compared to the standard AAS procedure. Furthermore it does not require additional measurements as in the case of AAS and AFTs: rather our technique derives its reference function from the data itself. The procedure can be extended to any number of artifacts or any desired information by introducing the multiple number of reference functions.

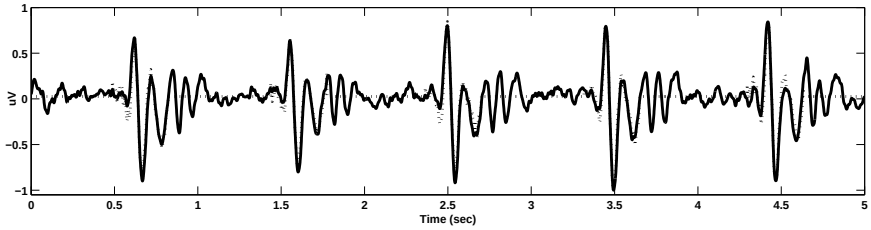

(a) Normalized IC corresponding to the BCG artifact

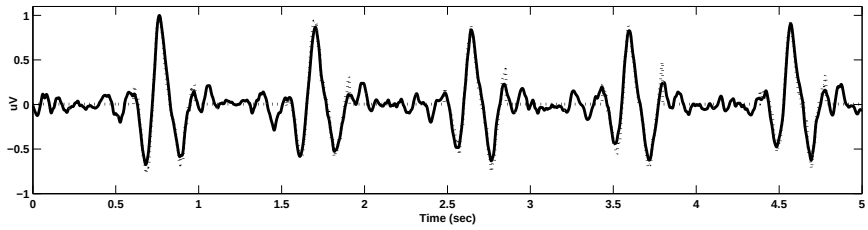

(b) Normalized IC corresponding to the EOG plus BCG artifacts

Figure 4.4: The two extracted ICs (solid) and the normalized reference functions (dotted).

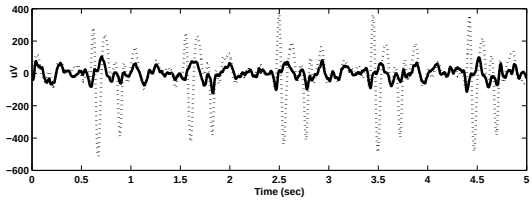

(a) Refs. generated from channels O1 and EOG

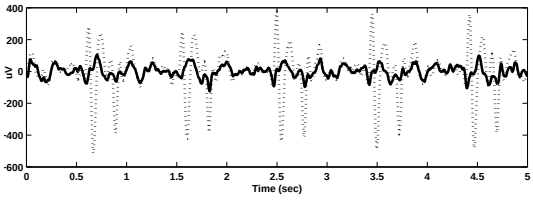

(b) Refs. generated from channels O2 and EOG

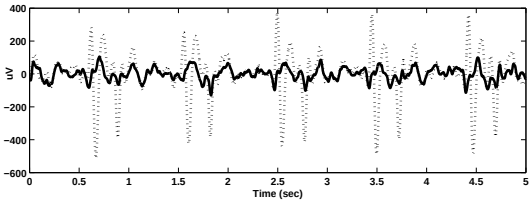

(c) Refs. generated from channels P8 and EOG

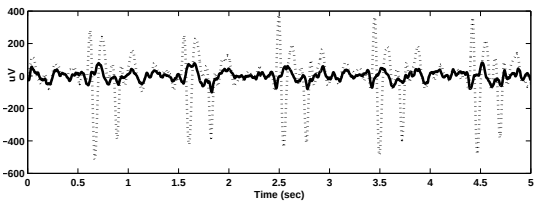

(d) Refs. generated from channels CP6 and EOG

Figure 4.5: Comparison of artifact attenuation at the EEG channel P4, before(dotted) and after artifact attenuation (solid), when refs. generated from different channels using the TT-R.

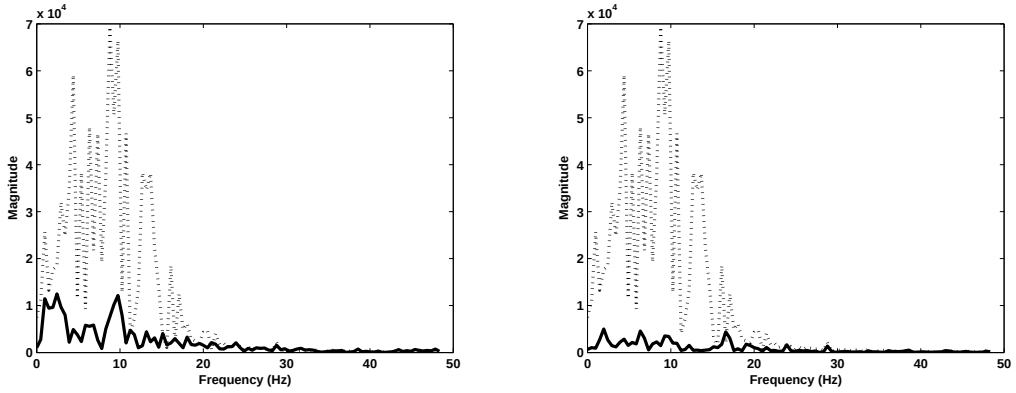

(a) (b)

Figure 4.6: Power spectrum plots of channel O2,(a) reference functions generated using the TT-R and (b) PC-R techniques, before (dotted) and after artifact attenuation (solid).

The role of reference functions for constrained ICA is to direct the algorithm into the direction of desired ICs. Therefore, reference function generation should depends on each application area. In the area of artifact rejection in EEG data, temporal and morphological information about the artifact is useful. In this chapter, we have introduced three ways of generating the reference functions for the constrained ICA algorithm. In our first technique (CH-R), we used a channel that is severely affected by BCG artifact and the EOG channel as reference functions. For EEG measured inside MRI scanner the artifacts not only get amplified but also their relative timing and shape get distorted. As mentioned in table 4.1, it did improve the overall INPS values but the improvement is not very significant as compared to AAS because of the different morphological distortions of artifacts for each channel. The other limitation of the CH-R method is that some useful information may also be discarded. In our second method (TT-R), we kept only the approximate timing and representative shape information for the BCG from one EEG channel and for BCG and EOG artifacts from EOG channel. The INPS values improved because in this case more accurate information about the artifacts are provided as compared to the previous method. To include more information, about the representative timing and morphological infor-

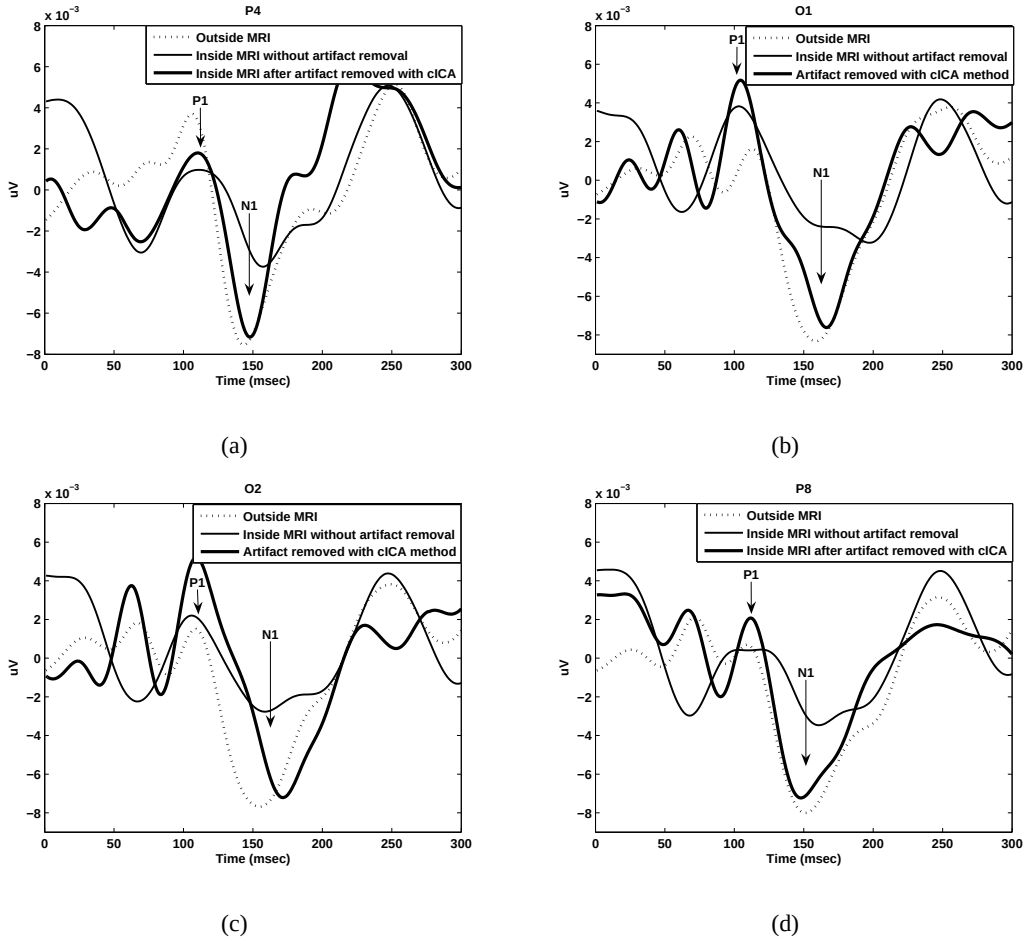

Figure 4.7: Visual evoked potentials at (a) P4, (b) O1, (c) O2 and (d) P8 channels, the response outside MRI (dotted), inside MRI without artifact attenuation (thin solid), and after artifact attenuation(thick solid). The reference functions generated using the PC-R technique.

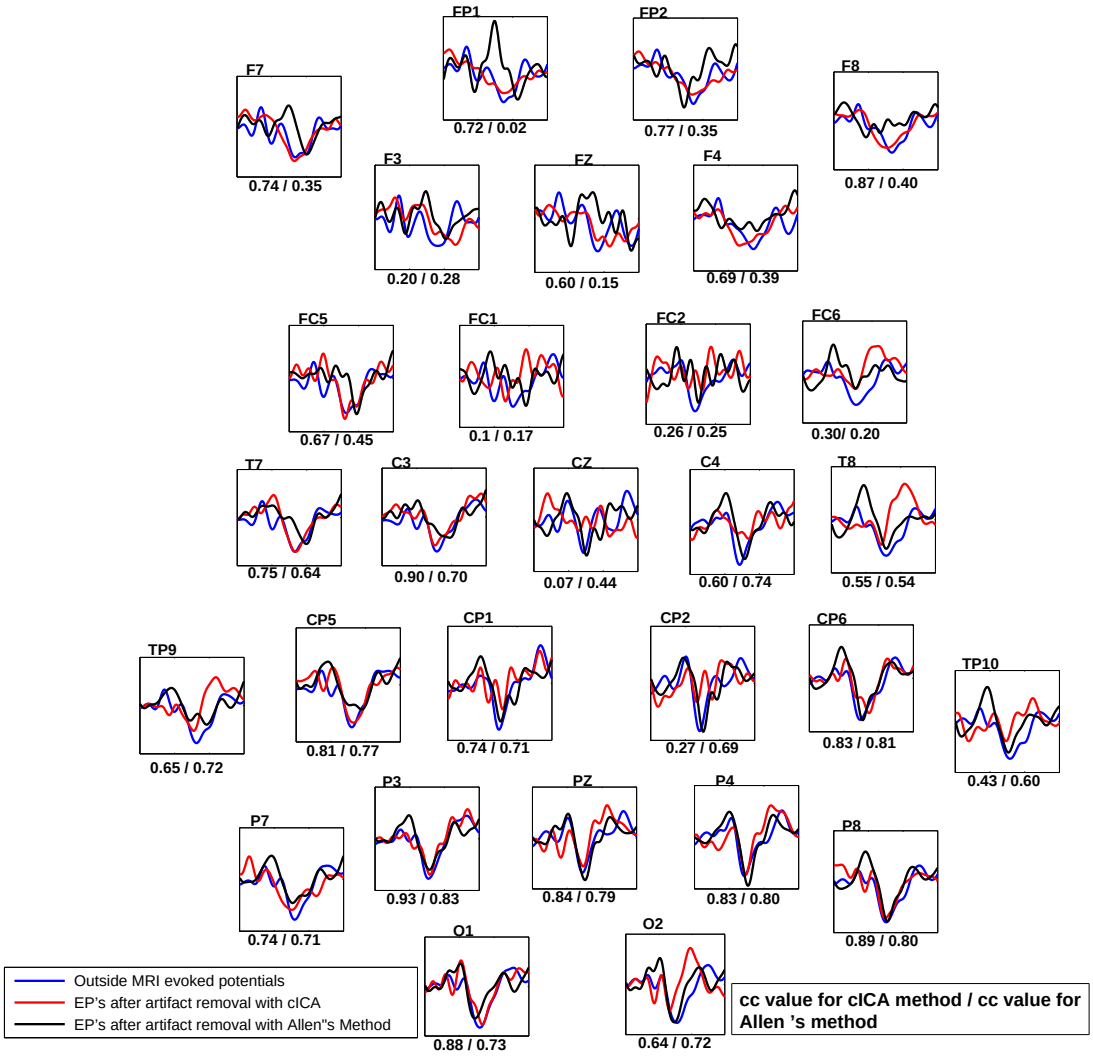

Figure 4.8: Comparison of outside VEPs and those obtained using the constrained ICA method and the AAS (Allen's) method.

mation, into the reference function we relied on the basic structure of PCA (i.e., projections on the maximum variance bases preserving general timing and morphology). Based on this idea the PC-R technique gave us the best results as presented in table 4.1. Although we have shown three different ways of generation of reference functions with progressively improving results, other variations could be used depending on the application area.

Previously, various methods for artifact rejection [34, 37, 40, 38, 39] in EEG recording have been proposed. For example, the BCG artifact induced by the pulsatile parenchyma brain motion can be reduced using the standard AAS method [34]. In this method a noise template is estimated by averaging every channel with epochs time-locked to the complex ECG waveform and slow baseline trends are removed using Linear regression. The estimated noise template is then subtracted from each 1-s section of EEG. However this method suffers from less representative templates. Motion sensor signal was utilized in an adaptive filter scheme to remove the motion-related artifacts [37]. The BCG and motion affect on EEG are very much non-stationary as we have proved and the artifact attenuation methods depend much on the accuracy of the corresponding template. Constrained ICA with our designed reference functions perform better because we identify the artifacts as independent components (ICs). Then we subtract them form the EEG recordings, after projecting them back to the measurement space, to get the artifact attenuated EEG signals. Based on the results we have presented in this chapter, our proposed scheme outperforms the current standard schemes with some convenient features.

In the work presented in this chapter, we have validated our technique only with the BCG and EOG artifacts in the data. We believe that constrained ICA with the proposed reference function generation schemes could be an effective tool for attenuating the BCG and EOG artifacts from EEG data measured inside MRI. The proposed technique could facilitate the simultaneous EEG and fMRI studies involving continuous as well as evoked responses of the brain. If the gradient artifact is present even after its removal using the AAS method; assuming that it is independent, it can further be attenuated with the proposed method by designing a reference function for it.

Chapter 5

Constrained Spatiotemporal ICA For Spatiotemporal Data

In general, Independent component analysis (ICA) is a statistical blind source separation technique, used either in spatial or temporal domain. The spatial or temporal ICAs are designed to extract maximally independent sources in respective domains. The underlying sources for spatiotemporal data (sequence of images) can not always be guaranteed to be independent, therefore spatial ICA extracts the maximally independent spatial sources, deteriorating the temporal sources and vice versa. For such data types, spatiotemporal ICA tries to create a balance by simultaneous optimization in both the do-mains. However, the spatiotemporal ICA suffers the problem of source ambiguity. Recently, con-strained ICA (c-ICA) has been proposed which incorporates a priori information to extract the desired source. In the study presented in this chapter, we have extended the c-ICA for better analysis of spatiotemporal data. The pro-posed algorithm, i.e., constrained spatiotemporal ICA (constrained st-ICA), tries to find the desired independent sources in spatial and temporal domains with no source ambiguity. The performance of the proposed algorithm is tested against the conventional spatial and temporal ICAs using simulated data. Furthermore, its performance for the real spatiotemporal data, functional magnetic resonance images (fMRI), is compared with the SPM (conventional fMRI data analysis tool). The functional maps obtained with the proposed algorithm reveal more activity as compared to SPM.

5.1 Introduction

Independent component Analysis (ICA), a blind source separation (BSS) method based on higher order statistics, decomposes the linear memory-less observations into their underlying maximally in-dependent sources and their corresponding mixing weights [7, 6]. There are two conventional modalities in which ICA can be used to decompose the spatiotemporal data into a set of spatial or temporal ICs i.e., spatial ICA and temporal ICA. Spatial ICA finds underlying independent spatial sources and the mixing matrix contains corresponding set of time sequences; temporal ICA finds independent temporal sequences and the obtained mixing matrix gives the corresponding set of spatial modes. With the success of ICA in medical signal processing there is a strong interest in ICA for the analysis of spatiotemporal data e.g., fMRI images. fMRI is a non-invasive technique used to study spatiotemporal brain functions in both research and clinical areas [55]. It can measure small changes in the MR signal caused by small changes in blood oxygenation level, when specific areas of brain are performing the given task [56]. By acquiring successive images from multiple slices of head in time, image intensity variation at each voxel represent the blood oxygenated level dependent (BOLD) response to a given task. Therefore, it is possible to determine active brain regions for a given task by correlating each voxel signal in MR image sequences to the experimental paradigm. The spatial resolution in fMRI images can go up to 1mm, making it a preferred technique for accurate source localization.

In 1998, McKeown et al. [27] for the first time introduced ICA for fMRI data analysis, with the as-sumption that fMRI data is a mixture of spatially independent components. Biswal and his colleagues [57] applied the ICA in the temporal domain for fMRI un-mixing. So far, most of the applications of ICA for fMRI are based on ICA using the spatial mode (Spatial ICA). However the choice of spatial or temporal ICA is controversial: Comparison and discussion on the underlying assumptions for the use of spatial and temporal ICA is given in [58]. Some authors have also applied ICA on the fMRI data in the complex domain [59] considering that the phase information which is normally discarded in usual ICA application provides vital information. ICA has been successful in the identification of various source signals in fMRI [48] which are considered

challenging for the second order techniques such as correlation and regression analysis.

The foremost assumption for ICA application is that the underlying sources should be independent. However, for spatiotemporal data like fMRI image sequences it is difficult to fulfill this independence criterion for both the spatial and temporal domains (i.e., independent sources in spatial domain as well as independent sources in temporal domain). In such cases, spatial or temporal ICA tries to find a set of maximally independent sources in one domain at the cost of their corresponding unconstrained set of sources in the other domain. Lately, Spatiotemporal ICA [60, 61] has been proposed to create a balance by jointly optimizing the sources in spatial and temporal domains. Stone and his colleagues [60, 61] suggested that skew symmetric source distribution is more realistic assumption for fMRI studies. Suzuki et. al. [62] also assumed a skew symmetric distribution in his study. In 2002, Seifritz and his team used a combination of spatial and temporal ICA to analysis the spatiotemporal data [63]. They first used the spatial ICA to locate a region of interest and finally temporal ICA to find the temporal response of human auditory cortex. However, for the higher dimensional data like fMRI, spatiotemporal ICA gives large number of independent components making the subsequent analysis very complicated and subjective. In other words, there exists source ambiguity for ICAs in the conventional spatial, temporal, and spatiotemporal modes.

The existing ICA models are blind source separation methods; they do not take advantage from the a priori information that might be available about the desired source. In the case of fMRI data, the paradigm information is vital. The conventional ICAs use this information for sorting the ICs found instead of utilizing it in the un-mixing process. Recently, Lu and Rajapakse introduced an algorithm, constrained ICA, [9] that can incorporate a priori information in the un-mixing process. In temporal mode, this algorithm has been applied for fMRI data analysis [9]. Constrained ICA has also been applied for artifact removal from EEG signals [2]. However constrained ICA, which is the same as the spatial or temporal ICA except that it includes the constraints in the cost function, also suffers from the same disadvantage as of spatial or temporal ICA i.e., the maximal independent component in one domain and deteriorated components in the

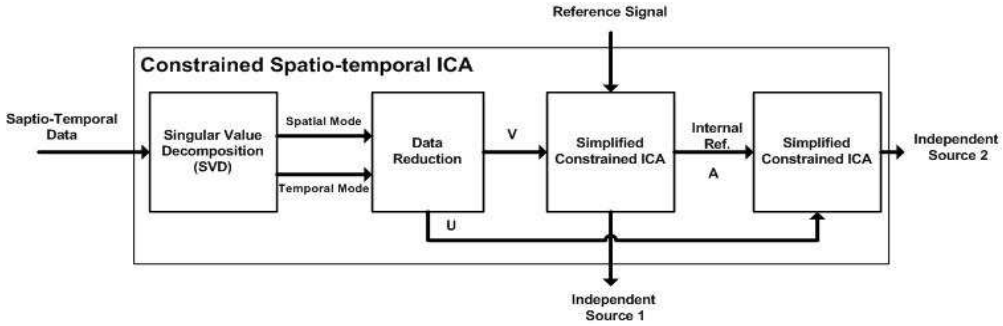

Figure 5.1: The schematic diagram of the constrained spatiotemporal ICA.

corresponding domain.

As mentioned above, there exists a problem of source ambiguity in the case of spatiotemporal ICA. In case of, constrained ICA source identification problem is solved by incorporating the a priori information. However, the performance of earlier for spatiotemporal data is better than the later. Considering the spatiotemporal nature of fMRI data, we extend constrained ICA into constrained spatiotemporal ICA (constrained st-ICA) that finds independent, yet desired temporal and spatial sources thus solving the source ambiguity problem for spatiotemporal data. The proposed method is based on the singular value decomposition (SVD) and cascade of two simplified one unit ICA-R blocks as shown in the schematic diagram Fig. 5.1. The performance of the algorithm against the conventional ICAs is tested using the simulated data. To analyze the performance for real spatiotemporal data, it is applied to fMRI data and its results are compared to those of the conventional fMRI data analysis tool i.e., Statistical Parametric Mapping (SPM). The functional maps obtained with the pro-posed algorithm reveal more active brain regions compared with the SPM. Based on the results we strongly believe that the proposed algorithm could be used for spatiotemporal data analysis.

5.2 Independent Component Analysis

Independent component Analysis (ICA) is a stochastic method that assumes that a linear memory-less observation matrix $\mathbf{X} = (\mathbf{x}_1, \mathbf{x}_2, \ldots, \mathbf{x}_m)^t$ can be decomposed into underlying set of independent sources $\mathbf{S} = (\mathbf{s}_1, \mathbf{s}_2, \ldots, \mathbf{s}_n)^t$ i.e.,

$$\begin{aligned} \hat{\mathbf{S}} &= \mathbf{XW} \\ or \quad \mathbf{X} &= \mathbf{SA} \end{aligned} \tag{5.1}$$

where $\mathbf{A}$ is the mixing matrix and $\mathbf{W}$ is the unmixing matrix. General implementations of ICA can be found in the literature [8, 46, 6, 7].

If the observation matrix contains image sequence then equation 5.1 can be written as $\mathbf{X} = \mathbf{S}\Lambda\mathbf{T}^t$. where $\mathbf{S}$ represents the independent spatial sources and $\mathbf{T} = (\mathbf{t}_1, \ldots, \mathbf{t}_k)^t$ are the corresponding independent time courses and Λ are diagonal scaling parameters.

5.2.1 Spatial ICA and Temporal ICA

he observation matrix X can be decomposed into $\mathbf{X} = \mathbf{UDV}^t$ using singular value decomposition, where $\mathbf{U}$ is an $m \times m$ eigenimage matrix, V is an $n \times n$ matrix of corresponding eigensequences, and $\mathbf{D}$ is a $m \times n$ diagonal matrix of singular values. By retaining the k singular value we can reduce the rank of the matrix.

$$\mathbf{X} \approx \hat{\mathbf{X}} = \hat{\mathbf{U}}\hat{\mathbf{D}}\hat{\mathbf{V}}^t \tag{5.2}$$

Spatial ICA assumes that the $m \times k$ eigenimage matrix $\hat{\mathbf{U}}$ can be decomposed into k spatially independent components $\mathbf{S} = (\mathbf{s}_1, \ldots, \mathbf{s}_k)^t$. The corresponding time courses can be obtained as follows.

$$\begin{aligned} \hat{\mathbf{X}} &= \mathbf{SA}_s\hat{\mathbf{D}}\hat{\mathbf{V}}^t \\ &= \mathbf{ST}_s \end{aligned} \tag{5.3}$$

where rows of $\mathbf{T}_s = \mathbf{A}_s\hat{\mathbf{D}}\hat{\mathbf{V}}^t$ contain corresponding time courses.

On the other hand Temporal ICA assumes that $n \times k$ eigensequence matrix can be decomposed into k independent temporal components $\mathbf{T} = (\mathbf{t}_1, \ldots, \mathbf{t}_k)^t$. The corresponding spatial modes can be obtained as follows.

$$\begin{aligned} \hat{\mathbf{X}} &= \hat{\mathbf{U}}\hat{\mathbf{D}}\mathbf{A}_t^t\mathbf{T}^t \\ &= \mathbf{S}_t\mathbf{T}^t \end{aligned} \tag{5.4}$$

where each column of $\mathbf{S}_t = \hat{\mathbf{U}}\hat{\mathbf{D}}\mathbf{A}_t^t$ contain the corresponding spatial modes.

5.2.2 Spatiotemporal ICA

The Spatiotemporal ICA [60, 61] is based on the assumption that some times underlying spatial and temporal sources are not completely independent. In these cases the spatial or temporal ICA will not produce good results in their corresponding unconstrained temporal and spatial domains respectively. Spatiotemporal ICA treats the spatial and temporal domains equally by maximizing the following cost function.

$$h_{st}(W_s, \Lambda) = \alpha H(\mathbf{Y}_s) + (1-\alpha)H(\mathbf{Y}_t) \tag{5.5}$$

where W_s is the spatial un-mixing matrix, Λ is scaling matrix, α is the relative weighting factor, $H(\mathbf{Y}_t)$ is the temporal entropy, $\mathbf{Y}_t = \sigma_t(\mathbf{y}_t)$ are the cdfs of temporal signals, $\mathbf{y}_t = \hat{V}W_t$ are extracted temporal signals, $H(\mathbf{Y}_s)$ are the spatial entropy, $\mathbf{Y}_s = \sigma_s(\mathbf{y}_s)$ is the cdfs of spatial signals and $\mathbf{y}_s = \hat{U}W_s$ are extracted spatial signals,

5.2.3 Constrained ICA

When *a priori* information about the desired source is available, we can incorporate this information as constrained in the ICA cost function [9]. The constraint could be in the temporal or in the spatial domain depending on the configuration of ICA (Temporal or Spatial) being used. This constraint referred to as the reference function must carry some information about the desired

source. During the optimization process it guides the algorithm in the direction of desired independent source. Let the reference be $\mathbf{r}(t) = (r_1(t), r_2(t), ..., r_k(t))^t$. The closeness constraint for single IC can be written as

$$g(\mathbf{w}) = \varepsilon(\mathbf{w}^t\mathbf{x},\ r_i) - \xi \leq 0 \tag{5.6}$$

where ε is some closeness measure between the estimated output $\mathbf{w}^t\mathbf{x}$ and the reference signal r_i. The closeness threshold parameter is denoted by ξ. The measure of closeness can take any form, such as mean squared-error (MSE), correlation or any other suitable closeness (or similarity) measures. One interesting improvement in constrained ICA can be found in [64].

5.3 Constrained Spatiotemporal ICA

The spatiotemporal data where the underlying independence criterion is difficult to establish; the conventional ICA algorithms have some weaknesses, i) spatial or temporal ICA tries to find the maximally independent components in the spatial or temporal domains respectively affecting the components in the corresponding domains, ii) ordering of the output sources are random (source ambiguity), iii) the number of sources found for the high dimensional data are very large (such as sequences of fMRI images), making the subsequent analysis laborious and highly subjective. The stICA tries to overcome the first above mentioned disadvantage of conventional ICA by simultaneously optimizing the spatial and temporal domains. However, it suffers from source ambiguity and large number of de-rived sources for high dimensional data; same as that of conventional ICAs. The cICA finds only a specific or a subset of sources and also solves a source ambiguity problem by incorporating a priori information. However, the cICA being exactly the same as that of conventional ICA (same contrast function, same optimization procedure) else than it includes some constrains into the contrast function suffers from the above mentioned first disadvantage of the conventional ICA. In the proposed con-strained st-ICA we have tried to collect the advantages of st-ICA and cICA to overcome the above mentioned disadvantages of conventional ICA.

In this algorithm, we exploited the salient features of singular value decomposition (SVD) along with one unit cICA algorithm. The SVD: (i) decomposes the observation data into a set of spatial modes (left singular matrix) and the corresponding set of temporal sequences (right singular matrix), (ii) both left and right singular matrices are orthonormal and (iii) the rank reduction can be done by selecting an appropriate number of k vectors as mentioned in section **??**. Based on these properties, corresponding underlying sources in the two domains can be found independently if some a priori information about the desired source is available. As shown in Fig. 5.1 there are two simplified/fast cICA blocks, we first explain the cICA and the simplifications/modifications that come naturally with our proposed constrained spatiotemporal ICA algorithm then at the end complete algorithm will be explained.

Let there are n independent source signals $\mathbf{s}(t) = [s_1(t),\ s_2(t), ..., s_n(t)]^{\mathrm{t}}$ and m the number of observed mixtures $\mathbf{x}(t) = [x_1(t), x_2(t), ...x_m(t)]^{\mathrm{t}}$. The a priori information, which represents some traces of the desired independent source, can be represented in terms of the reference signal $r(t)$. The information in the signal $r(t)$ may be incorporated as closeness constraint onto the ICA contrast function. The closeness constraint for single IC can be written as

$$\mathrm{g}(\mathbf{w}) = \varepsilon(\mathbf{w}^{\mathrm{t}}\mathbf{x},\ r) - \xi \leq 0 \tag{5.7}$$

(6) where ε is some closeness measure (e.g. Mean square error or correlation). The closeness threshold parameter is denoted by ξ . Various ICA algorithms use different contrast functions depending on the application area in which they are used. However the ICA contrast function based on negentropy is very reliable and flexible. In the original one unit cICA algorithm there are two constrains i.e., equality constraints and the inequality constraints. Equality constraints are to keep the unity variance and the inequality constraints are to incorporate the a priori information. In our case, the input data has inherently unit variance because both the modes are orthonormal; we don't need the equality constraints. Therefore the optimization equation for the constrained

spatiotemporal ICA is as follows.

$$\begin{aligned} &maximize \ : \ \mathrm{J}(y) \approx \rho[E\{\mathrm{G}(y)\} - E\{\mathrm{G}(v)\}]^2 \\ &Subject\,to: \ \mathrm{g}(\mathbf{w}) \leq 0 \ \ or \ \ \hat{g}(\mathbf{w}) = g(\mathbf{w}) + b^2 = 0 \end{aligned} \tag{5.8}$$

where $J(y)$ denotes the one-unit ICA contrast function introduced by [8], ρ is a positive constant, v is a zero mean, unit variance Gaussian variable, $G(.)$ is a non-quadratic function as defined in [8], $g(\mathbf{w})$ is the closeness constraint mentioned in equation 5.7 and b is the slack variable. Equation 5.8 is a constrained optimization problem which can be solved by explicitly manipulating for the optimum b^* through the use of an augmented Lagrangian function. Learning of the weights is achieved through a Newton-like learning process.

$$\begin{aligned} \mathrm{C}(\mathbf{w}, \mu) &= \mathrm{J}(y) + \mu^{\mathrm{t}} \hat{g}(\mathbf{w}) + \tfrac{1}{2}||\hat{g}(\mathbf{w})||^2 \\ \mathrm{C}(\mathbf{w}, \mu) &= \mathrm{J}(y) - \tfrac{1}{2\gamma}[\max^2\{\mu + \gamma g(\mathbf{w}), \ \ 0\} - \mu^2] \end{aligned} \tag{5.9}$$

where C represents the new contrast function to be optimized, μ is the Lagrange multiplier and γ is the scalar penalty parameter. Learning of the weights can be achieved through Newton like learning process.

$$\begin{aligned} &\mathbf{w}_{k+1} = \mathbf{w}_k - \eta(C'')^{-1}C' \\ &\mathbf{w}_{k+1} = \mathbf{w}_k - \eta\mathbf{R}_{\mathbf{xx}}^{-1}(H'')^{-1}C' \\ &\text{where} \\ &C'' = H''\mathbf{R}_{\mathbf{xx}} \qquad \mathbf{R}_{\mathbf{xx}} = E\{\mathbf{x}\mathbf{x}^{\mathrm{t}}\} = \mathbf{I} \\ &\text{therefore} \\ &\mathbf{w}_{k+1} = \mathbf{w}_k - \eta(H'')^{-1}C' \\ &\mathbf{w} \ \leftarrow \ \tfrac{\mathbf{w}}{|\mathbf{w}|} \\ &\text{and} \\ &C' = \bar{\rho}E\{\mathbf{x}G'_y(y)\} - \tfrac{1}{2}\mu E\{\mathbf{x}g'_y(\mathbf{w})\} \\ &H'' = \bar{\rho}E\{\mathbf{x}G''_{y^2}(y)\} - \tfrac{1}{2}\mu E\{\mathbf{x}g''_{y^2}(\mathbf{w})\} \end{aligned} \tag{5.10}$$

The optimum multipliers can be found by iteratively applying the gradient ascent method.

$$\mu_{k+1} = \max\{0, \ \mu_k + \gamma g(\mathbf{w}_k)\} \tag{5.11}$$

The presented cICA algorithm is simple and fast compared to cICA presented by Lu [9]. There are no equality constrains and matrix inversion ($\mathbf{R_{xx}}^{-1}$) at each iteration is avoided to achieve speed [64].

Given the spatiotemporal data, the spatial and temporal modes can be obtained via SVD. Appropriate data reduction is also done. A priori information and the appropriate SVD mode (spatial or temporal) after data reduction are given to the first cICA block. The outputs will be the independent source and the mixing vector of that domain. From the mixing vector reference signal for the corresponding independent source in the other domain can be generated as given in equation 5.12. This reference signal and the other reduced SVD mode are presented to the second cICA block. The output will be the independent component of this domain, corresponding to the previously extracted independent component. Constrained st-ICA, fMRI data as a specific example, can be described as follows:

step 0: The observation matrix $\mathbf{X}$ contains the fMRI image sequences.

step 1: Reduce the dimension of the observation matrix $\mathbf{X}$ using SVD. Find $\hat{\mathbf{U}}$ and$\hat{\mathbf{V}}$ according to equation 5.2. The matrix $\hat{\mathbf{U}}$ contains spatial mode and $\hat{\mathbf{V}}$ contains temporal modes.

step 2: In the case of fMRI data some a priori information in the temporal domain is readily available. Generate the temporal reference signal $\mathbf{r}_t$ from that information; inverted fMRI experiment protocol.

step 3: Zero mean and normalize the temporal reference signal $\mathbf{r}_t$.

step 4: Call the simplified constrained ICA block with eigensequence matrix $\hat{\mathbf{V}}$ and reference $\mathbf{r}_t$ as the inputs. Upon convergence the output will be the independent temporal sequence.

step 5: To determine the corresponding independent image mode, find the approximate image mode and used it as the spatial reference $\mathbf{r}_s$. The approximate spatial mode can be found as follows:

$$\begin{aligned} \mathbf{r}_s &= \hat{\mathbf{X}}((\hat{\mathbf{V}}\mathbf{w}_t)^t)^{-1} \\ \mathbf{r}_s &= \hat{\mathbf{X}}(\mathbf{T}^t)^{-1} \end{aligned} \tag{5.12}$$

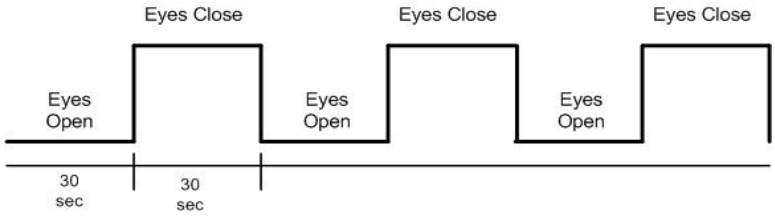

Figure 5.2: Experimental protocol for fMRI data collection.

where $\mathbf{w}_t$ is the un-mixing vector found in step 4 and $\mathbf{T}$ is the time sequence recovered.

step 6: Zero mean and normalize the spatial reference $\mathbf{r}_s$.

step 7: Call the constrained ICA block with eigenimage matrix and reference $\mathbf{r}_s$ as the inputs. Upon convergence the output will be independent image source corresponding to the independent temporal sequence found in step 4.

5.4 fMRI Experiment and Data Acquisition

fMRI data was acquired on a 3.0T MR scanner (Magnum 3.0, Medinus, Korea) using a T2-weighted EPI sequence (TR = 2850ms, TE = 36ms, flip angle =70 , 64 x 64 matrix, FOV = 240 x 240 mm, slice thickness = 4mm, voxel size = 3.75 x 3.75 x 4mm3) with 29 transaxial slices covering the whole brain regions. To minimize motion artifact, we tightly fixed the head using sponge in the head coil.

A well-established protocol for alpha activity modulation for human brain is closing (thus inducing the alpha activity) and opening (thus suppressing the alpha activity) of the eyes [27]. By adopting this experimental protocol, after several minutes of dark adaptation, we asked each subject (5 male, 263 years old) to open his eyes for 30 sec and then close for 30 sec. This cycle was repeated three times to obtain 60 flash image for one complete experiment. Fig. 5.2 shows experimental protocols.

5.5 Results

5.5.1 Synthetic Data Set

The performance of the proposed constrained st-ICA algorithm was tested using the simulated data. Four temporal and spatial sources were generated as shown in Fig. 5.3(a). Each temporal source is of 100 sample points and each spatial source is of 40 x 40 matrix. As evident in the Fig. 5.3(a) neither temporal nor spatial sources are independent. These simulated sources are mixed together to create a spatiotemporal data. The results of spatial ICA and temporal ICA on this mixture data set are shown in Fig. 5.3(b) and 5.3(c) respectively. Both, the spatial and temporal ICA try to find maximal independent sources in the spatial or temporal domains, deteriorating the sources in the other (corresponding) domain. On the other hand, constrained st-ICA finds independent sources in two stages with minimal inter domain affect. It employs a priori information so that only the desired sources (connected sources) should be extracted from the two domains. The results of constrained st-ICA are shown in Fig. 5.3(d). The results indicate that the quality of temporal sources obtained with constrained st-ICA is superior to those obtained with spatial ICA and the obtained spatial sources are superior to those obtained with temporal ICA. The reason for this is that the cost function of temporal or spatial ICA are designed to find maximally independent temporal or spatial sources respectively thus effecting the sources in their cor-responding domains. However, this is not the case with the proposed constrained st-ICA as explained in detail in the constrained spatiotemporal ICA section. Also, the time consumed by spatial or tempo-ral ICA (Pentium (R) 4 CPU 3.01 GHz, 1GB of Ram) to derive sources is in the range of 5 - 6 Sec. whereas, for the constrained st-ICA the time to extract the desired source is in the range of 3.0 - 3.5 sec.

5.5.2 fMRI Data Set

For real life application, the proposed algorithm is applied for fMRI analysis. The fMRI data col-lected for each individual is realigned and convolved with a Gaussian filter (8 x 8 x 8) for

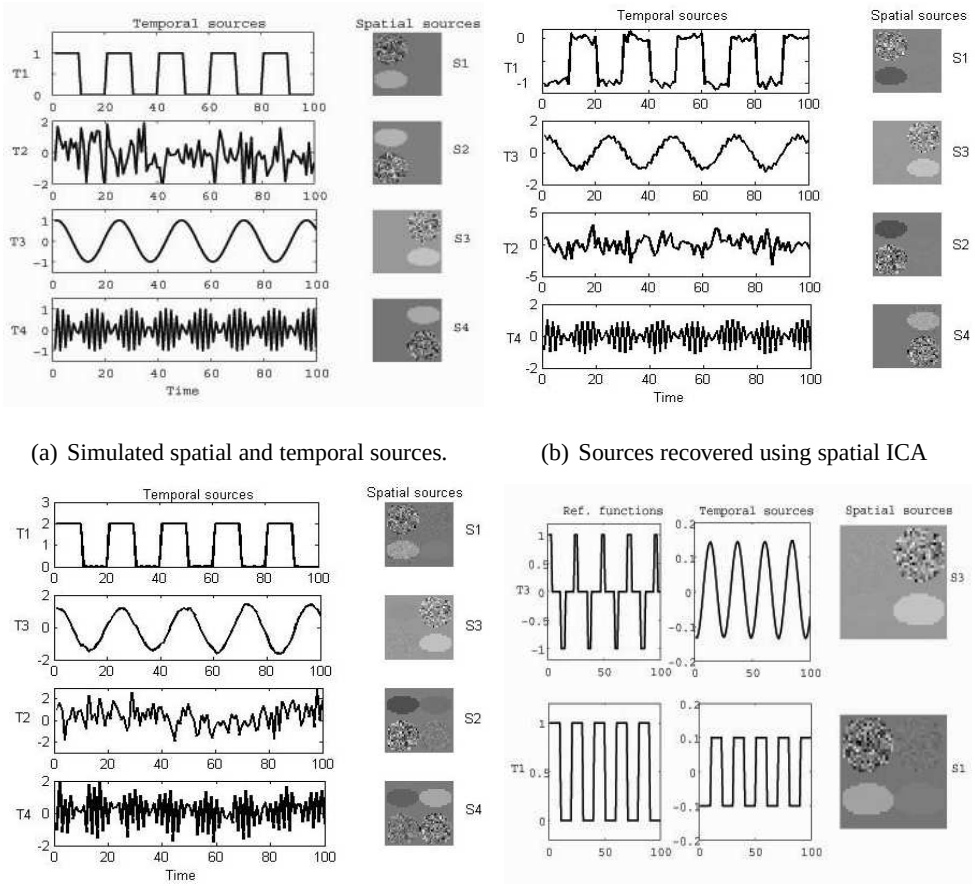

(a) Simulated spatial and temporal sources.

(b) Sources recovered using spatial ICA

(c) Sources recovered using temporal ICA

(d) Sources recovered using constrained stICA

Figure 5.3: (a) Simulated Sources (b) The result of spatial and (c) temporal ICA, Deteriorations in the corresponding domain are clearly visible. (d) Constrained st-ICA gives better results compared to other ICAs. In (d) first column are the ref. functions used, centre column are the temporal sources and right column are the spatial sources recovered.

smoothing. The data from each individual was processed separately on a single volume basis. Each row of an ob-servation matrix contains an image. The ON-OFF stimulation (inverted) (Fig. 2) was used as the initial reference. Independent spatial and temporal components are recovered according to the algo-rithm presented above in the constrained spatiotemporal ICA section.

Once a component map is recovered, it is converted to the z-map [27] according to the Equation 5.13.

$$z_{ij} = \frac{s_{ij} - m_i}{\sigma_i} \geq threshold \tag{5.13}$$

where i is the row index, j is the column index,$\mathbf{S}$ is the spatial component recovered, m_i the mean, and σ the standard deviation of the i^{th} row of $\mathbf{S}$. The threshold value selected for our implementation was 0.6. Details of how to calculate the threshold value can be found in [27].

The time courses (temporal sources) recovered with the constrained st-ICA is shown in Fig. 5.4. The time courses have higher correlation with the ON-OFF stimulation reference (cc = 0.87 0.88) compared to SPM (cc = 0.66 0.75) results. The functional maps (spatial sources) obtained with constrained st-ICA are compared with those obtained with SPM. The results for the slice 14, 15 and 16 for three different subjects are presented in Fig. 5.5. In the previous alpha modulation fMRI experiments, the functional maps are known to have activity in the frontal and occipital regions [65]. The functional maps by constrained st-ICA reveal more frontal activities, which is missed by SPM in most of the cases. The results indicate that the pro-posed constrained st-ICA may be a more effective method for fMRI data analysis.

5.6 Summary

In this chapter a new algorithm, constrained-stICA is proposed. The method tries to find the desired independent spatial and temporal components by separating the input image sequences into spatial and temporal modes that can be analyzed independently by incorporating the a priori information. The conventional ICA algorithms, for data sets like image sequences, try to find maximum independent component without taking into considering the fact that if the extracted

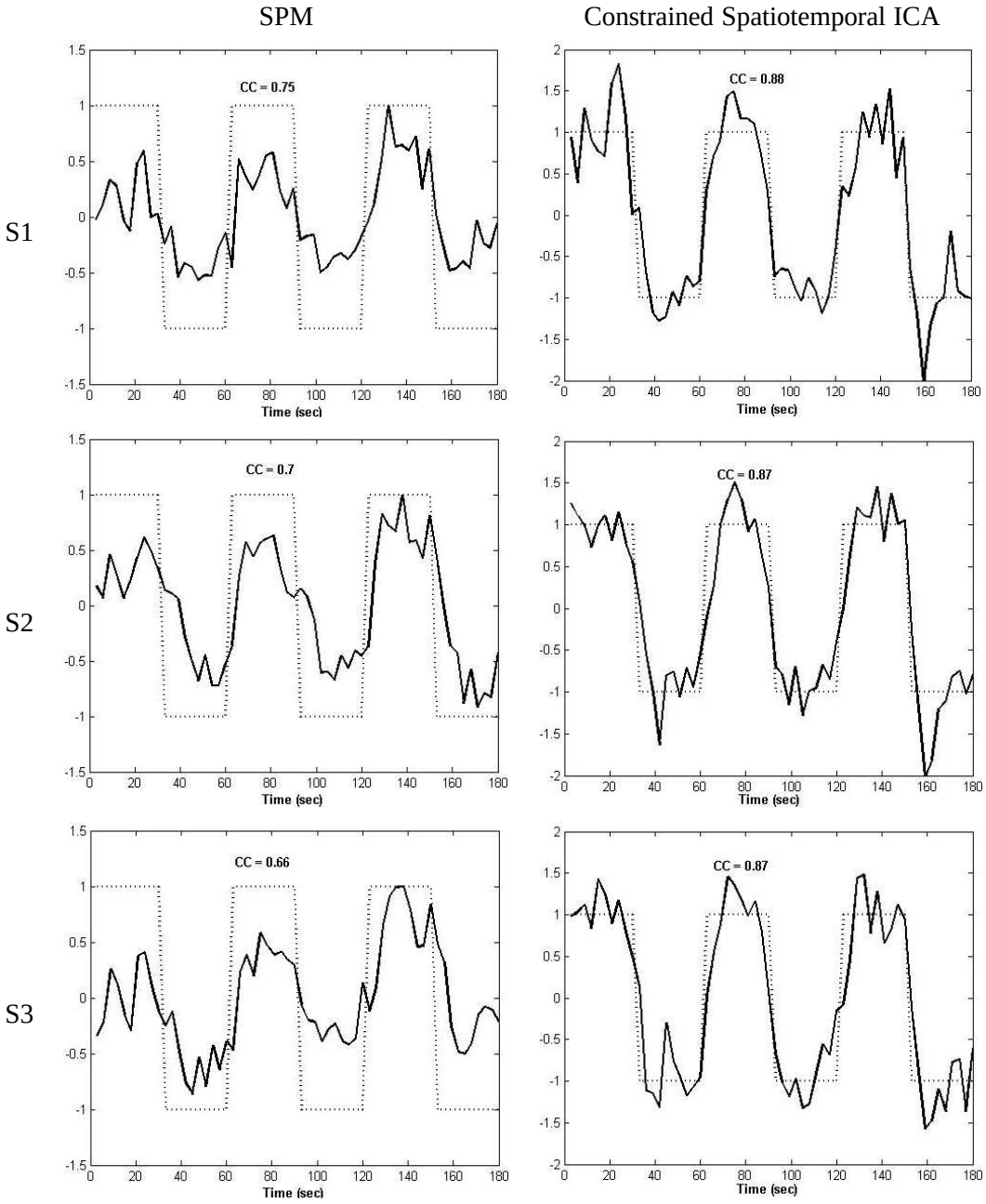

Figure 5.4: Time sequences (solid) obtained with constrained st-ICA has higher correlation with the ref. signal (dotted), inverted ON-OFF stimulation sequence, compared with those obtained with SPM.

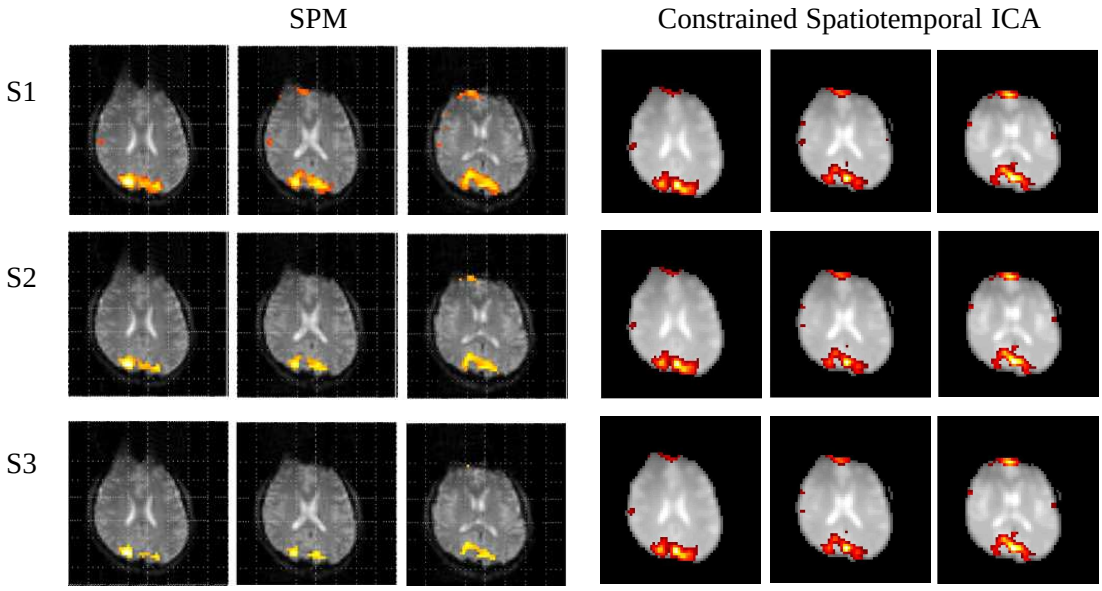

Figure 5.5: SPM and constrained spatiotemporal ICA processed fMRI data. Z-score maps (slice 14,15,16) obtained with constrained st-ICA shows frontal activity which was missed by SPM in most of the cases.

IC is not independent how badly the IC in the corresponding domain may be affected. If the conventional ICA is applied separately on spatial and temporal domains obtained with SVD. There is no way that the output of the two ICAs can be connected together as the ordering of the components is random.

In the study presented in this chapter, we have validated the performance of the proposed algorithm by comparing the results of simulated data set with the conventional ICAs. Furthermore as a real application, we have applied the algorithm on a set of fMRI data and the compared the results with the SPM, which is the conventional technique for fMRI analysis. The results of the proposed algorithm on the simulated data as well as the fMRI data indicate that the proposed algorithm could be more effective technique for the analysis of spatiotemporal data.

Chapter 6

Alpha Source Extraction and Localization in EEG Signals

The alpha activity of brain has a frequency range of 8-12 Hz. In order to extract the alpha activity from EEG data; in this chapter a new procedure based on independent component analysis (ICA), which can incorporate the *a prior* frequency information into the ICA to extract independent components in the desired frequency range is presented. We named this procedure as augmented ICA (Au-ICA). The performance of the proposed procedure for alpha extraction has been compared to that of the conventional band-pass filtering via the scalp alpha power maps and cortical source maps of the alpha activity. Our results demonstrate that the alpha power maps and cortical source maps obtained with our method reveal more localized alpha generating regions of brain as compared with the conventional methods. Furthermore they match more closely to the activated regions of brain, mapped using functional magnetic resonance imaging (fMRI) thus validating our results. We believe that the Au-ICA is a more effective method of extracting brain activity reflected in the specific frequency range of EEG signals. The results presented here emphasize that the proposed method may be used for accurate source localization or imaging maps from EEG signals.

6.1 Introduction

Numerous attempts have been made to elucidate the generators of the brain activities. In late 1920's Berger did the first EEG recording. The recorded signal has a 10 Hz frequency, later

named it as the alpha rhythms. This signal is clearly present in EEG recorded at the occipital area of the 95 percent of the normal adults and have a frequency range of 8 to 12 Hz. It is characterized by being blocked by visual input or mental effort as well as by drowsiness or sleep [66].

The alpha rhythms are an important phenomena of the brain: not only the physiological nature but also their sources are important. Numerous studies have been carried out to find the sources of the alpha activity of the brain. The alpha rhythms have been localized within the primary and secondary visual area of occipital and partly parieto-occipital cortex [67] using the multichannel EEG and MEG.

Simultaneous EEG and MEG provides spatio-temporal resolution on the range of millisecond and centimeter. whereas, simultaneous EEG and fMRI provides resolution on the order of milliseconds and millimeter scale. Owing to the better spatio-temporal resolution, simultaneous EEG and fMRI gives new prospects to the source localization, particularly to study the brain functions in resting state [68]. In 2002, Goldman [69] conducted a study involving simultaneous EEG and fMRI for the first time. In this study, after removing the artifacts from the EEG, average alpha powers for the four channels containing occipital electrodes were calculated. A voxel-wise correlation was perfomed with alpha power time series obtained by convolving the alpha power curves with the *a prior* hemodynamics response. Goldman and his group found out that alpha power is negatively correlated to MRI signal in multiple regions of occipital, superior temporal, inferior frontal, and cingulate cortex and is positively correlated to thalamus and insula. Lauf and co-researchers in 2003 [70] also found out a negative correlation between the alpha power and parietal and frontal cortical activity for the subjects who's EEG are measured with eyes-closed rest inside the MR scanner. The claims of Goldman were also verified by [71] in 2006. However, mandelkow *et. al.* [72] claimed that with the current EEG-MRI methodologies based on correlation analysis: it is difficult to detect the alpha rhythms. His analysis was based on the cross-spectral coherence between simultaneously recorded EEG and MRI time series.

Apart from these common approaches, a novel method had also been developed where sta-

tistically independent sources for the alpha activities are sought by an algorithm called mixture density independent component analysis (ICA) [65]. Since the brain waves is a mixture of various electrical activities of the brain processes, if the alpha wave is assumed as one of sources contributing to the mixture linearly, ICA can separate the alpha wave from the rest of the brain waves. Another study conducted by feige [73] using ICA, with open versus closed eyes and auditory stimulation versus silence condition, found out inverse relationship between EEG alpha amplitude and BOLD signals in primary and secondary viusal areas. They concluded that a correlation with some time lag between the thalamus and in the anterior midbrain is an indicative of some activity preceding the actual EEG change by some seconds.

The standard implementations of one unit ICA algorithm can extract a single IC. However, the recovered IC is favored by the used contrast function. If *a priori* information about the desired independent source is available, we can use that information to force the ICA algorithm to converge in the direction of desired source. Constrained ICA [9] is an approach to incorporate the *a priori* information into the ICA contrast function. Based on the constrained ICA Ahn and his colleagues tried to map the alpha activity [74]. However the generation of a reference function is a difficult task when only frequency range of the desired source is known.

In this study, the desired independent source (alpha activity) has a frequency range of 8-12 Hz, the only *a priori* information available about the desired source. we propose a new method called augmented ICA (Au-ICA) to use this information to extract the alpha activity from the EEG signals as shown in Fig. 1. The proposed algorithm can extract ICs in any desired frequency range. The performance of the proposed method for the extraction of the alpha activity has been compared to that of the conventional band-pass filtering. The alpha power maps are constructed to compare the identified focal regions of the brain responsible for alpha activity. The results indicate that alpha power maps are far more focalized with the proposed method. To further analyze the results, the cortical source maps are constructed via distributed source imaging. The cortical source maps are validated by independent fMRI analysis (fMRI data collected with the same protocols) to find the activated regions of brain. Our results clearly show that the localized

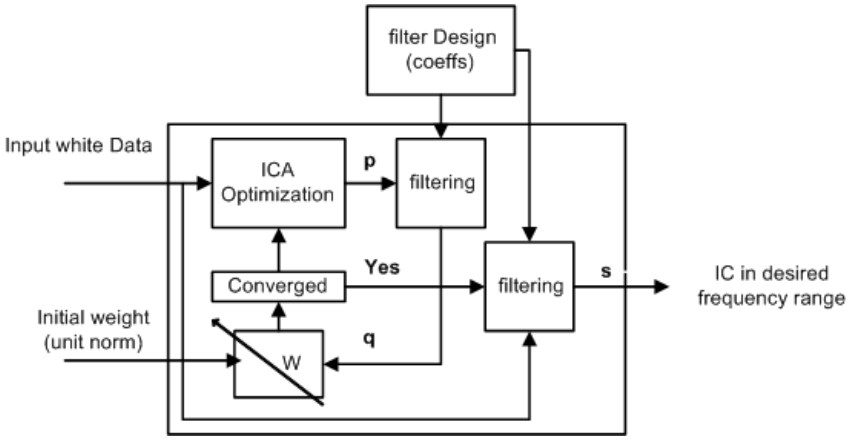

Figure 6.1: Schematic diagram of Au-ICA

alpha sources from the Au-ICA better match the alpha activated regions of fMRI, thus indicating that Au-ICA can extract the alpha rhythms from EEG recordings more effectively than the conventional approaches. We believe that the signal extraction, when frequency range of the desire source is known, based on the proposed method is an effective approach as a pre-processing tool toward more accurate EEG source localization.

6.2 Methods

6.2.1 Experimental Design

The alpha rhythms are apparent when the eyes of subject are close in full awake condition and they got suppressed with opening of the eyes. For alpha activity modulation, we have adopted a well-established protocol as presented by henning [71]. In this study, five healthy volunteers participated (5 males, 26$\pm$3 years old). The subjects' medical history did not show any cues of attention-related or sleep disorders. In the first experimental protocol, after several minutes of dark adaptation, each subject was asked to open his eyes for 30 sec and then close for 30 sec on acoustical cues. This cycle was repeated three times for EEG and fMRI experiments, which were

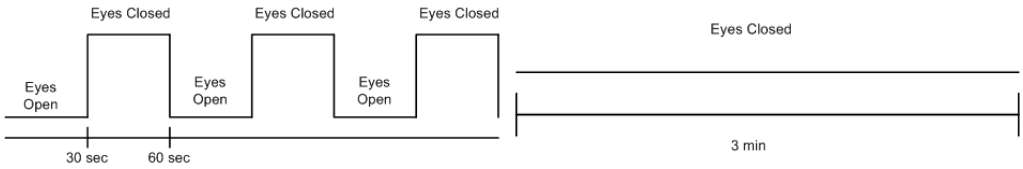

(a) Protocol I: both for EEG and fMRI (b) Protocol II: EEG only

Figure 6.2: Experimental protocols used to acquire the data

conducted separately.

The second experimental protocol was designed to monitor the alpha activity in the natural settings. The same subjects' was asked to close their eyes throughout the experimental period of 3 min. Fig. 6.2, shows these two experiment protocols.

6.2.2 Acquisition of EEG and fMRI Data

A 32-channel EEG recording system (BrainAmp, Brain Products GmbH, Germany) was used to acquire EEG data using the first and second experimental protocols. Continuous EEG recordings were performed with the sampling rate of 1kHz and low-pass filtered at 40Hz. All EEG recordings were performed with the standard 10-20 uni-polar system referenced to FCz. The ground electrode was positioned between Cz and Fz. Electrode-skin impedance was kept below 1K ohm. To minimize motion artifacts in EEG on the scalp electrodes of the subjects, we tightly fixed the EEG cap on the scalp using the adhesive tapes.

The fMRI data were acquired on a 3.0T MR scanner (Magnum 3.0, Medinus, Korea) using a T2-weighted EPI sequence (TR = 2850ms, TE = 36ms, flip angle =70 , 64 x 64 matrix, FOV = 240 x 240 mm, slice thickness = 4mm, voxel size = 3.75 x 3.75 x 4mm^3) with 29 transaxial slices covering the whole brain regions. To minimize motion artifact, we tightly fixed the head using sponge in the head coil. During the data acquisition, we used only the first experimental protocol (i.e., opening and closing of the eyes). The purpose of fMRI experiment was to validate the localized sources of the alpha activity identified in the alpha power maps and cortical source

maps of EEG.

6.2.3 Augmented Independent Component Analysis

Let us denote the multi-channel observations by $\mathbf{x}(t) = (x_1(t), x_2(t), \ldots, x_n(t))^T$ and the underlying source components by $\mathbf{s}(t) = (s_1(t), s_2(t), \ldots, s_m(t))^T$.

$$\mathbf{x}(t) = \mathbf{A}\mathbf{s}(t) \tag{6.1}$$

where the matrix A of size $n \times m$ represents linear memory-less mixing channels. Details mathematical explanation about ICA is provided in Chapter 2. The one-unit ICA algorithms extracts one source at a time, the extraction of the sources depends on the contrast function used. If negentropy is used as a contrast function, the one unit algorithm will extract a source with maximum entropy.

$$J(y) \approx \rho[E\{G(\mathbf{w}^t\mathbf{x})\} - E\{G(v)\}]^2 \tag{6.2}$$

where $J(y)$ is the contrast function, G is the non-quadratic function and v being the gaussian random variable as defined by the [6]. When one desires a source other than the maximum entropy then conventional ICA based on above contrast function is of little use. If *a priori* information about the desired source is available, constrained ICA [9] can be employed to extract that source. However, when the only known information about the desired source is the frequency range then it is very difficult to generate the reference function, required by the constrained ICA, due to phase matching problems. In such cases, the following procedure can be adopted to extract

the IC in the desired frequency range.

1.Zero mean and whiten the data to get $\mathbf{z}$.

2.Choose an initial vector $\mathbf{w}$ of unit norm.

3.Optimization equations

$J(y) \approx [E\{G(y)\} - E\{G(v)\}]^2$ (Negentropy)

$\frac{\partial J}{\partial \mathbf{w}} = \gamma E\{\mathbf{z}g(\mathbf{w}^t\mathbf{z})\}$ (The output is constrained to have unit variance)

where g is the used nonlinearity

$F(z) = E\{\mathbf{z}g(\mathbf{w}^t\mathbf{z})\} + \beta\mathbf{w} = 0$ (Contrast function after using Lagrange Multiplier)

$\frac{\partial F}{\partial \mathbf{w}} = E\{\mathbf{z}\mathbf{z}^t g'(\mathbf{w}^t\mathbf{z})\} + \beta\mathbf{I}$

Using the newton learning method.

$\Delta\mathbf{w}=\eta\frac{J'(y)}{J''(y)}$ (After some simplifications the update equation)

$\mathbf{w} \leftarrow \mathrm{E}\{\mathbf{z}\mathrm{g}(\mathbf{w}^{\mathrm{t}}\mathbf{z})\} - \mathrm{E}\{\mathrm{g}'(\mathbf{w}^{\mathrm{t}}\mathbf{z})\}\mathbf{w}$.

4. $\mathbf{p}=\mathbf{w}\mathbf{z}$.

5. $\mathbf{q}=f(\mathbf{p})$. where f is the filtering operation.

6. $\mathbf{w}= \mathrm{inv}(\mathbf{z}\mathrm{q}^{-1})$.

7. $\mathbf{w}=\mathbf{w}/||\mathbf{w}||$.

8. go to step 3 untill convergence.

9. $\mathbf{s}=f(\mathbf{w}\mathbf{z})$.

where $\mathbf{p}$ is the signal at each iteration, $\mathbf{q}$ is the signal after the filtering process at each iteration and $\mathbf{s}$ is the independent component in the desired frequency range. Details about optimization equations in step 3 can be found in [8]. The coefficients of the filter are designed according to frequency range for which independent component is sought and used during the filtering process in the above mention procedure according to the schematic diagram shown in Fig. 6.1.

6.2.4 Analysis of fMRI Data

The SPM99 software [75] was used for an individual analysis of fMRI data. The standard procedures for realignment, normalization, and spatial smoothing (10mm FWHM) were performed. The reference function was designed according to the protocol I as a box-car function. It is believed that the alpha activity reflected in the blood oxygenation level-dependent (BOLD) effect is negatively correlated with the alpha modulation protocols, as this observation is supported by many recent studies [70, 65, 71]. In accordance with these previous studies, we have also analyzed fMRI data in the same way: the negative correlation maps were obtained at $p<0.001$, uncorrected.

6.3 Results

6.3.1 Alpha Signal Extraction from EEG Signals

Fig. 3, show a set of representative results of conventional and proposed method respectively. Fig. 6.3(a), shows the extracted alpha waves (indicated with a solid black line) from the O1 channel signal (gray line) using bandpass filtering, whereas Fig. 6.3(b) shows the Au-ICA extracted alpha (a black line) superimposed on the same original signal. In both Figs. 6.3(a) and 6.3(b), the onset of alpha activity due to eye-closing (data collected with the protocol I) is clearly discernable. Figs. 6.3(c) and 6.3(d), show the similar results when the data was collected with the protocol II. In both cases, Au-ICA extracted alpha signals show more distinct alpha spindles in comparison to the alpha waves extracted by the bandpass filtering. Fig. 4, shows the power spectrum plots of some representative EEG channels when processed with the proposed method (black) and bandpass filtering (gray). The variation in the magnitude spectrum (8-12 Hz) from channel to channel compared with the conventional method clearly indicating the superior extraction performance of the Au-ICA method.

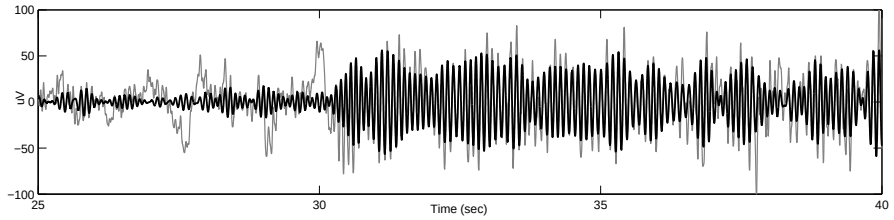

(a) Bandpass filtering

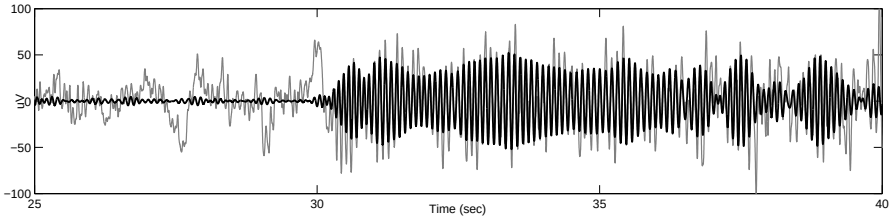

(b) Augmented ICA

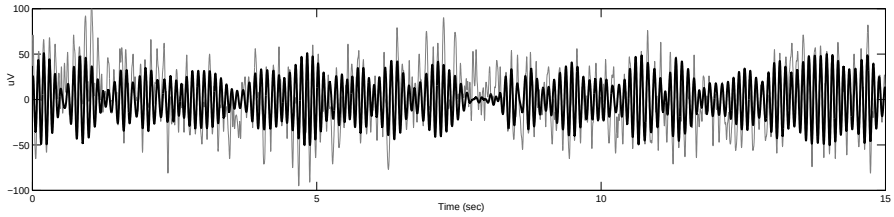

(c) Bandpass filtering

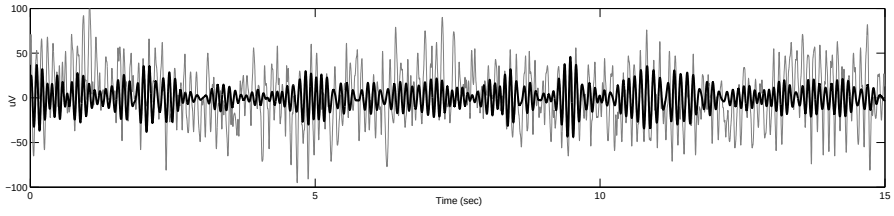

(d) Augmented ICA

Figure 6.3: Recovered alpha signal in black superimposed on the raw EEG signal in gray from the channel O1. (a) and (b) EEG acquired with the experiment protocol I, (c) and (d) EEG acquired with the experimental protocol II

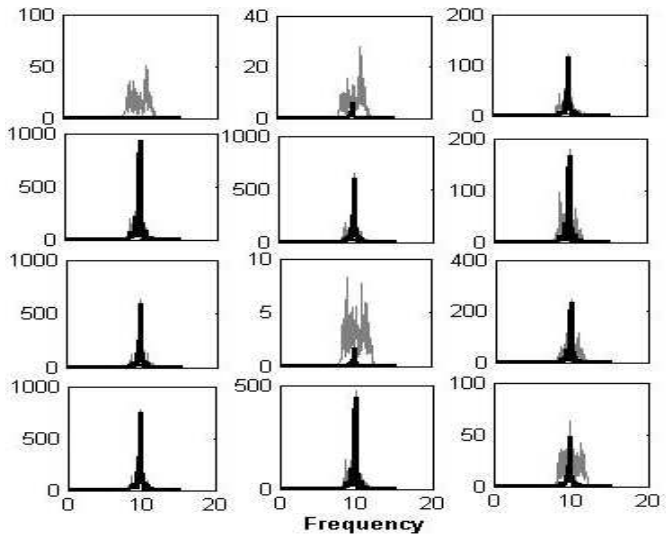

Figure 6.4: Power spectrum plots of alpha signals recovered with Au-ICA (black) superimposed on those recovered with bandpass filtering (gray).

6.3.2 EEG Alpha Power Maps

The alpha signal extraction performance of the proposed method is estimated by comparing the alpha power maps with the conventional method. To plot the alpha power maps, the extracted alpha signal is projected back into the measurement space and the contributions of the alpha signal to all the observed channels are determined as follows:

$$\begin{aligned} \mathbf{a} &= \mathbf{x}\ \mathbf{s}^{-\dagger} \\ \mathbf{R} &= \mathbf{a}\ \mathbf{s} \end{aligned} \tag{6.3}$$

where, $\dagger$ is the pseudo inverse and $\mathbf{R}$ is a matrix of contributions of the extracted alpha in all the channels. The alpha power maps are plotted from the $\mathbf{R}$ matrix with the help of the BESA software [76]. Fig. 6.5, shows a set of alpha power maps from one subject. Fig. 6.5(a), shows the alpha power maps with EEG data (protocol I) processed with band-pass filtering. Fig. 6.5(b), shows the alpha power maps from the Au-ICA extracted alpha signals of the same subject. More localized alpha power sources are clearly noticeable in Fig. 6.5(b). Fig. 6.5(c), shows the alpha

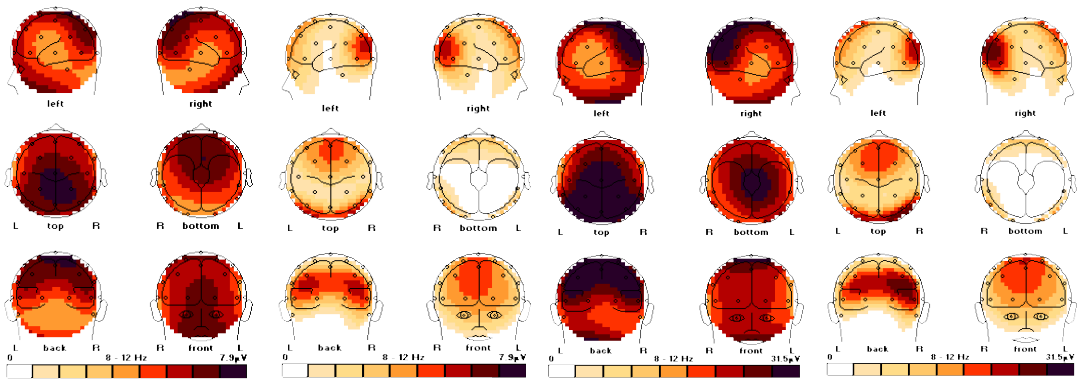

(a) Bandpass filtering (b) Augmented ICA (c) Bandpass filtering (d) Augmented ICA

Figure 6.5: Alpha power maps obtained via BESA. (a) and (b) data acquired with the protocol I, (c) and (d) EEG acquired with the protocol II.

power maps from the band-pass filtered EEG data with the protocol II. Fig. 6.5(d), shows the alpha power maps from the Au-ICA extracted alpha EEG signals. From the independent EEG experiments using the protocols I and II, similar and consistent power maps were obtained using Au-ICA as shown in Figs. 6.5(b) and 6.5(d).

6.3.3 EEG Cortical Source Maps

The alpha power maps represent the alpha power distribution on the scalp, whereas the cortical source maps indicate the actual current sources related to the alpha activated regions. To investigate the spatial correspondence of the alpha sources obtained with Au-ICA, we compared the cortical source maps to the fMRI activation maps obtained via SPM99 [75].

Figs. 6.6(a) and Fig. 6.6(b), show cortical source maps from the band-pass and Au-ICA extracted alpha EEG signals from the same eyes-closed period respectively. The functional maps of fMRI in Fig. 6.6(c), indicate that the associated alpha activated regions include the frontal and occipital lobes which are consistent with the localized areas in the cortical source maps of EEG using Au-ICA. Similarly Figs. 6.6(d) and 6.6(e), shows the cortical source maps from the band-

pass and Au-ICA extracted alpha EEG signals with the experimental protocol II respectively. Our results confirm that the alpha sources in Figs. 6.6(b) and 6.6(e) are more focal than those in Figs. 6.6(a) and 6.6(d). The cortical maps of EEG data using Au-ICA show alpha activated regions involving the frontal and occipital lobes that spatially match the alpha power maps as shown in Figs. 6.5(b) and 6.5(d).

Note that the activated visual cortex in Fig. 6.6 is not due to the visual stimulation, but due to the alpha activity: as mentioned earlier (Section 6.2.4) the activated regions are negatively correlated with the protocol.

6.4 Summary

Blind source separation and extraction techniques hold promise toward biomedical signal analysis. However, there is always a need of extracting only the interesting sources. *a priori* information about the interesting sources is available at some stage of processing. For the EEG analysis, normally the frequency range of interesting signals is known in advance. In this chapter, we have proposed a method based on ICA, named as augmented ICA, that can incorporate the *a priori* information about frequency to extract only the independent component that lie in the desired frequency range of EEG signals i.e., alpha rhythms.

There have been many studies using EEG, fMRI, and simultaneous EEG-fMRI [70], yet general consensus has not been made on the true sources of alpha activity. However, the studies by [69] and [70] reported multiple regions (occipital, parietal and inferior frontal lobes) are responsible for the generation of alpha activities, based on the negative BOLD of fMRI. Our findings in the work presented in this chapter match very closely to these regions, supporting our approach.

Our results, more focalized alpha power and cortical maps, suggest that Au-ICA seems to be capable of extracting the desired frequency range signals more effectively from raw EEG data than the conventional methods. The results also suggest that the conventional band-filter based approaches to extract alpha (or any other specific frequency range) in EEG signals might

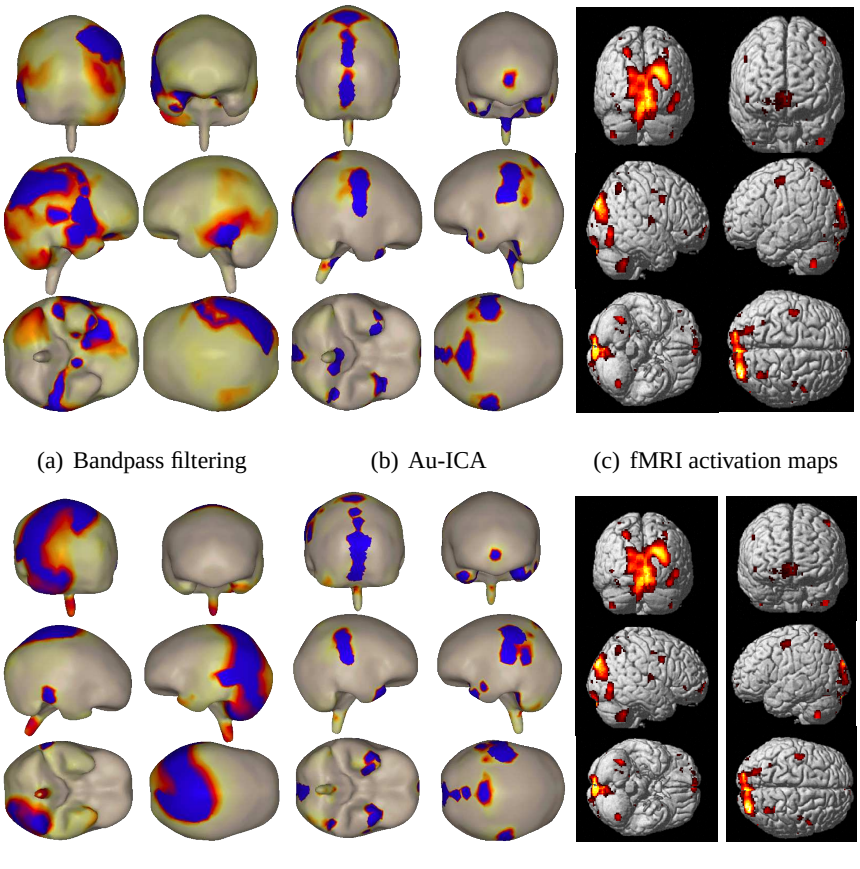

(a) Bandpass filtering (b) Au-ICA (c) fMRI activation maps

(d) Bandpass filtering (e) Au-ICA (f) fMRI activation maps

Figure 6.6: EEG cortical source maps, (a) and (b) with EEG data acquired with the protocol I, (d) and (e) with the protocol II. fMRI activation maps for the data acquired with the protocol I

not reveal the true source generating areas of the brain (although they seem to recover the alpha generating regions which are very much blurred and enlarged) because they work on each EEG channel independently. In contrast, Au-ICA treat all the EEG signals simultaneously in the process of extracting the independent component.

We consider that the Au-ICA approach could be more useful as a preprocessing step in the analysis of alpha activities of EEG and can be extended to extract other kinds of brain activities upon the availability of some *a priori* information about their frequency range.

Chapter 7

Extraction of Event Related Potentials (P300)

A brain computer interface (BCI) uses electrophysiological activities of the brain such as natural rhythms and evoked potentials to communicate with some external devices. P300 is a positive evoked potential (EP), elicited approximately 300ms after an attended external stimulus. A P300-based BCI uses this evoked potential as a means of communication with the external devices. Until now this P300-based BCI has been rather slow, as it is difficult to detect a P300 response without averaging over a number of trials. Previously, independent component analysis (ICA) has been used in the extraction of P300. However, the drawback of ICA is that it extracts not only P300 but also non-P300 related components requiring a proper selection of P300 ICs by the system. In this study we propose an algorithm based on constrained independent component analysis for P300 extraction which can extract only the relevant component by incorporating a priori information. A reference signal is generated as this a priori information of P300 and constrained ICA is applied to extract the P300 related component. Then the extracted P300 IC is segmented, averaged, and classified into target and non-target events by means of a linear classifier. The method is fast, reliable, computationally inexpensive as compared to ICA and achieves an accuracy of 98.3% in the detection of P300.

7.1 Introduction

Recently, a new technology has emerged enabling direct communication between human brain and computer, known as brain-computer interface (BCI). This is done by utilizing certain electrophysiological activities that reflect the function of the brain [77]. BCI using non-invasive means

has been a subject of much research and certain natural rhythms such as alpha and beta-rhythms have been used for BCI [78][79][80]. However, the main drawback using these natural brain rhythms in BCI is that they require extensive training for controlling the natural brain waves. That is why the usage of evoked potentials (EP) for BCI is being extensively researched as they do not require subject training. P300 is a positive EP that is elicited approximately 300ms after an attended external stimulus.

In 1988, Farwell and Donchin first introduced the idea of using P300 in BCI. They introduced some P300 detection methods for BCI such as stepwise discriminant analysis (SWDA), peak picking, area and covariance [81]. Later Donchin added discrete wavelet transform (DWT) to SWDA [82]. P300 detection usually requires extensive averaging and more the number of trials the better the accuracy and reliability of the BCI system. However, increasing the number of trials increases the processing time for detection, which is one drawback of the P300-based BCI.

Independent component analysis (ICA) has been used for the extraction of P300 signals in [83] and [84]. ICA is a statistical technique that is used to separate a mixture of signals into its components provided that the components are independent of each other [8]. The main drawback of ICA is that the number of components is equal to the number of observations. Therefore, one has to apply additional signal processing methods to ascertain which components contain the P300 response. Spatially constrained ICA (scICA) is a semi-blind source separation technique which extracts only the relevant sources and has been previously used for the detection of P300 in [85]. scICA incorporates a priori information of the typical P300 spatial distribution. The spatial distribution is found by running ICA on the available data set and creating a template, which is used as a single spatial constraint to constrain the mixing matrix. Hence, one has to train the spatial constraints before extracting the desired P300 sources. In this study, we propose to use constrained ICA described in [9] and [2] for P300 extraction. The advantage of constrained ICA is that it can extract only the relevant source blindly, without any training of the constraints being applied. The potential of constrained ICA has already been investigated in other areas like extraction of rhythmic activity [86] and artifact rejection [2].

7.2 P300 Extraction using Constrained ICA

The BCI competition 2003 data set IIb [87] provided by the Wadsworth center for our experiment is used. In this data set, the user was presented with a 6 x 6 matrix of characters. The data set consists of 64 EEG channels in which the users task was to focus on characters in a word that was prescribed by the investigator. For each character, the user display was as follows: the matrix was displayed for a 2.5 s period and during this time each character had the same intensity. Subsequently each row and column in the matrix was randomly intensified for 100ms. After intensification of a row or column, the matrix was blank for 75ms. Row or column intensifications were block randomized in blocks of 12. Each set of 12 intensifications was repeated 15 times for each character. Each sequence of 15 sets of intensifications was followed by a 2.5 s period, during which the matrix was blank.

The details about the constrained ICA algorithm can be found in chapter 2. The main steps for our algorithm are described as follows:

1) Bandpass Filtering: The data was bandpass filtered from 0-10 Hz because spectral analysis showed P300 to be within this frequency range.

2) Reference Signal Generation: Designing a proper reference function plays the key role in the extraction of P300-related ICs. A rectangular pulse shape reference function is designed for each of the rows and columns separately. When the target row or column is flashed, after approximately 300 ms, a P300 signal is generated. Hence, when designing the reference function for a particular row or column, we assume that it is the intended target and hence the rectangular pulse is generated in the reference function within 250 to 350 ms interval after the stimulation of the particular row or column. Therefore, we get 12 reference functions, one for each row and column. A general representation of how the reference function is generated is shown in Fig. 7.1 *3) cICA:* cICA was applied on the block of data by using the reference function generated in order to detect which rows or columns elicited P300 responses. As we generated a reference signal for each row or column, hence in effect we derive 12 ICs from the cICA algorithm.

4) Segmentation and Averaging: From the beginning of stimulation of the particular row or

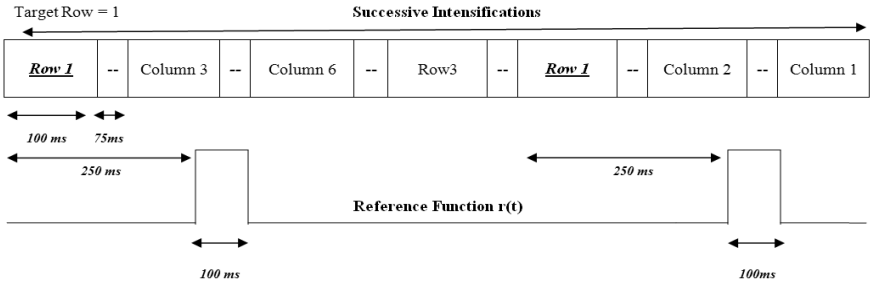

Figure 7.1: Representation of reference signal generation

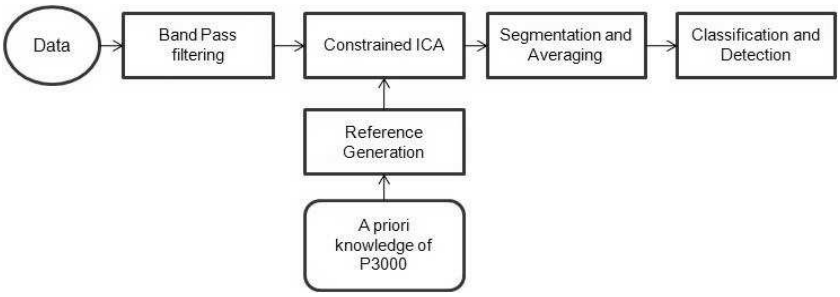

Figure 7.2: Schematic diagram of P300 extraction process

column each IC was segmented into 15 epochs of 650 ms intervals and averaged.

5) P300 Detection: Each averaged segment was correlated with a P300 template. The correlation coefficients and maximum amplitude of the averaged segment were used as features to classify the events into the target and non-target events. A linear classifier was designed which was able to classify the target and non-target events successfully. The feature with the classification boundary is illustrated in Fig. 7.4(b).

The schematic diagram of the process is given in Fig. 7.2

7.3 Results

Before the application of cICA, the existence of P300 was confirmed by averaging target and non-target events at the electrode channel Cz. Fig. 7.3(a) shows a portion of the reference signal generated for a specific row or column. The extracted components by using the constrained ICA algorithm are illustrated in Fig. 7.3(b) and Fig. 7.3(c). The extracted IC containing P300 responses is shown in Fig.7.3(b). It can be seen from the figure that P300 can be extracted quite effectively using this technique. Fig. 7.3(c) shows the extracted IC for the non-target event. In order to increase the reliability and the accuracy of the algorithm we segment the target events into 15 epochs and perform averaging to improve the SNR. Fig. 7.4(a) shows a comparison of the resulting P300 from the extracted signal after averaging, for both target and non-target events. Using this algorithm, we were easily able to separate the target and non-target events by the means of a simple linear classifier, as illustrated in Fig. 7.4(b). The linear classifier was trained with 10 target and 10 non-target events. We used 30 target and 30 non-events in the testing phase and achieved a 98.3% accuracy. Accuracy can be increased if a more complex classifier was used.

7.4 Summary

P300 extraction based on constrained ICA gives better performance as compared to other methods such as ICA. In the conventional ICA, signal is decomposed into several components depending on the number of multichannel observations and most of them do not contain P300 information. In the procedure presented in this chapter, constrained ICA converges only on that independent component containing P300 information, thereby reducing the computation needed to extract P300 signal without compromising the reliability and accuracy of P300 detection and extraction. With a typical Pentium IV personal computer, ICA takes about 45 seconds to extract all the components whereas constrained ICA run on the same data can extract the desired component in only 2 seconds. Hence, a better communication rate can be achieved using the

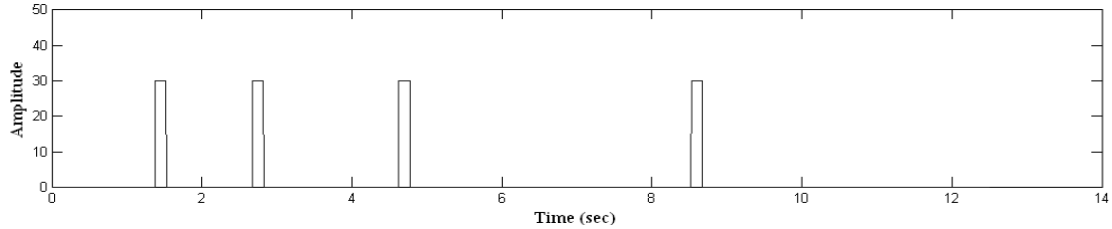

(a) Reference signal

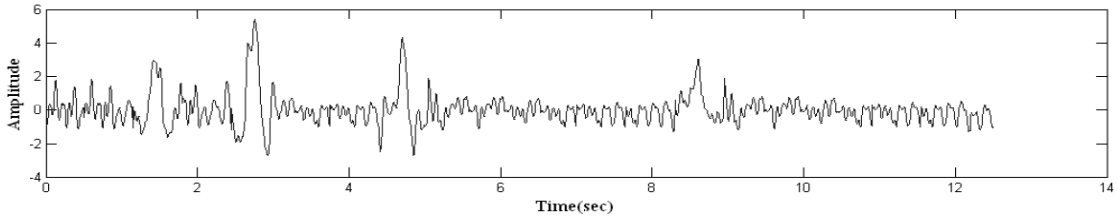

(b) Extracted IC from target data

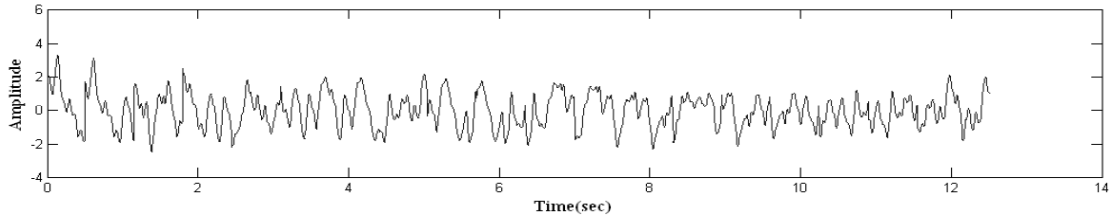

(c) Extracted IC from non target data

Figure 7.3: (a) A part of reference signal showing 4 pulses (b) Corresponding extracted IC from target data (c) Corresponding extracted IC from non-target data

constrained ICA method in a P300-based BCI system.

Designing the proper reference signal plays a very important role in our extraction algorithm. The role of reference function is to direct the constrained ICA algorithm is the direction of the desired ICs. Therefore, reference signal has to be close to the desired P300 component. We have used the rectangular shape as a reference as it is easy to generate. Because we don't know which row or column elicits a P300 response, we have designed a reference signal for all rows and columns and developed a detection scheme to ascertain those components containing the P300 signal. After finding the demixing matrix there is no dense computation involved in our detection and classification scheme since the cICA algorithm yields that IC closest to the desired component, hence detection of P300 in the IC is not that difficult. We were able to classify the target and non-target events quite efficiently by means of a simple linear classifier.

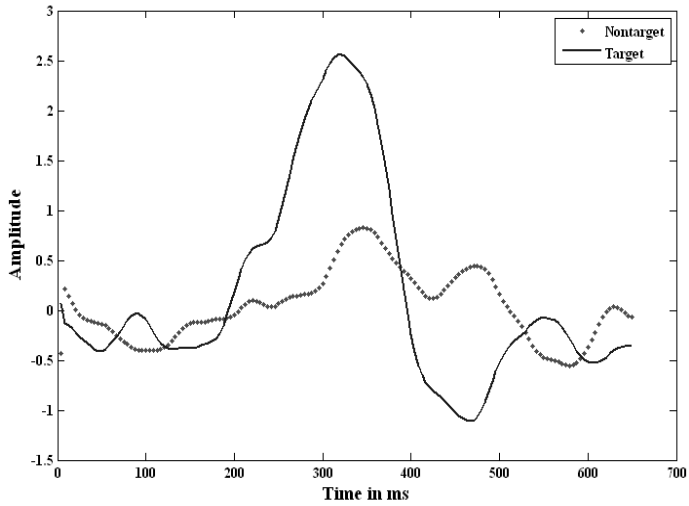

(a)

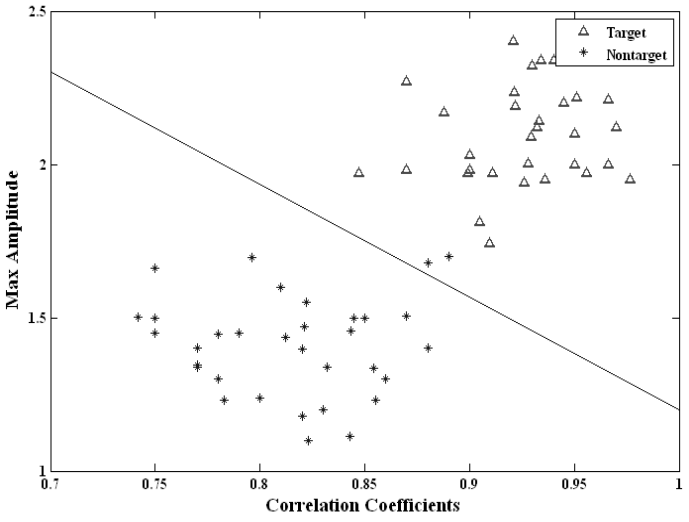

(b)

Figure 7.4: (a) Comparison of averaged segment containing P300 and non P300 signals (b) Plot of feature space with a linear classifier

Chapter 8

Conclusions and Future Work

Blind source separation techniques has many applications, ranging from pattern extraction / analysis, medical diagnostics, image processing to financial series analysis. However, blind source separation based on independent component analysis has gained great deal of popularity in the bio-signal analysis. ICA has been extensively used for different bio-signal analysis applications like, artifact rejection from EEG for MEG data, analysis of evoked potentials and source extraction. Similarly, ICA has been used for fMRI analysis to find the sources. ICA has been used for other bio-medical signals like ECG and PCG analysis.

However ICA has some limitations; i) number of output components is equal to the number of observations, ii)source ambiguity, iii) random ordering of the output components, iv) loss of amplitude information in output components. These disadvantages can be over-comed by incorporating the more information into the basic ICA model. This has been achieved in constrained ICA algorithm proposed by Lu and Rajapakse. They proposed two basic formulation of constrained ICA, i.e. less-complete ICA and ICA with reference. In the first formulation of constrained ICA (i.e., less-complete ICA) the additional information is incorporated directly into the ICA contrast function. Whereas, in second formulation (i.e ICA with reference) the constrained ICA algorithm tries to find an independent component closer to the provided reference signal (template signal). The reference signal does need to be perfect match of the desired independent component. The reference signal should carry some information of the the desired output as it has to guide the algorithm in the desired direction.

Electroencephalogram (EEG) and functional magnetic resonance imaging (fMRI) are im-

portant non-invasive brain imaging techniques. EEG has temporal resolution in the range of millisecond range and fMRI has spatial resolution in the range millimeter. By combining the two modalities advantages of the two can be combined for studying the brain functionality at superior temporal and spatial resolution. However, the artifacts in EEG recording inside MRI scanner get amplified to an extent that it makes EEG data practically useless. The prominent artifacts includes imaging artifacts, BCG and EOG artifacts. Imaging artifacts can be removed using average artifact subtraction (AAS) methods. Number of studies has been conducted to remove EOG artifact from EEG signals measured inside MRI using ICA. The use of ICA for artifact rejection has difficulties because of disadvantages mentioned above; The procedure can neither be standardize nor automated. Through this thesis an BCG and EOG artifact attenuation method from EEG signals measured inside MRI is presented in chapter 4. The presented method is simple, standardized and is almost automatic. The technique uses constrained ICA with *a priori* information about the artifacts as references or constraints. The role of reference functions for constrained ICA is to direct the algorithm into the direction of desired ICs. In the area of artifact rejection in EEG data, temporal and morphological information about the artifact is useful. In this study, three different ways of generating the reference functions for the constrained ICA algorithm has been present. The performance of the proposed procedure is rigorously tested using quantitative and comparative measures, indicating the better performance of the proposed method.

The spatiotemporal data like sequence of images (fMRI data) has interesting sources in both the temporal as well as in spatial domains. The independence of sources in both the domains depends on the experimental conditions and some times it is difficult to maintain those conditions. The standard ICA algorithm can be used in two different modes i.e, spatial and temporal ICA modes. The contrast functions of these standard ICA algorithm are designed to extract maximum independent components. For spatiotemporal data, the spatial or temporal ICA tries to find maximal independent components of one domain deteriorating the independent components of the corresponding domain. The other disadvantage is that the standard ICAs produce very large

number of ICs for fMRI data. Spatiotemporal ICA algorithm has been proposed by J.V. Stone for spatiotemporal data like fMRI data. The algorithm tries to create a balance by jointly optimizing the spatial and temporal domains. However, it suffers from source ambiguity and large number of ICs. For the spatiotemporal data like fMRI images, a priori information is available like the experimental protocol. Through this thesis, an algorithm constrained spatiotemporal ICA has been proposed. The algorithm find the independent components of both the domains with minimal inter domain effect. Only the desired components are extracted therefore no source ambiguity. The performance of the algorithm is tested on simulated as well as on the real data fMRI data set. The results of the proposed algorithm are very encouraging.

Blind source separation and extraction techniques hold promise toward biomedical signal analysis. When *a priori* information about the interesting sources is available, there is always a need of extracting only the interesting sources. In case of EEG, the frequency range of interesting signals is known in advance e.g., we know that the frequency range of alpha signals (8Hz 12Hz) and that of beta signals (18Hz to 20Hz). The constrained ICA algorithm can incorporate *a priori* information to extract only the desired IC. However, when the available information is in different domain than that of signals itself, like in this case available information is in frequency domain and the EEG signals are in time domain, the basic constrained ICA algorithm is of little use. we have proposed a method based on ICA, named it as augmented ICA, that can incorporate the *a priori* information about frequency to extract only the independent component of desired frequency range. The performance of the algorithm is showed by extracting the alpha rhythms from EEG data.

A brain computer interface (BCI) is method of creating a communication link between the brain and external computing device. BCI uses natural brain rhythms or evoked potentials for communication. Evoked potentials are the averaged EEG signals time locked to external stimulus. P300 is a positive evoked potential (EP), elicited approximately 300ms after an attended external stimulus. Until now P300-based BCI has been rather slow, as it is difficult to detect a P300 response without averaging over a number of trials. In the conventional ICA, EEG signal is

decomposed into several components depending on the number of multichannel observations and most of them do not contain P300 information, making the overall process slow. In this thesis P300 extraction based on constrained ICA is presented. P300 extraction based on constrained ICA gives better performance as compared to other methods such as ICA. In the procedure presented in this chapter, constrained ICA converges only on that independent component containing P300 information, thereby reducing the computation needed to extract P300 signal without compromising the reliability and accuracy of P300 detection and extraction. The performance of the proposed procedure indicate that it will facilitate the development of P300 based BCI systems.

The presented procedures and algorithms have application in medical diagnostics, brain computer interface, telecare / ubiquitous health care and brain games. The EEG signals must be artifact free so that desired patterns or abnormality in those become visible. Also, to extract control signals for BCI applications; the procedures based on constrained ICA presented in this thesis are important. Alpha signal, one of the important EEG signal, which are present with eyes closed and fully awake condition. Shape of the alpha tells the overall state of mind and also could be a control signal in BCI applications. Augment ICA presented in this chapter could be an effective method to extract alpha. telecare or ubiquitous applications are becoming reality with the advancement in science and technology. Based on the proposed methods features extracted or other signals like P300 or alpha signals can be transmitted to other locations for experts opinion. The source extraction for bothe spatial and temporal domains for fMRI data also have applications in medical diagnostics and tele health and ubiquitous health care applications. Another, very interesting application for the ideas proposed in thesis could be brain games i.e. playing game through thoughts. One of the possible future directions is to develop above mentioned applications based on the proposed procedures.

Appendix A

List of Publications

Journal Papers:

1. Nguyen Duc Thang, *Tahir Rasheed*, Young-Koo Lee, Sungyoung Lee, Tae-Seong Kim,“Content Based Facial Image Retrieval Using Constrained Independent Component Analysis”, *Journal of information science*. Conditionally accepted.

2. *Tahir Rasheed*, Young-Koo Lee, Sungyoung Lee and Tae-seong Kim,“Constrained Spatiotemporal ICA and Its Application for fMRI Data Analysis”, *Journal of Biomedical Engineering Research*.

3. *Tahir Rasheed*, Young-koo Lee, Soo Yeol Lee and Tae-seong Kim,“Attenuation of artifacts in EEG signals measured inside a MRI scanner using constrained independent component analysis”, *Physiol. Meas.* 30 (2009) 387404 .

4. S. H. Ahn, *Tahir Rasheed*, W. H. Lee, T.-S. Kim, M. H. Cho and S. Y. Lee,“Constrained Independent Component Analysis Based Extraction and Mapping of the Brain Alpha Activity in EEG”, *Journal of Biomedical Engineering Research* (2008) 405-413.

5. Bilal Ahmed, *Tahir Rasheed*, Mohammad A. U. Khan, Abdur Rashid and Saghir Ahmad,“Rib suppression in Chest Radiographs using ICA Algorithm”, *Information Technology Journal* 6(7) (2007) 1085-1089.

6. *Tahir Rasheed*, Myung Ho In, Young-Koo Lee, Sungyoung Lee, Soo Yeol Lee, and Tae-Seong Kim,“Constrained ICA Based Ballistocardiogram and Electro-oculogram Artifacts

Removal from Visual Evoked Potential EEG Signals Measured inside MRI", *Proceedings of international Conference on Neural Information Processing (LNCS)*(2006) 1088-1097.

International Conference Papers:

7. *Tahir Rasheed*, Young-koo Lee, Sungyoung Lee and Tae-Seong Kim,"Extraction and Localization of Alpha Signals Using Augmented ICA", *International conference on computer modeling and Simulation*, Sanya, China (2010).

8. *Tahir Rasheed*, Young-koo Lee and Sungyoung Lee,"Principal subspace analysis based BCG artifact removal in single channel EEG signal measured inside MRI scanner", *International conference on bio-science and bio-technology*, Jeju island, Korea (2009).

9. Asad Masood Khattak, Adil Mehmood Khan, *Tahir Rasheed*, Young-koo Lee and Sungyoung Lee, "Comparative Analysis of XLMiner and Weka for Association Rule Mining and Clustering", *The International Conference on Database Theory and Application*, Jeju island, Korea (2009).

10. Ji-Hwan Kim, Nguyen Duc Thang, *Tahir Rasheed* and Tae-Seong Kim,"Forearm Motion Tracking with Estimating Joint Angles from Inertial Sensor Signals", *The 2nd International Conference on BioMedical Engineering and Informatics*, Tianjin, China (2009).

11. Ozair Idrees Khan, Sang-Hyuk Kim, *Tahir Rasheed*, Adil Mehmood Khan and Tae-Seong Kim,"P300 extraction using constrained independent component analysis", *31st Annual international conference of the IEEE engineering in medicine and biology society*, Hilton Minneapolis, Minnesota, USA (2009).

12. Asad Masood Khattak, Khalid Latif, sungyoung Lee, Young-koo Lee and *Tahir Rasheed*,"Building an Integrated Framework for Ontology Evolution Management", *12th Conference on Creating Global Economies through Innovation and Knowledge Management*, Malaysia (2009).

13. *Tahir Rasheed*, Young-Koo Lee and Tae-Seong Kim,"Constrained Spatiotemporal ICA and Its Application for fMRI Data Analysis", *IEEE International Conference on Biomedical Engineering*, Singapore (2008).

14. Bilal Ahmed, *Tahir Rasheed*, Young-Koo Lee, Sungyoung Lee and Tae-Seong Kim,"Facial Image Retrieval through Compound Queries Using Constrained Independent Component Analysis", *IEEE International Conference on Tools with Artificial Intelligence*, Patras, Greece (2007) 544-548.

15. Bilal Ahmed, *Tahir Rasheed*, Young-Koo Lee, Sungyoung Lee and M. A. U. Khan,"Rib Suppression for Enhancing Frontal Chest Radiographs using Independent Component Analysis", *International Conference on Adaptive and Natural Computing Algorithms*, Warsaw, Poland (2007) 300-308.

16. *Tahir Rasheed*, Bilal Ahmed, Young-Koo Lee, Sungyoung Lee, M. Bettayeb and M. A. U. Khan,"Rib Suppression in Frontal Chest Radiographs: A Blind Source Separation Approach", *IEEE International Symposium on Signal Processing and its Applications*, Sharjah, UAE (2007).

17. *Tahir Rasheed*, Tae-Seong Kim, Young-Koo Lee, SooYeol Lee and SungYoung Lee,"Constrained ICA-based Ballistocardiogram Artifacts Removal from EEG Signals Acquired inside MRI", *Organization for Human brain Mapping 12th annual meeting*, Florence, Italy (2006).

18. *Tahir Rasheed*, T.-S. Kim, Y.-K. Lee, M. H. In, W.H. Lee, S. Y. Lee and S. Y. Lee,"Constrained ICA based Ballistocardiogram and Electro-oculogram Artifacts Removal from EEG Signals Acquired inside MRI", *International Society of Magnetic Resonance in Medicine*,Seattle, Washington, USA (2006).

Bibliography

[1] T. Rasheed, T. S. Kim, Y. K. Lee, M. H. In, W. H. Lee, S. Y. Lee, and S. Y. Lee. Constrained ICA based ballistocardiogram and electro-oculogram artifacts removal from EEG signals acquired inside MRI. In *Proc. Intl. Soc. Mag. Reson. Med.*, volume 14, page 2843, May 2006.

[2] T. Rasheed, Y. K. Lee, S. Y. Lee, and T. S. Kim. Attenuation of artifacts in EEG signals measured inside a MRI scanner using constrained independent component analysis. *Physiological Measurement*, 30:387–404, 2009.

[3] P. Huber. Projection pursuit. *The Annals of Statistics*, 13(2):435–475, 1985.

[4] P. Comon. Independent component analysis–A new concept? *Signal Process*, 36(7):287–314, 1994.

[5] Aappo Hyvarinen. Survey on independent component analysis. *Neural Computing Surveys*, 2:94–128, 1999.

[6] Aapo Hyvärinen and Erkki Oja. A fast fixed-point algorithm for independent component analysis. *Neural Computation*, 9:483–492, 1997.

[7] A. J. Bell and T. J. Sejnowski. An information-maximization approach to blind separation and blind deconvolution. *Neural Computation*, 7:129–1159, 1995.

[8] Aapo Hyvärinen, Juha Karhunen, and Erkki Oja. *Independent component analysis*. John Whily & Sons, Inc., 2001.

[9] Wei Lu and Jagath C Rajapakse. Approach and application of constrained ICA. *IEEE Transactions on Neural Networks*, 16(1):203–212, 2005.

[10] Wei Lu and Jagath C. Rajapakse. Constrained independent component analysis. In *Advances in Neural Information Processing Systems (NIPS2000)*, volume 13, pages 570–576. MIT Press, 2000.

[11] Wei Lu and Jagath C Rajapakse. ICA with reference. *Neurocomputing*, 69:2244–2257, 2006.

[12] X.-R. Cao and R.-W. Liu. General approach to blind source separation. *IEEE Trans. Signal Process.*, 44(3):562–571, 1996.

[13] A. Cichocki, R. Thawonmas, and S. Amari. Sequential blind signal extraction in order specified by stochastic properties. *Electron. Lett.*, 33(1):64–65, 1997.

[14] A. Hyvrinen and E. Oja. Simple neuron models for independent component analysis. *Int. J. Neural Syst.*, 7(6):671–687, 1996.

[15] A. Cichocki, J. Karhunen, W. Kasprzak, and R. Vigrio. Neural networks for blind separation with unknown number of sources. *Neurocomput.*, 24(1-3):55–93, 1999.

[16] A. Papoulis. *Probability, Random Variables, and Stochastic Processes*. New York: McGraw-Hill, 1991.

[17] M. Girolami and C. Gyfe. Extraction of independent signal sources using a deflationary exploratory projection pursuit network with lateral inhibition. *Proc. Inst. Electr. Eng. Vision Image, and Signal Processing*, 144(5):299306, 1997.

[18] Aapo Hyvärinen. New approximations of differential entropy for independent component analysis and projection pursuit. *Advances in Neural Information Processing Systems*, 10:273–279, 1998.

[19] M. Zibulevsky and B. A. Pearlmutter. Blind source separation by sparse decomposition. *Neural Computat.*, 13(4), 2001.

[20] J. Luo, B. Hu, X.-T. Ling, and R.-W. Liu. Principal independent component analysis. *IEEE Transaction on Neural Networks,* 10(4):912917, 1999.

[21] L. Pauling and C.D. Coryell. The magnetic properties and structure of hemoglobin, oxyhemoglobin and carbonmonoxyhemoglobin. *PNAS*, 22:210–216, 1936.

[22] Scott Makeig, Anthony J. Bell, Tzyy-Ping Jung, and Terrence J. Sejnowski. Independent component analysis of electroencephalographic data. *Advances in Neural Information Processing Systems 8, MIT Press, Cambridge MA*, 1996.

[23] M. Hamalainen, R. Hari, R. Ilmoniemi, J. Knuutila, and O. V. Lounasmaa. Magnetoencephalographytheory, instrumentation, and applications to noninvasive studies of the working human brain. *Reviews of Modern Physics*, 65(2):413–497, 1993.

[24] S. Blanco, H. Garcia, R. Quian Quiroga, L. Romanelli, and O. A. Rosso. Stationarity of the eeg series. *IEEE Engineering in Medicine and Biology Magazine*, pages 395–399, 1995.

[25] M. Scherg and D. von Cramon. Two bilateral sources of the late aep as identified by a spatiotemporal dipole model. *Electroencephalography and Clinical Neurophysiology*, 62:32–44, 1985.

[26] J. Mosher, P. Lewis, and R. Leahy. Multidipole modelling and localization from spatiotemporal meg data. *IEEE Trans. Biomedical Engineering*, 39:541–557, 1992.

[27] M. J. McKeown, S. Makeig, G. G. Brown, T. P. Jung, S. S. kindermann, A. J. Bell, and T. J. Sejnowski. Analysis of fMRI data by blind separation into independent spatial components. *Human Brain Mapping*, 6:160–188, 1998.

[28] M. J. McKeown and T. J. Sejnowski. Independent component analysis of fMRI data: Examinating the assumptions. *Human Brain Mapping*, 6(5-6):368–372, 1998.

[29] G. Bonmassar, K. Anami, J. Ives, and J. W. Belliveau. Visual evoked potential (VEP) measured by simultaneous 64-channel EEG and 3T fMRI. *Neuroreport*, 10:1893–1897, 1999.

[30] K. Krakow, P. J. Allen, M. R. Symms, L. lemieux, O. Josephs, and D. R. Fish. EEG recording during fMRI experiments: image quality. *Human Brain Mapping*, 10:10–15, 2000.

[31] R. I. Goldman, J. M. Stern, J. Engel, and M. S. Cohen. Acquiring simultaneous EEG and functional MRI of the alpha rhythm. *Clin. Neurophysiol*, 111:1974–1980, 11 2000.

[32] G. Bonmassar, N. Hadjikhani, J. R. Hinton, D. Hinton, and J. W. belliveau. Influence of EEG electrodes on simultaneous EEG/fMRI measurments. *Human Brain Mapping*, 14:108–115, 2001.

[33] A. Salek-Haddadi, M. Merschhemke, L. Lemieux, and D. R. Fish. Simultaneous EEG-corelated ictal fMRI. *NeuroImage*, 16:32–40, 2002.

[34] P. J. Allen, G. Polizzi, K. Krakow, D. R. Fish, and L. Lemieux. Identification of EEG events in the MR scanner: The problem of pulseartifact and a method for its subtraction. *NeuroImage*, 8:229–239, 1998.

[35] P. J. Allen, O. Josephs, and R. Turner. A method for removing imaging artifact from continuous EEG recorded during functional MRI. *NeuroImage*, 12:230–239, 2000.

[36] J. Sijbers, J. van Audekerke, M. verhoye, A. Van der Linden, and D. Van Dyck. Reduction of ECG and gradient related artifacts in simultaneous recorded human EEG/MRI data. *Magn.Reson.Imaging*, 18(7):881–886, 2000.

[37] G. Bonmassar, P. L. Purdon, I. P. Jaaskelainen, K. Chiappa, V. Solo, E. N. Brown, and J. W. Belliveau. Motion and ballistocardiogram artifact removal for interleaved recording of EEG and EPs during MRI. *Neuroimage*, 16:1127–1141, 2002.

[38] E. Comi, P. Annovazz, A. M. Silva, M. Cursi, V. Blasi, M. Cadioli, A. Inuggi, A. Falini, G. Comi, and L. Leocani. Visual evoked potentials may be recorded simultaneously with fMRI scanning: A validation study. *Human Brain Mapping*, 24:291–298, 2005.

[39] R. Becker, P. Ritter, M. Moosmann, and A. Villringer. Visual evoked potentials recovered from fMRI scan periods. *Human Brain Mapping*, 26:221–230, 2005.

[40] K. H. Kim, H. W. Yoon, and H. W. Park. Improved ballistocardiac artifact removal from the electroencephalogram recorded in fMRI. *Journal of Neuroscience Methods*, 135:193–203, 2004.

[41] Myung Hoo In, Soo Y Lee, Tae S Park, Tae-S Kim, and Min H Cho. Ballistocardiogram artifact removal from EEG signals using adaptive filtering of EOG signals. *Physiological measurements*, 27:1227–1240, 2006.

[42] T. P. Jung, C. Humphries, T. W. Lee, S. Makeig, M. J. McKeown, V. lraggui, and T. J. Sejnowski. Extended ICA removes artifacts from electroencephalographic recordings. *Adv. Neural Inf. Process. Syst.*, 10:894–900, 1998.

[43] R. K. Niazy, C. F. Beckmann, G. D. Iannetti, J. M. Brady, and S. M. Smith. Removal of fMRI envirnoment artifacts from EEG data using optimal basis sets. *Neuroimage*, 28:720–737, 2005.

[44] G. Srivastava, S. Crottaz-Herette, K. M. Lau, G. H. Glover, and V. Menon. ICA-based procedures for removing ballistocardiogram artifacts from EEG data acquired in the MRI scanner. *Neuroimage*, 24:50–60, 2005.

[45] D. Mantini, M. G. Perrucci, S. Cugini, A. Ferreti, G. L. Romani, and C. D. Gratta. Complete artifact removal for EEG recorded during continuos fMRI using independent component analysis. *NeuroImage*, 31:598–607, 2007.

[46] T. W. Lee. *Independent component analysis: Theory and Applications*. Kluwer Academic Publisher, Boston, 1998.

[47] T. P. Jung, S. Makeig, M. Waterfield, J. Townsend, E. Courchesne, and T. J. Sejnowski. Removal of eye activity from visual event-related potentials in normal and clinical subjects. *Clin.Neurophysiol.*, 111:1745–1758, 2000.

[48] T. P. Jung, S. Makeig, M. Waterfield, J. Townsend, E. Courchesne, and T. J. Sejnowski. Analysis and visualization of single-trail event-related potentials. *Human Brain Mapping*, 14:166–185, 2001.

[49] W. Nakamura, K. Anami, T. Mori, O. Saitoh, A. Cichocki, and S. Amari. Removal of ballistocardigram artifacts from simultaneously recorded EEG and fMRI data using independent component analysis. *IEEE Transactions on Biomedical Engineering*, 53(7):1294–1308, 7 2006.

[50] J. James Christopher and J. Gibson Oliver. Temporally constrained ICA: An application to artifact rejection in electromagnetic brain signal analysis. *IEEE Transactions on Biomedical Engineering*, 50(9):1108–1116, 9 2003.

[51] T. Rasheed, M. H. In, Y. K. Lee, S. Y. Lee, S. Y. Lee, and T. S. Kim. Constrained ICA based ballistocardiogram and electro-oculogram artifacts removal from visual evoked potential EEG signals measured inside MRI. In *13th International Conference on Neural Information Processing, Hong Kong*, pages 126–129, 2006.

[52] T. D. Lagerlund, F. W. Sharbrough, and N. E. Busacker. Spatial filtering of multichannel electroencephalographic recordings through principal component analysis by singular value decomposition. *Journal of Clinical Neurophysiology*, 14(1):73–82, 1997.

[53] C. G. Benar, Y. Aghakhani, Y. Wang, A. Izenberg, A. Al-Asmi, F. Dubeau, and J. Gotman. Quality of EEG in simultaneous EEG-fMRI for epilepsy. *Clinical Neurophysiology*, 114:569.580, 2003.

[54] S. Tong, A. Bezerianos, J. Paul, Y. Zhu, and N. Thakor. Removal of ECG interference from the EEG recordings in small animals using independent component analysis. *J. Neurosci. Methods*, 118:11–7, 2001.

[55] J. J. Pekar. A brief introduction to functional MRI - history and today's developments. *IEEE Engineering in Medicine and Biology Magazine*, 25(2):24–26, 2006.

[56] P. A. Bandettini. Processing strategies for time-course data sets in functional MRI of the human brain. *Magnetic Resonance in Medicine*, 30:161, 1993.

[57] B. B Biswal and J. L. Ulmer. Blind source separation of multiple signal sources of fMRI data sets using independent component analysis. *J. Comput. Assist. Tomogr.*, 23:265–271, 1999.

[58] V. D. Calhoun, T. Adali, G. D. Pearlson, and J. J. Pekar. Spatial and temporal independent component analysis of functional MRI data containing a pair of task related waveforms. *Human Brain Mapping*, 13:43–53, 2001.

[59] V. D. Calhoun, T. T. Adali, Pearlson G. D., Van Zijl P. C. M., and Pekar J. J. Independent compo-nent analysis of fMRI data in the complex domain. *Magnetic Resonance in Medicine*, 48:180–192, 2002.

[60] J.V. Stone, J. Porrill, N.R. porter, and N.M. Hunkin. Spatiotemporal ICA of fMRI data. *Computational Neuroscience Report*, 202, 2000.

[61] J. V. Stone, J. Porrill, N. R. Porter, and I. D. Wilkinson. Spatiotemporal independent component analysis of event-related fMRI data using skewed probability density functions. *Neuroimage*, 15(2):407–421, 2002.

[62] K. Suzuki. Fast and precise independent component analysis for high field fMRI time series tailoried using prior information on snatiotempooral structure. *Human Brain Mapping*, 15:54166, 2002.

[63] E. Seifritz, F. Esposito, F. Hennet, H. Mustovic, J. G. Neuhoff, D. Beilecen, G. Tedeschi, K. Scheffler, and F. D. Salle. Spatiotemporal pattern of neural processing in the human auditory cortex. *Science*, 297(5587):1706–1708, 2002.

[64] Q. H. Lin, Y. R. Zheng, F. L. Yin, H. Liang, and V. D. Calhoun. A fast algorithm for one-unit ICA-R. *An international journal of information sciences*, 177:1265–1275, 2007.

[65] J. W. Jeong, T. S. Kim, S. H. Kim, and M. Singh. Application of independent component analy-sis with mixture density model to localize brain alpha activity in fMRI and EEG. *International Journal of Imaging Systems and Technology*, 14(04):170–180, 2004.

[66] E. Niedermeyer. Alpha rhythms as physiological and abnormal phenomena. *Int. J. Psychophysiol*, 26:31–49, 1997.

[67] I. Manshanden, J. C. De Munck, N. R. Simon, and F. H. Lopes da Silva. Source localization of MEG sleep spindles and the relation to source alpha band rhythms. *Clin Neurophysiol*, 113:1937–1947, 2002.

[68] A. Salek-Haddadi, K. J. Friston, L. Lemieux, and D. R. Fish. Studying spontaneous EEG activity with fMRI. *Brain Res.*, Rev.43:110–113, 2003.

[69] Robin I Goldman, John M Stern, Jerome Engel Jr, , and Mark S Cohen. Simultaneous EEG and fMRI of the alpha rhythm,. *NeuroReport*, 13(18):2487–2492, December 2002.

[70] H. Laufs, A. Kleinschmidt, A. Beyerle, E. Eger, A. Salek-Haddadi, C. Preibisch, and K. Krakow. EEG-correlated fMRI of human alpha activity. *NeuroImage*, 19:463–476, 2003.

[71] Stephan Henning, Klaus-Dietmar Merboldt, and Jens Frahm. Task- and EEG-correlated analyses of BOLD MRI responses to eyes opening and closing. *Brain Research*, 1073-1074:359–364, 2006.

[72] H. Mandelkow, P. Halder, D. Bradeis, M. Soellinger, N. de Zanche, R Luechinger, and P. Boesiger. Heart beats brain: The problem of detecting alpha waves by neuronal current imaging in joint EEG-MRI experiments. *NeuroImage*, 37:149–163, 2007.

[73] Bernd Feige, Klaus Scheffler, Fabrizio Esposito, Francesco Di Salle, Jurgen Hennig, and Erich Seifritz. Cortical and subcortical correlates of electroencephalographic alpha rhythm modulation. *J Neurophysiol.*, 93:2864–2872, December 2005.

[74] S. H. Ahn, W. H. Lee, M. H. In, T. S. Kim, and S. Y. Lee. Extraction and localization of alpha activity of the brain in EEG and fMRI using constrained ica. In *Proceedings of the 29th Annual International Conference of the IEEE EMBS Cit Internationale, Lyon, France*, volume 3, pages 5493–5496, 2007.

[75] SPM99. Available at. `http://www.fil.ion.ucl.ac.kr.uk/spm`, 2006.

[76] BESA. Available at. `http://www.besa.de`, 2006.

[77] J. R .Wolplaw, N. Birbaumer, D. J. McFarland, G. Pfurtscheller, and T.M. Vaughan. Brain-computer interfaces for communication and control. *Clin.Neurophsiol.*, 113:767–791, 2002.

[78] G.E. Fabiani, Dennis J. McFarland, J.R.Wolplaw, and G. Pfurtscheller. Conversion of eeg activity into cursor movement by a brain-computer interface. *IEEE Trans Neural Systems and Rehab. Engineering*, 12(3):767–791, 2004.

[79] A.Kostov and M. Polak. Parallel man-machine training in development of EEG- based cursor control. *IEEE Trans. Rehab.Eng.*, 8(2):203–205, 2000.

[80] J. R .Wolplaw, D. J. McFarland, and T. M. Vaughan. Brain computer interface research at the wadsworth center. *IEEE Trans. Rehab. Eng.*, 8(2):222–226, 2000.

[81] L.A. Farwell and E. Donchin. Taking off the top of your head:toward a mental prosthesis utilizing event related brain potentials. *Electroenceph. Clin. Neurophysiol.*, 70:510–523, 1988.

[82] E. Donchin, K. M. Spencer, and R. Wijesinghe. The mental prosthesis: Assessing the speed of a p300-based brain-computer interface. *IEEE Trans. Rehab. Eng.*, 8:174–179, 2000.

[83] N. Xu, X. Gao, B. Hong, and S. Gao. BCI competition 2003-data set iib : Enhancing p300 wave detection using ICA-based subspace projections for BCI applications. *IEEE Trans. Biomedical Engineering*, 51(6):1067–1072, 2004.

[84] H. Serby and E. Yom-Tov. An improved p300-based brain computer interface. *IEEE Trans. Neural Networks and Rehab.*, 13:89–98, 2005.

[85] S. Wang and C.J. James. Enhancing evoked responses for BCI through advanced ICA techniques. In *Advances in Medical, Signal and Info. Proc.*, pages 1–4, July 2006.

[86] S. Wang and Christopher J. James. Extracting rhythmic brain activity for brain-computer interfacing through constrained independent component analysis. *Computational Intelligence and Neuroscience*, 2007.

[87] B. Blankerz, K. R. Mueller, G. Vurio, T. M. Vaughan, G. Shalk, J. R. Wolplaw, A. Schloegl, C. Neuper, G. Pfurtcheller, T. Hinterberger, M. Schroeder, and N. Birbaumer. The bci competition 2003: Progress and perspectives in detection and discrimination of EEG single trials. *IEEE. Trans. Biomed. Eng.*, 51:1044–1051, 2004.